ASE-1708

FINAL REPORT

SOUNDING ROCKET FLIGHT OF A DIRECTIONAL NEUTRON DETECTOR

Contract NASW-1540

REPORT PERIOD

29 December 1966 to 30 September 1967

Prepared for

National Aeronautics and Space Administration

NASA Headquarters

Washington, D. C. 20546

Prepared by

American Science and Engineering

11 Carleton Street

Cambridge, Massachusetts 02142

Date: November 28, 1967

FOREWORD

This report presents an account of NASA sounding rocket flight 14.297 CE, the payload for which was prepared by American Science and Engineering under contract NASW-1540. The payload contained a directional neutron detector developed by AS&E under contract NASW-1523. This detector was conceived by J.R. Waters and developed under his direction. Other major contributors to the program were R. Becker, S. Frankenthal, E. Kellogg, H. Manko and R. Tietsch.

The eventual goal is to search for neutrons coming from the sun. This rocket flight and the previous development program showed that such a detector could be flown in a rocket without damage or degraded performance. However, certain improvements are required before it might be used to search for solar neutrons.

CONTENTS

CONTENTS (continued)

ILLUSTRATIONS

ILLUSTRATIONS (continued)

ILLUSTRATIONS (continued)

TABLES

ABSTRACT

A directional neutron detector was built, along with appropriate electronics, a sun sensing device, and a nose cone ejection system. The phosphor for the scintillation counter was constructed of small glass tubes filled with scintillation fluid encased in clear epoxy, and completely sourrounded by a cosmic ray anti-coincidence shell of CsI. The experimental apparatus was integrated into a Nike-Apache sounding rocket and launched from Wallops Island, Va. on 13 June 1967. Pulse height and pulse shape information telemetered to the ground station for subsequent two parameter analysis determined the type of radiation detected, as well as its energy spectrum. Except for the inadequate rejection of cosmic ray particles, the system functioned as planned, demonstrating the suitability of this type of detector for solar neutron measurements.

1.0 PURPOSE OF THE EXPERIMENT

1.1 Neutron Sources Outside the Atmosphere

Space experiments involving the measurement of intensity, spectrum, or direction of particle fluxes or of electromagnetic radiation are important in astrophysical or geophysical considerations, since the sources and production mechanism for all such radiations must be explained.

Measurement of neutron flux outside the earth's atmosphere can provide particularly useful information. Because of the attenuation length of neutrons in matter and the half life for radioactive decay, both of which are relatively short, such neutrons would be expected only from the earth's upper atmosphere, from the region just outside the sun's atmosphere, or from the space vehicle containing the detection system. Of these sources, neutrons from the earth and spacecraft would have less fundamental interest, since they would usually be secondary to radiation generated by energetic cosmic ray particles, which themselves are easily observable. Solar neutrons, on the other hand, are presumed to result from disturbances just outside the solar atmosphere which are remote from direct observation.

Following solar flares, protons, electrons and other charged particles of very high energy have been observed. Several authors have calculated neutron production rates, based on estimates of the fluxes and energies of the charged particles contained in the flare. While it is established that there must be neutron production in an amount that would be detectable, there is a wide variation in predictions of intensities and energy spectrum of the neutrons. Presumably, an actual measurement of the neutron yield would provide information on the process which produced them.

Hess[1] has considered a model whereby protons in flares, impinging on the surface of the sun, produce neutrons with a conversion efficiency of about 1 per cent. This would cause a neutron flux of 26/cm^2 sec at the earth if it were not for neutron decay. Of course, the amount of decay depends on the flight time and hence, on the energy of the neutrons.

Lingenfelter, Flamm, Canfield, and Kellman[2] have performed a more detailed investigation using a similar model. They conclude that a flux of as much as 7×10^4/cm^2 would arrive at the earth during the first hour following an extremely intense flare. The time dependence of the arrival would appear as in Figure 1-1.

Fireman[3] has measured large concentrations of tritium and He^3 in recovered Discoverer 17 material. A likely interpretation of his data is that these elements were produced by nuclear reactions in the sun during the 3^+ flare of December 12, 1960. If that were so, neutron fluxes at the earth of up to 10/cm^2 sec might have been seen during the intense portion of a flare of this importance. This yield is not insignificant compared to the proton induced neutrons considered by Lingenfelter et al. These D-D neutrons would be identified by their longer transit time and, in recoil detectors, by the size of the output pulse.

It should be possible to detect such fluxes, provided that the observations are made at the appropriate time. It would be most desirable to have the detector on a satellite to monitor neutron flux during quiet as well as active periods, and to be available for observations with little or no warning.

Measurements have been reported by several observers. Haynes[4] and Bame and Asbridge[5] have reported upper limits of 0.02 and 0.01 neutrons/cm^2 sec, respectively, during periods of little solar activity.

Following a recent experiment, Daniel, Joseph, Lavakare, and Sunnderajan[6] report an increase in the counting rate of a neutron sensitive

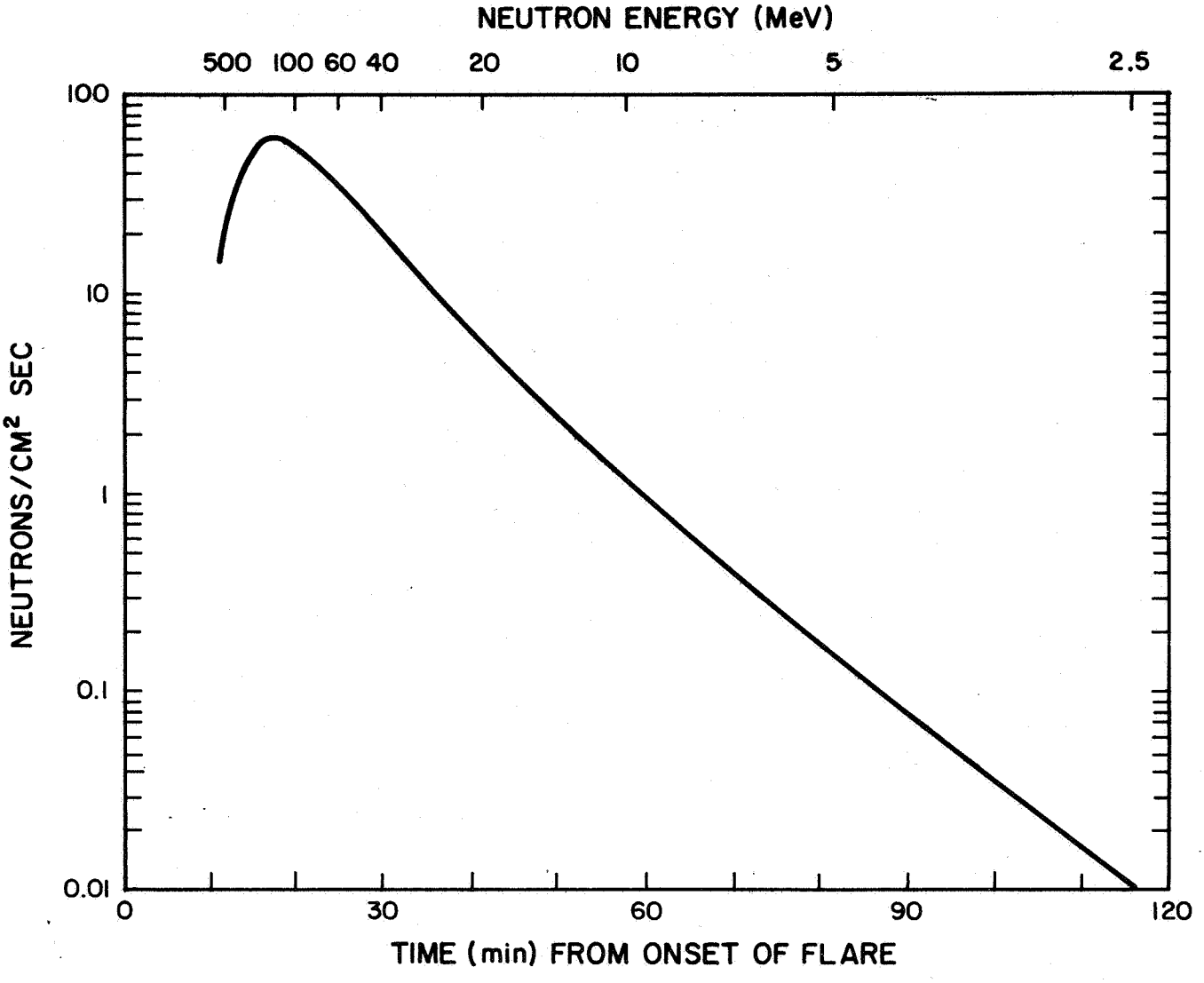

Figure 1-1 Neutrons from Solar Flare.
Predicted neutron flux arriving at the Earth after the onset of a flare.

detector during a period when activity from a solar sub-flare was monitored by optical and radio observations. The results are interesting, but by themselves, inconclusive.

1.2 Detector Design Considerations

To determine unambiguously that the sun is the source of detected neutrons, it is desired that the detector be more sensitive for neutrons from one direction than from another. Then, if a correlation between the counting rate and angle is observed as the detector is rotated, the actual source of the neutrons can be located.

In addition, the detector must be able to reject cosmic ray protons, gamma rays, or any incident radiation other than neutrons, but still count neutrons with reasonable efficiency. The detector must be rugged and compact, and have low power consumption if it is to operate on a space vehicle.

It was elected to reject the undesired events by pulse-shape discrimination (PSD) in a phoswich detector. A scintillation detector was employed which uses NE 213 fluid as the scintillator. Because of the nonlinear response of this scintillator material to the rate of energy deposition, proton recoils from neutron scattering give longer pulses than electron recoils from Compton scattering and other photon induced events. Cosmic ray events were to be rejected by enclosing the scintillator with a layer of CsI (Na). Cosmic ray protons going through the CsI (Na) would produce a pulse which is longer than neutron induced events. PSD circuits were designed which would allow rejection of the fast (gamma) pulses or the very slow (cosmic ray) pulses, and accept only the mid-range of pulse lengths that included detected neutrons.

Directionality was incorporated by allowing the scintillation fluid to flow into and around a matrix of closely packed glass tubes. Since the most energetic proton recoils are predominantly in the same direction as the incident neutron, neutrons incident along the direction of the tubes produce more light than neutrons perpendicular to the tubes. The effect can be understood qualitatively by considering an idealized case in which proton recoils originate in NE 213 fluid at the center of a glass tube when 3.0 MeV neutrons are incident.

Figure 1-2 shows the distribution in NE 213 of the ranges of proton recoils. Different ranges result from different scattering angles, and the horizontal scale, proportional to $\sin^2\theta$ is selected so that equal intervals represent equal probabilities. Also plotted is the distance to the inside tube wall along a line making an angle θ with respect to the tube axes, assuming the tube has an inside radius of 0.002 in. This path length, of course, varies with scattering angle. It is seen that for neutrons incident along the tubes, the entire range of the recoil is in the glass. About 40 percent of most energetic recoils are degraded in energy, however, when the incident neutrons are directed transverse to the glass tubes. It must be emphasized that a more detailed analysis is required to predict accurately the behavior of the detector. The analysis is further discussed in the next section.

1.3 Flight Test of the Detector

A detector has been constructed using the design concepts mentioned above. The glass tube structure was in the form of a cube, 1.50 in. on a side. Electronics suitable for a satellite were designed, assembled, and tested. To prove the suitability of the system for satellite applications, the initial unit was flown above the atmosphere in a Nike-Apache rocket.

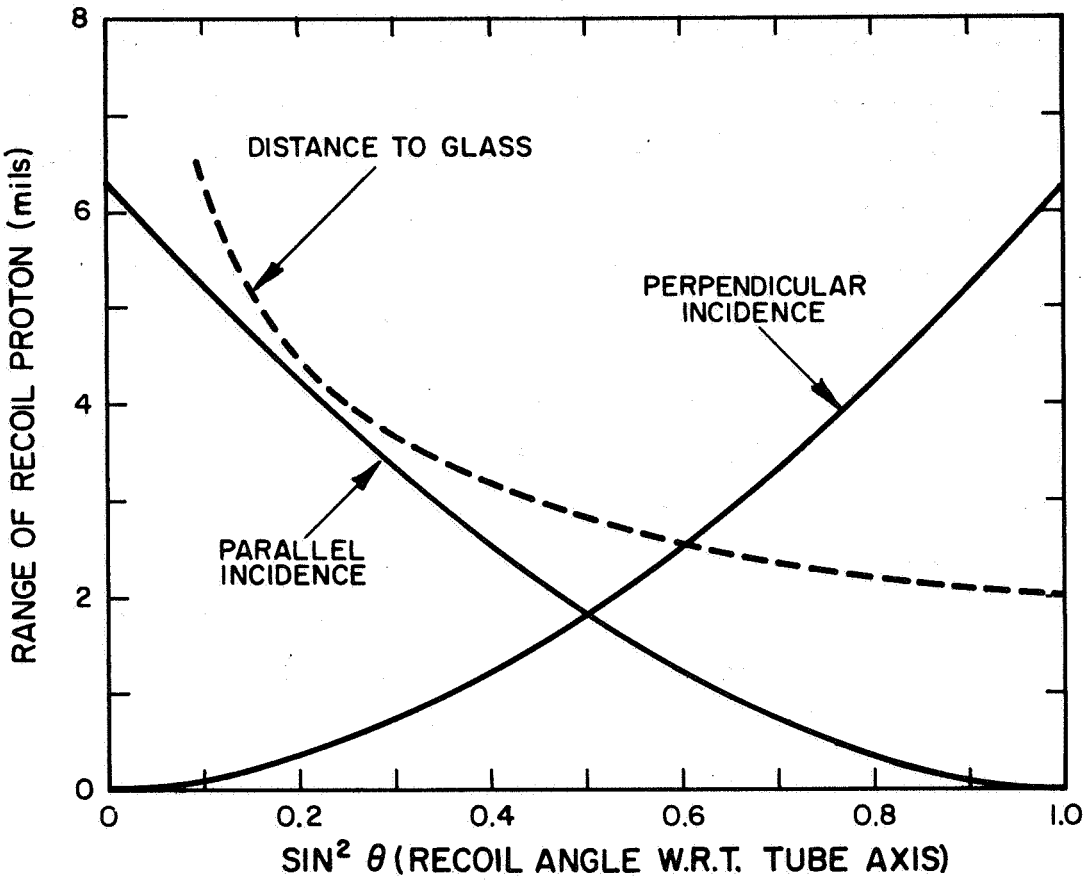

Figure 1-2 Distribution of Ranges.
Recoil protons in NE 213. 3.0 MeV Neutron energy.
Glass tube inner radius 0.002 inch.

The rocket flight, slightly over five minutes, was not ideal in that it provided no opportunity to observe solar neutron emission as a function of time. However, it was expected to provide at least an upper limit for neutron emission from the quiet sun. It was possible that a solar event could have occurred at such a time that solar neutrons could be detected during the flight, and in that case a measure of the intensity and energy distribution might be obtained.

2.0 DIRECTIONAL DETECTOR

2.1 Geometrical Considerations

The energy range over which the detector maintains directionality is determined by the inner radius of the glass tubes which contain the scintillation fluid. In order to utilize the same detector to search for 2.8 MeV D-D neutrons, as well as the more energetic breakup neutron spectrum calculated by Lingenfelter et al, it was necessary that the detector have good directionality at 2.8 MeV and at higher energies. Range-energy relationships indicated that a 0.002-inch inner radius would be appropriate in this case. Selection of the outer radius was a compromise between sensitivity and directionality. A choice of 0.003-inches outer radius was made, giving a scintillator/glass ratio of 0.493 : 0.507. This causes degradation of pulse height averaging to about 50 percent for neutrons incident perpendicular to the tubes, but maintains the sensitivity for neutron detection at a reasonable fraction of that from a homogeneous liquid scintillation cell.

The liquid scintillator cell was a 1.5 inch cube; the size being limited by multiple-scattering effects, light collection, cost and availability of space. Approximately 26 percent of incident 2.8 MeV neutrons should scatter from hydrogen in a cell the size selected. For a time integrated flux of 1.0 neutrons/cm^2 at 2.8 MeV there should be 4.0 recoil protons.

2.2 Pulse Shape Discrimination

The scintillation fluid chosen was NE 213 (supplied by Nuclear Enterprises, Ltd., Winnipeg, Manitoba) because of its excellent PSD properties. In particular, neutrons and gamma rays are readily distinguished by the fact that neutron pulses have a longer decay time.

Cosmic ray particles are expected to be a troublesome source of background. Their effect was reduced by completely enclosing the detector with a layer of CsI (Na) having a decay time of about 0.5 microseconds, much longer than neutron pulses from the NE 213. This technique for charged particle rejection is reported to have been used successfully by Haymes[4] resulting in only a slight deterioration of the discrimination between neutrons and gamma rays.

CsI (Na) was chosen over CsI (Tl) because of its greater light output. It is true, however, that the decay time of the CsI (Tl) is longer than for the CsI (Na), so that they are probably equivalent for use as an anticoincidence shield in the present application.

The CsI layer was 0.05 cm thick and any charged particle traversing this thickness would lose at least 400 keV of energy. Most cosmic ray particles would lose twice that, since they must enter and leave through the CsI. This should have provided sufficient slow decay component to the pulse to cause it to be rejected. Evidence presented later in this report, however, indicates that rejection was not as great as had been expected.

2.3 Directional Properties

Limiting the NE 213 liquid to the region inside and between closely packed glass tubes produced several desirable effects. Most important of these, as mentioned earlier, is that it can be easily demonstrated that a beam of neutrons is coming from a particular direction. Another effect was the reduction of the efficiency for detecting neutrons produced in the upper atmosphere and aboard the vehicle.

Alignment of the glass tubes was maintained in such a way that these background neutrons were incident on the detector in the least sensitive direction, with no correlation between sensitivity and angle. A final effect was that electron recoils from gamma-ray induced processes in the scintillator were of sufficiently long range that their pulse height was invariabily degraded by a factor of about two compared to that of a bulk scintillator; this reduced the ability of gamma pulses to break through the PSD and appear as neutrons.

A computer program to calculate the directional response was written. The program simulates the detector by tracking proton recoils from uniformly distributed scattering locations in the liquid scintillator through various polar and azimuthal angles of recoil. Each polar angle is weighted according to the lab cross section for n, p elastic scattering. See Figure 2-1.

Recoil protons for each combination of scattering location, polar and azimuthal angle are tracked through the sample. A power law form of the range energy relation is assumed, and the light output is assumed to follow the relations of Rothberg [7]:

$$L = 0.28E + 0.033\,E^2 \qquad E < 6 \text{ MeV}$$

$$L = 0.70E - 1.33 \qquad E \geq 6 \text{ MeV}$$

where E is the energy in MeV, and L is the light output in units such that L = E for electrons.

The fundamental input parameters for the calculation are neutron energy, glass tube inner and outer radii and the angle between the glass tube axes and the direction of the neutron's momentum. Most of the calculations, lab tests and flight analysis were done with this angle equal to 0° (parallel incidence) or 90° (perpendicular incidence).

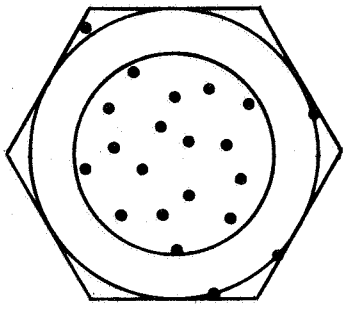

UNIFORMLY DISTRIBUTED
SCATTERING LOCATIONS

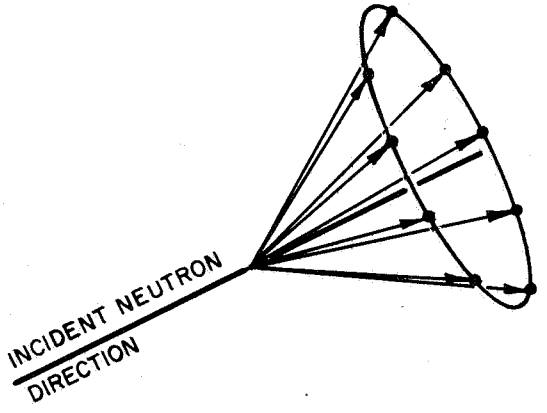

EQUALLY SPACED
AZIMUTHAL ANGLES
OF RECOIL PROTONS

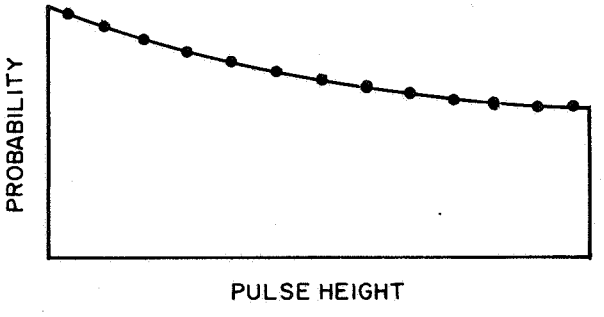

EQUALLY SPACED
PULSE HEIGHT
FOR POLAR ANGLES
OF RECOIL PROTONS

Figure 2-1 Selection of Events.
The approach to calculating the directional response is outlined.

Some of the computer outputs are illustrated in Figures 2-2 through 2-5. The response is plotted at energies of 1, 2, 3, 4, 5, 6, 7, 8, 10, 12 and 14 MeV for neutron tube angles as indicated.

The curves show that the detector will have good efficiency and good directional properties from 2.5 MeV up to about 8 MeV, as long as the incident neutron spectrum includes only a reasonably narrow range of energies. It would be expected to be useful for looking at the slower neutron from solar flares, since these neutrons will be produced over a short period of time and will arrive in the vicinity of the earth at a time determined by their energy.

The detector does not give highly directional response to a continuous neutron energy distribution. Therefore, one might question its practical usefulness. One important situation where it could be used to advantage is in observing the effects of the sudden onset phase of an intense flare. The neutrons would be time-of-flight analyzed, so would be monoenergetic at any given time. The detector would give directional response, and would be extremely useful in sorting out real solar neutrons from fluctuations in the background caused by other effects of the flare. One example of a side effect very difficult to sort out is a change in the rate of local neutron production in the spacecraft, due to increased charged particle fluxes from the sun. This effect could not be discriminated against by a non-directional detector.

2.4 Evaluation of Prototype

In order to test several concepts of the design, prototype detectors were built and studied. A sample of NE 213 fluid enclosed in a glass chamber one inch in diameter and one inch long, without glass tubes, was used in determining the pulse height response to various sources of radiation in the laboratory. It was also used in checking the quality of our electronics, in particular, the PSD circuits.

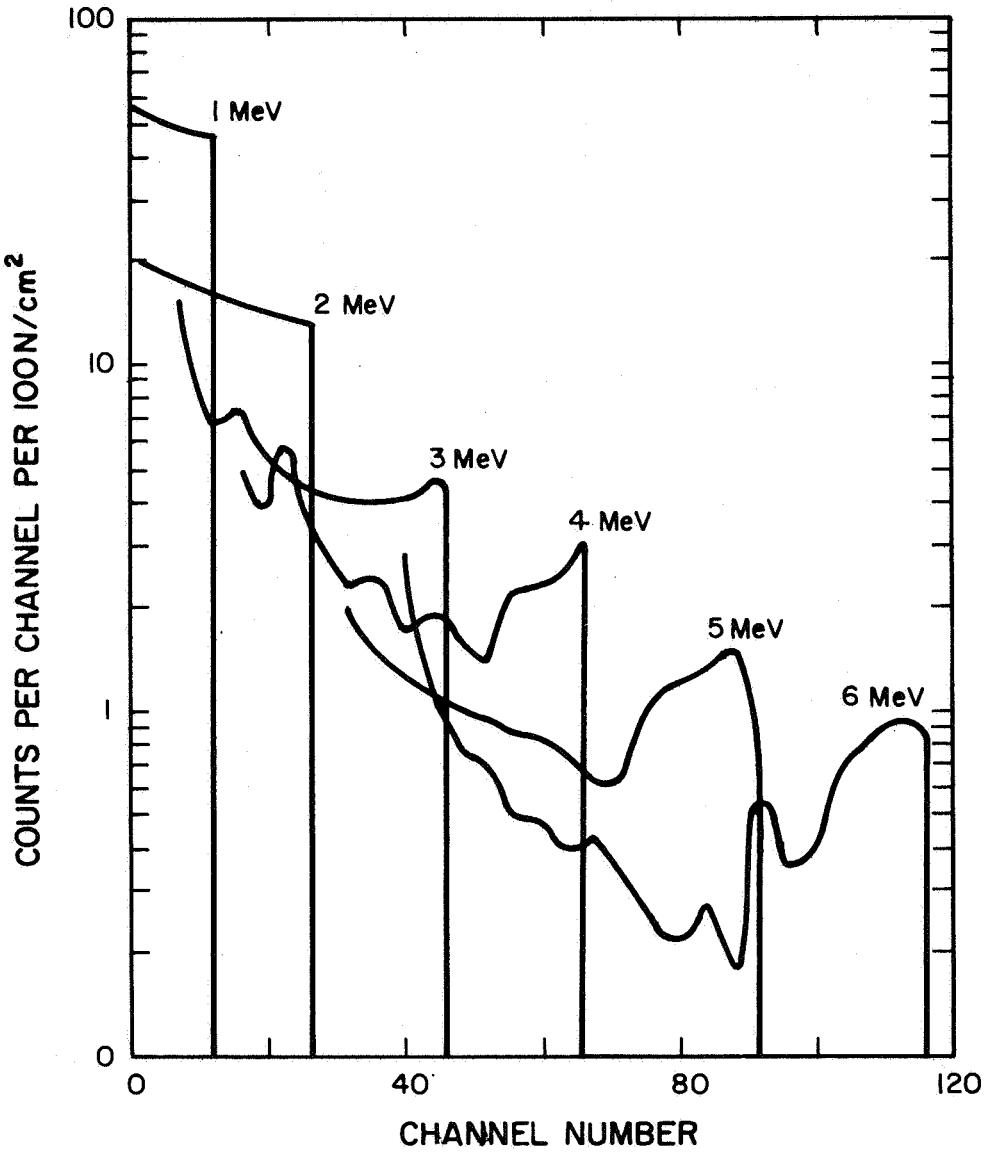

Figure 2-2 Calculated Spectra for Directional Detector. Neutrons incident parallel to tube axis.

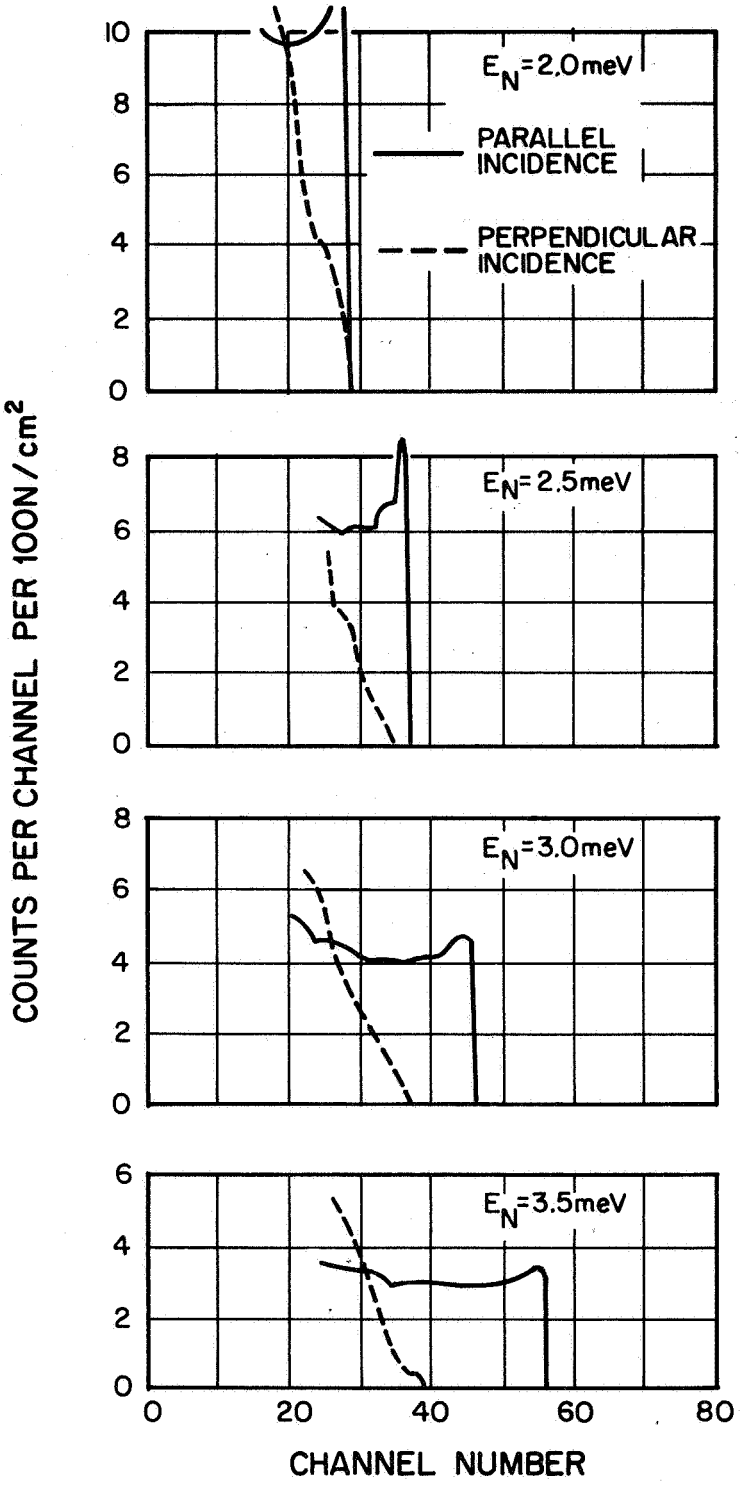

Figure 2-3 Calculated Spectra for Directional Detector: 2 to 3.5 MeV, parallel and perpendicular incidence.

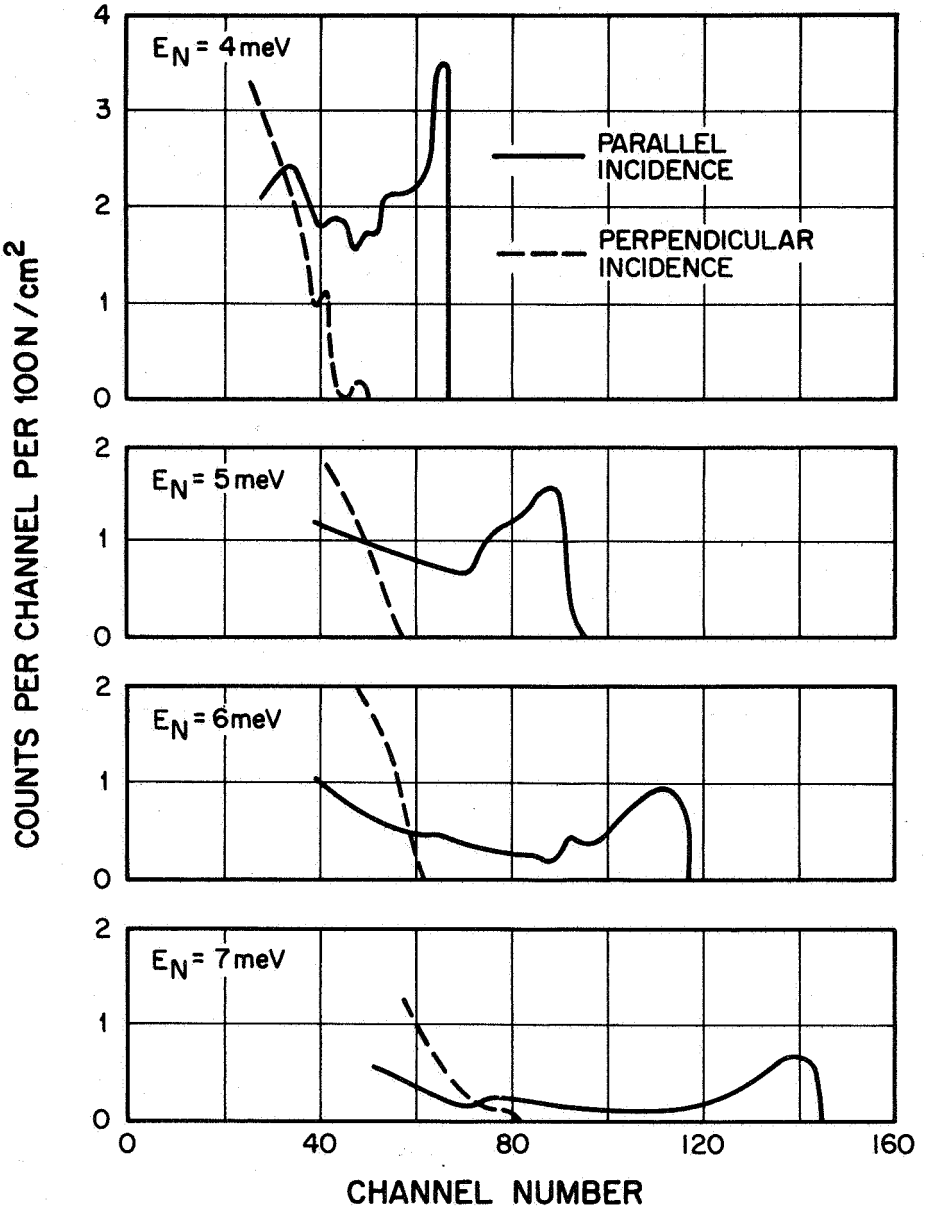

Figure 2-4 Calculated Spectra for Directional Detector: 4 to 7 MeV, parallel and perpendicular incidence.

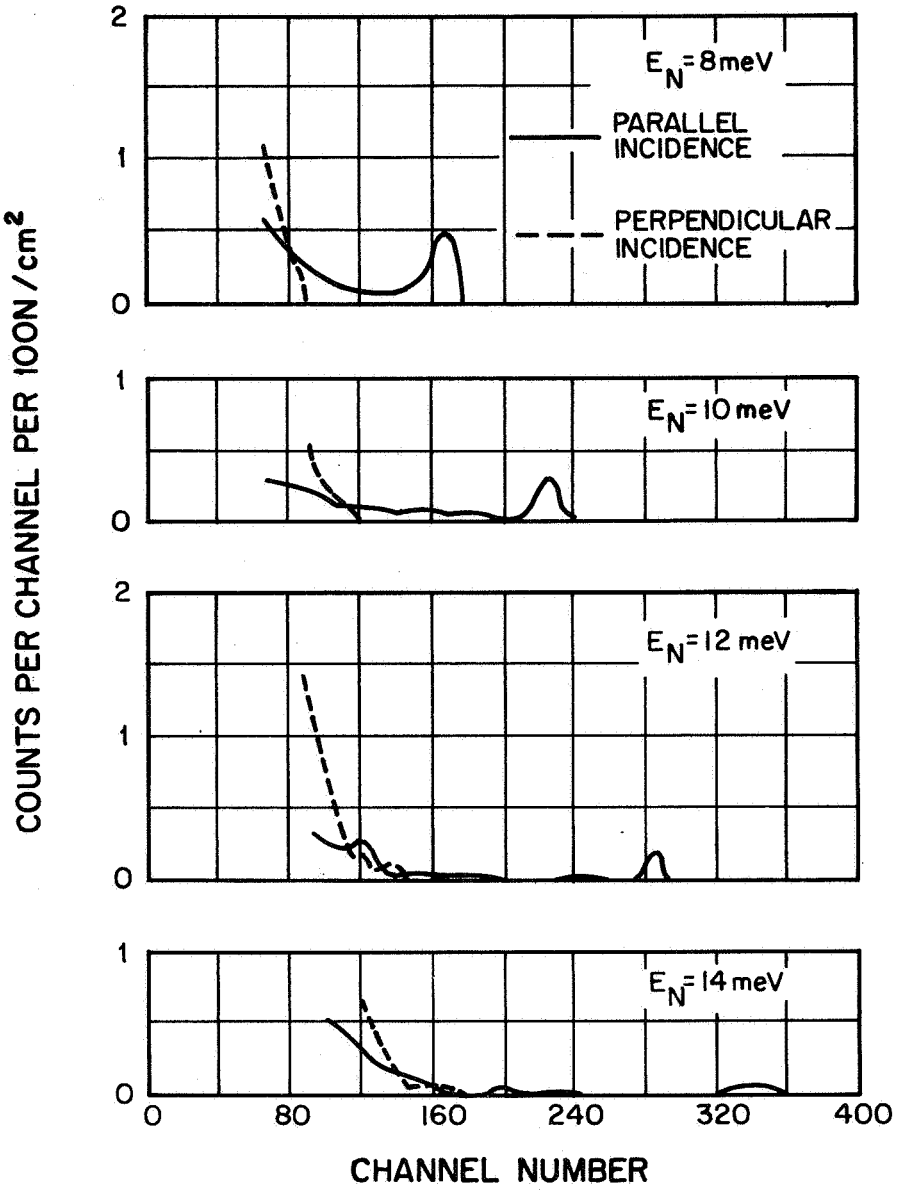

Figure 2-5 Calculated Spectra for Directional Detector: 8 to 14 MeV, parallel and perpendicular incidence.

Two detectors with glass tubes also were constructed. The one most similar to the flight scintillator contained 850 tubes of the same cross-section as was used in the flight. In order to fill the cell it was first evacuated. The NE 213 fluid was then allowed to flow in, filling the vacuum.

The directional response is shown in Figure 2-6. The calculated curves include 50 percent pulse height resolution, and were normalized along both axes. There is good agreement in the shapes and realtive light output for parallel and perpendicular incidence. The "directionality" shown in Figure 2-6 is defined as the ratio of the total number of counts above a given threshold for parallel incidence to those for perpendicular incidence. Figure 2-7 shows the effectiveness of PSD. The curves labeled "n-logic" are data identified as neutrons by the PSD circuit. They show the shape expected from 2.8 MeV neutrons incident parallel to the axis. The cutoff at about channel 35 is from a lower-level discriminator. Both "n-logic" curves are the same with and without the presence of Co^{60} gamma rays. The "γ-logic" data is strongly affected by the gamma rays, as expected. Figure 2-8 shows that some directionality is retained at 14 MeV.

2.5 Fabrication of the Flight Scintillator

For ruggedness and ease in handling, the glass tubes used for the flight were bonded together at elevated temperatures into hexagonal bundles of 270 each. These bundles were then cemented together to form the total glass structure. About 71,000 tubes were required. A portion of the assembly is shown in Figure 2-9. The cell was constructed by American Optical Co., Southbridge, Massachusetts.

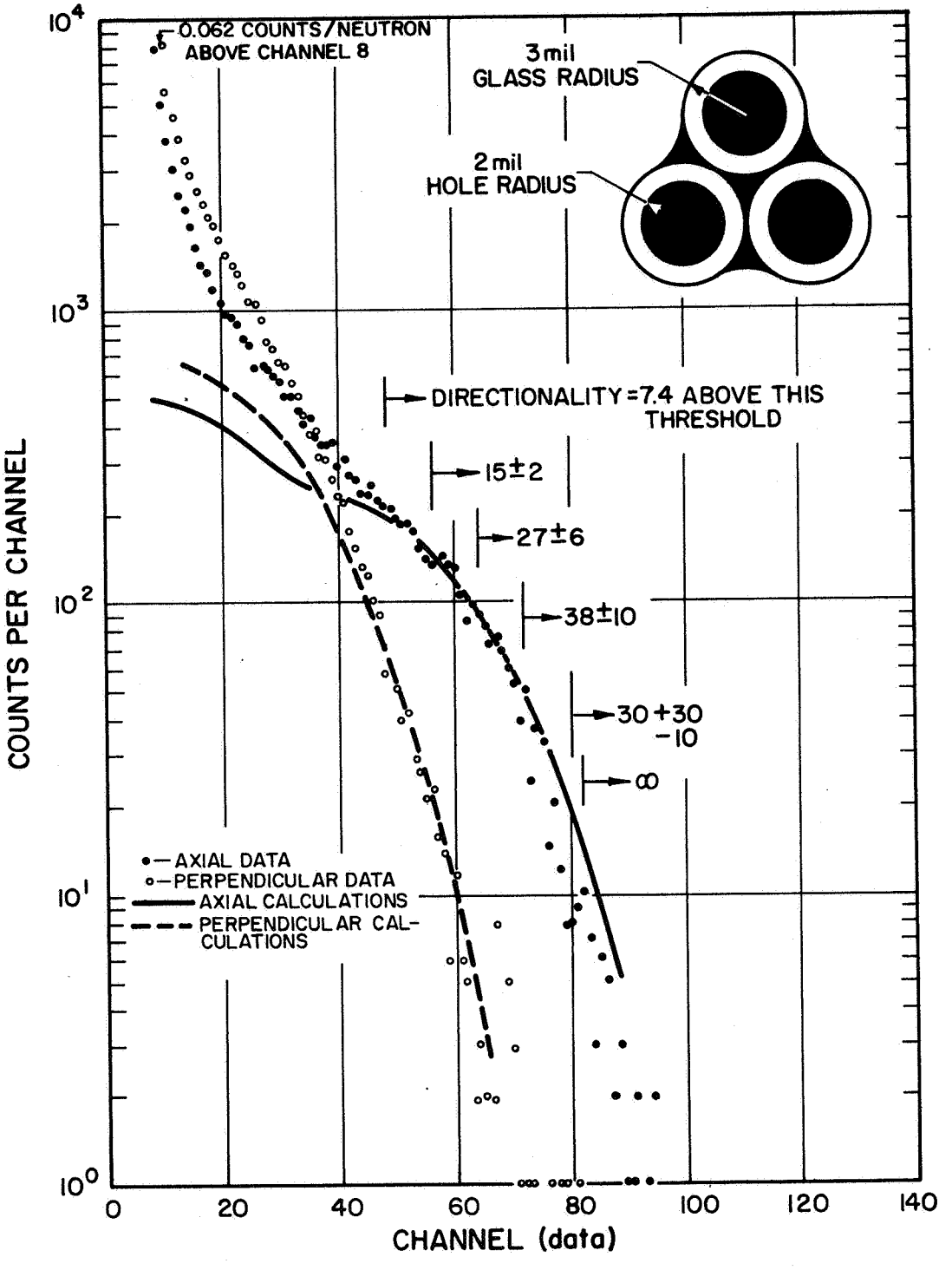

Figure 2-6 Directional Detector Response to 2.8 MeV Neutrons: Prototype. No PSD rejection of gammas was used here. Gammas are seen below about channel 40.

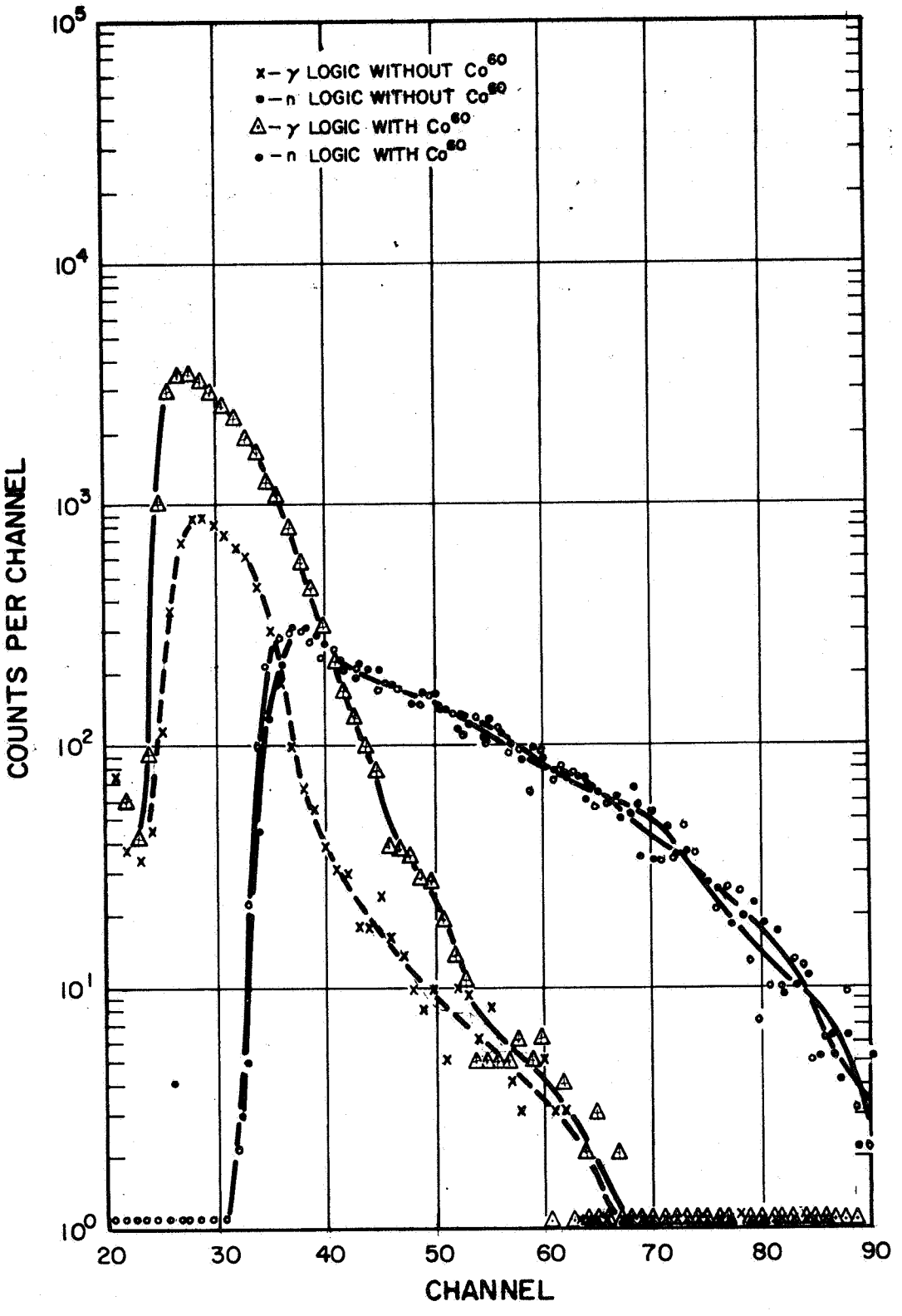

Figure 2-7 Gamma vs Neutron Response of Prototype.
Detector aligned parallel to D-D neutron source. Results with Co^{60} source present show gamma routed spectrum influenced strongly, but neutron routed spectrum unaffected.

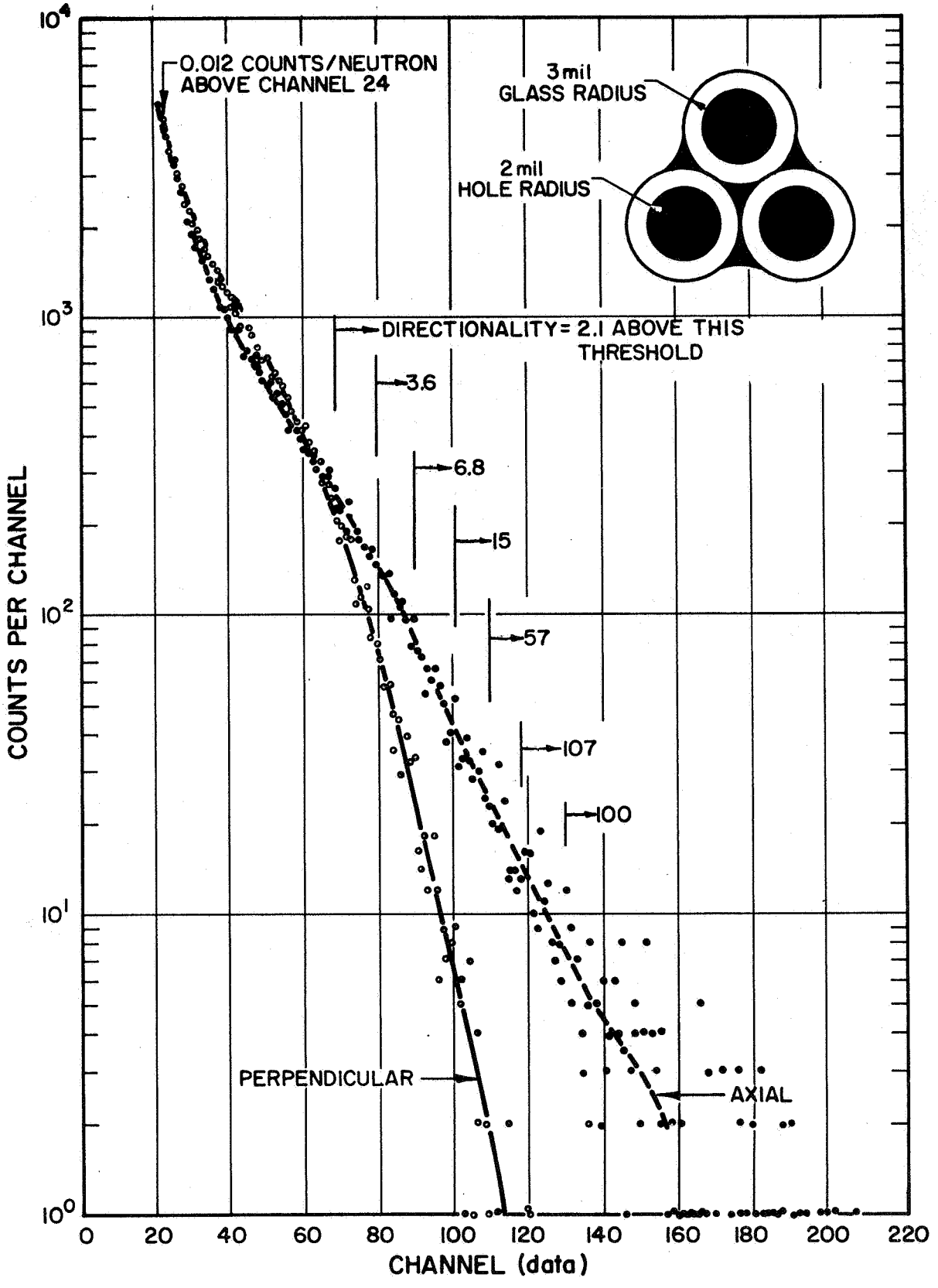

Figure 2-8 Directional Response to 2.8 MeV Neutrons: Prototype.

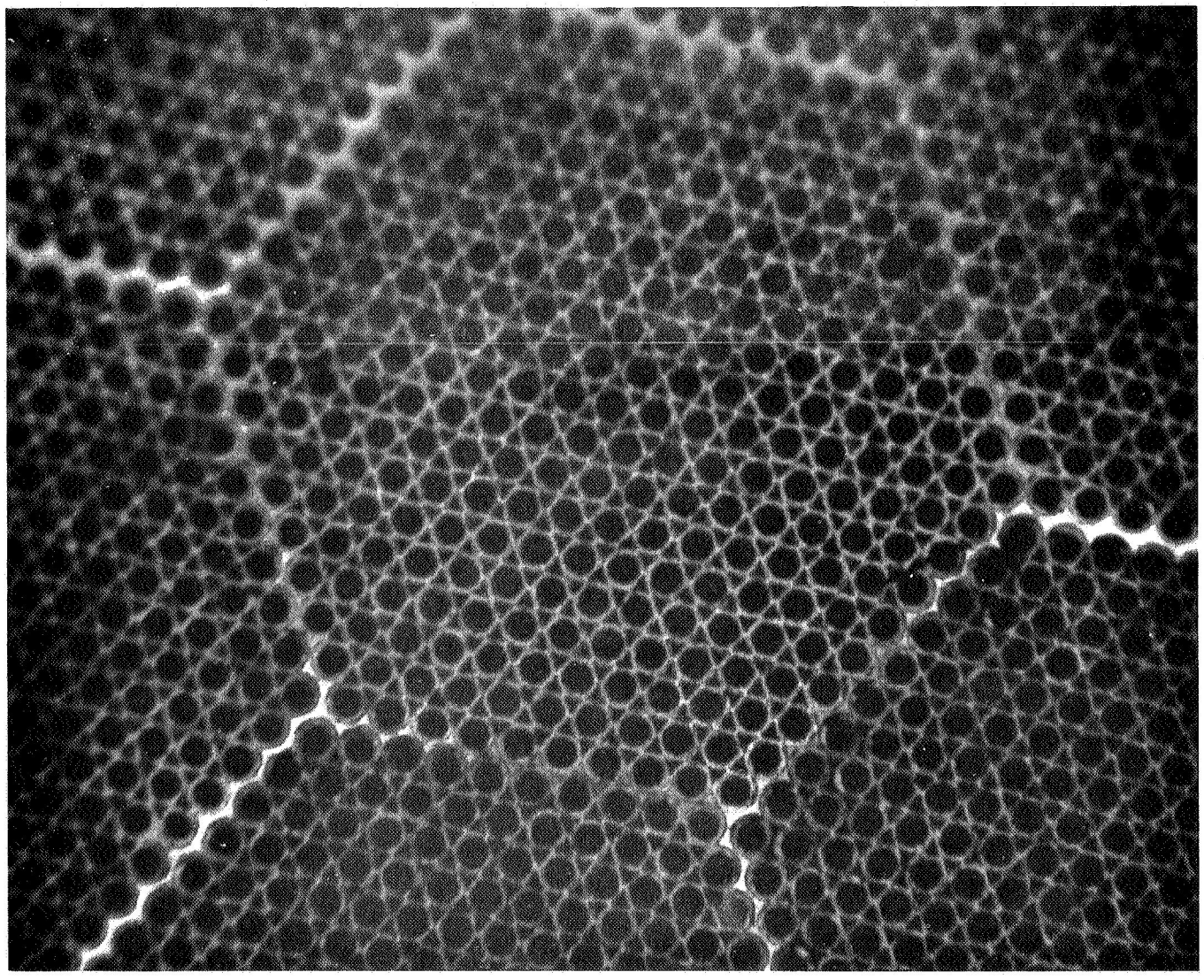

BV-003

Figure 2-9 0.006" Diameter

An epoxy enclosure (Allaco Crystal Clear) was cast around the glass block, with one end left open for filling. A cover, to be sealed to the enclosure by an O-ring and epoxy cement, completed the assembly. The cell was first filled with NE 213 fluid using the same procedure that had been employed for the prototype.

At this stage the scintillator did not have the optical qualities expected. The appearance of the glass block, when delivered from the manufacturer, was dull and cloudy, which was attributed to the high contrast in refractive index between glass and air. When the tubes were filled with fluid, which closely matched the glass in refractive index, there was not a noticeable improvement. The prototype detectors, on the other hand, had been so clear that the individual glass tubes were almost undiscernable. Studies continued on this scintillator, however, to determine as much from it as possible.

As a further step in the fabrication of the scintillator, the layer of CsI (Na) for charged particle rejection was bonded to the epoxy enclosure. This was done, with no detectable deterioration of the optical properties, by Harshaw Chemical Corporation, Cleveland, Ohio.

Prior to final evaluation and flight the scintillator was potted in a mu metal can. The inside of the can was painted with several coats of TiO_2. The potting material was General Electric RTV 602, a form of silicone rubber. This final encapsulation of the detector seemed to improve the optical properties, presumably because of the highly reflective inner surface of the mu metal can.

To learn more about the technique of fabricating a glass tube structure with good optical properties, a second unit was ordered from the same supplier, this one to be assembled without the use of cement between the hexagonal bundles of tubes. The optical properties of this structure did not seem to be better than the first one. An intensive effort at ultrasonic

cleaning of the inside of the glass tubes with a solvent provided some improvement, indicating that the difficulties in the initial unit may have been caused from clogging of the tubes by small chips of glass or abrasive.

2.6 Laboratory Tests of the Flight Scintillator

With the use of conventional commercially available electronics circuitry, tests of the efficiency, directionality, and PSD performance of the flight scintillator were made before and after the CsI (Na) anticoincidence shield was added.

A block diagram of the electronics is shown in Figure 2-10. The circuits shown in the diagram are of ORTEC manufacture. Signals at the points labeled PS, PH, and Routing were fed to a Nuclear Data 512-channel pulse height analyzer. The phototube was identical to the one used in the rocket flight, an RCA developmental tube, with a bialkali cathode, C70114F, which is essentially the same as a type 4461.

The method of achieving PSD is conventional. The anode signal generates a leading-edge timing pulse while the dynode signal, integrated at the preamp input and clipped in the amplifier, has a crossover time dependent on the decay time of the scintillator fluorescence. Thus, a time-to-amplitude converter, measuring the differential between the leading edge and crossover times, furnishes the desired pulse shape (PS) information. This PS signal can be fed directly to the signal input of the multichannel analyzer, or through a single channel analyzer to furnish a logic signal controlling the routing within the multichannel analyzer.

Figure 2-11 shows a typical spectrum of the PSD output, using a bulk liquid scintillator, when Co^{60} and Pu-Be sources are employed. The Pu-Be spectrum is shown with and without routing. Self-routing of the PS signal is useful in determining the proper settings of the single channel analyzer. Efficiency for detection of neutrons and Co^{60} gamma rays are 10 percent and 0.4 percent, respectively, which are typical values for a liquid scintillator of 0.785 $in.^3$ volume.

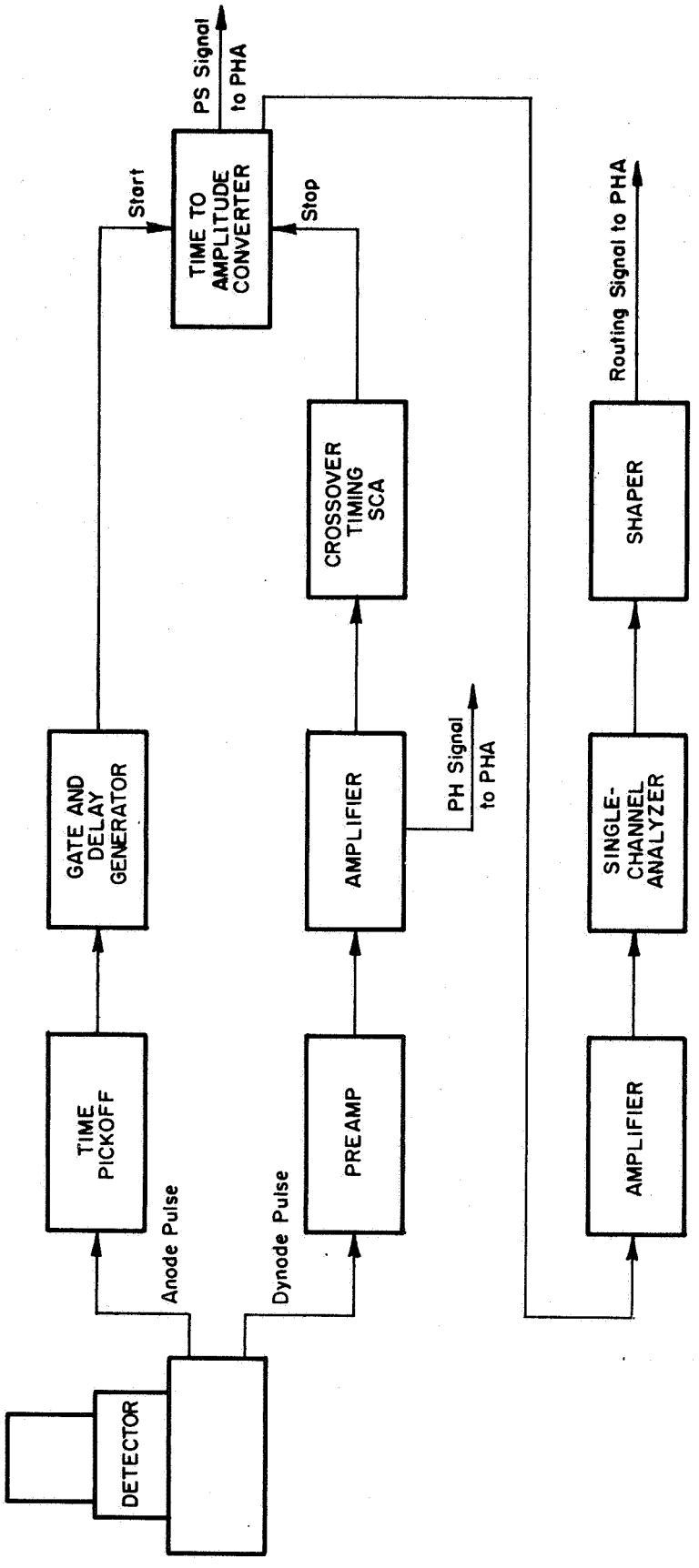

Figure 2-10 Block Diagram of Electronics: Laboratory Tests of Detector. These are referred to in the text as the commercial electronics.

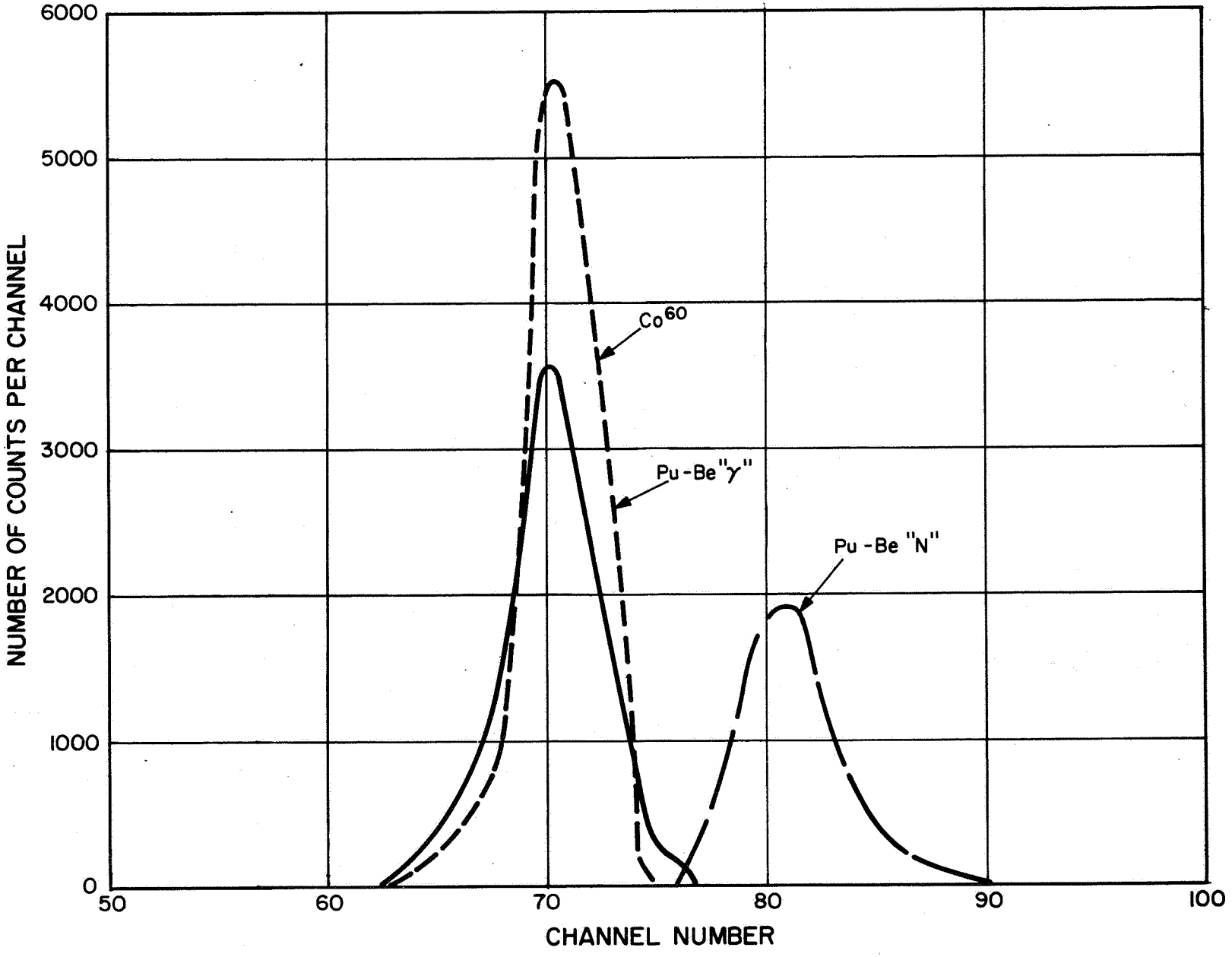

Figure 2-11 Pulse Shape Spectra: Bulk Scintillator, Commercial PSD Electronics. The solid curve shows events from Pu-Be labeled gamma rays by the circuitry. The events in the dashed peak were labeled neutrons, while those under the dotted peak were obtained in a different run using the Co^{60} source, and were labeled gammas. No events from Co^{60} were labeled neutrons.

When the bulk NE 213 sample is replaced by the flight scintillator, the light output is reduced by approximately one order of magnitude. This is attributed, in part, to the slight discoloration of the scintillator which was mentioned earlier, and possibly to the greater average distance of the scintillation fluid from the photocathode. Optimum behavior is achieved by partially compensating for this loss of light by increasing the photomultiplier high voltage supply about 100 volts and by increasing the amplifier gain.

No operating conditions could be found, however, for which the pulse height resolution or the PSD performance was as good as with the bulk NE 213 cell. Figure 2-12 shows the PS spectrum for D(d, n) He^3 neutrons from a 150 keV accelerator, as well as radiation from Co^{60} and Pu-Be source. It is clear that there is less discrimination between neutrons and gamma rays than that obtained with the bulk NE 213. These measurements were made before the CsI (Na) layer was attached.

Directional sensitivity for 2.8 MeV neutrons is demonstrated in Figures 2-13 and 2-14. The CsI layer had been added by this time. In both graphs spectra are shown in which radiation from the D (d, n) He^3 reaction is incident parallel and perpendicular to the glass tubes. Note that the efficiency is significantly different in the two cases.

In Figure 2-13 the PSD pulses are shown. The response to gamma rays, indicated by the peak around channel 16, is approximately the same for the two orientations, while the response to neutrons is quite directional.

The pulse height spectrum shown in Figure 2-14 has been gated by the condition that the PSD pulse be within the neutron peak. Directionality is again observed, but not exactly as would be expected on the basis of the theoretical predictions shown in Figure 2-3. The entire spectrum for perpendicular incidence is uniformly diminished in amplitude,

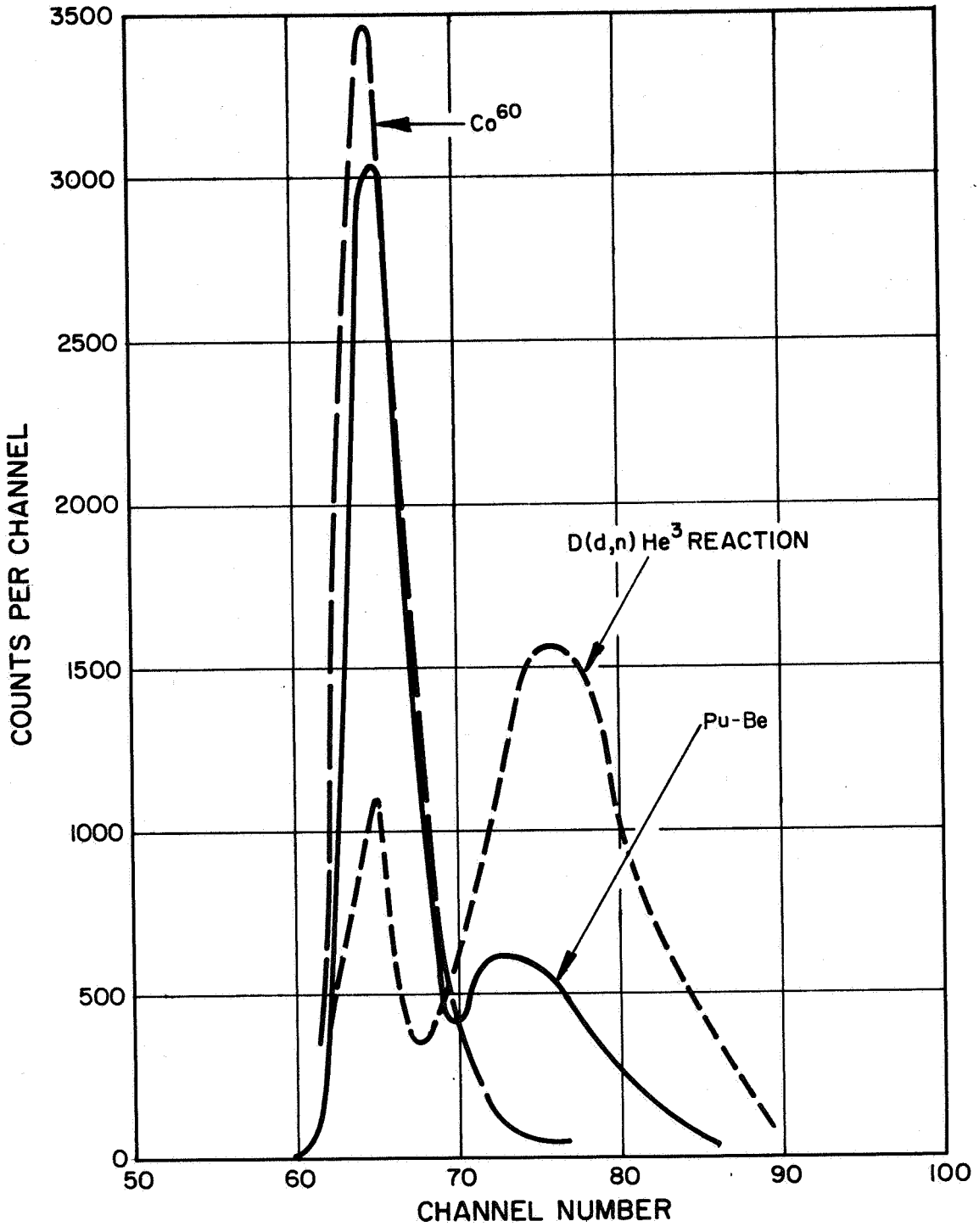

Figure 2-12 Pulse Shape Spectra: Flight Scintillator, Commercial PSD Electronics. The solid curve shows a large peak of gammas and a small, just resolved peak of neutrons from Pu-Be. The dashed curve from Co^{60} shows only a gamma peak. The dotted curve from the D(d,n) reaction at perpendicular incidence, shows a small gamma peak and a large neutron peak.

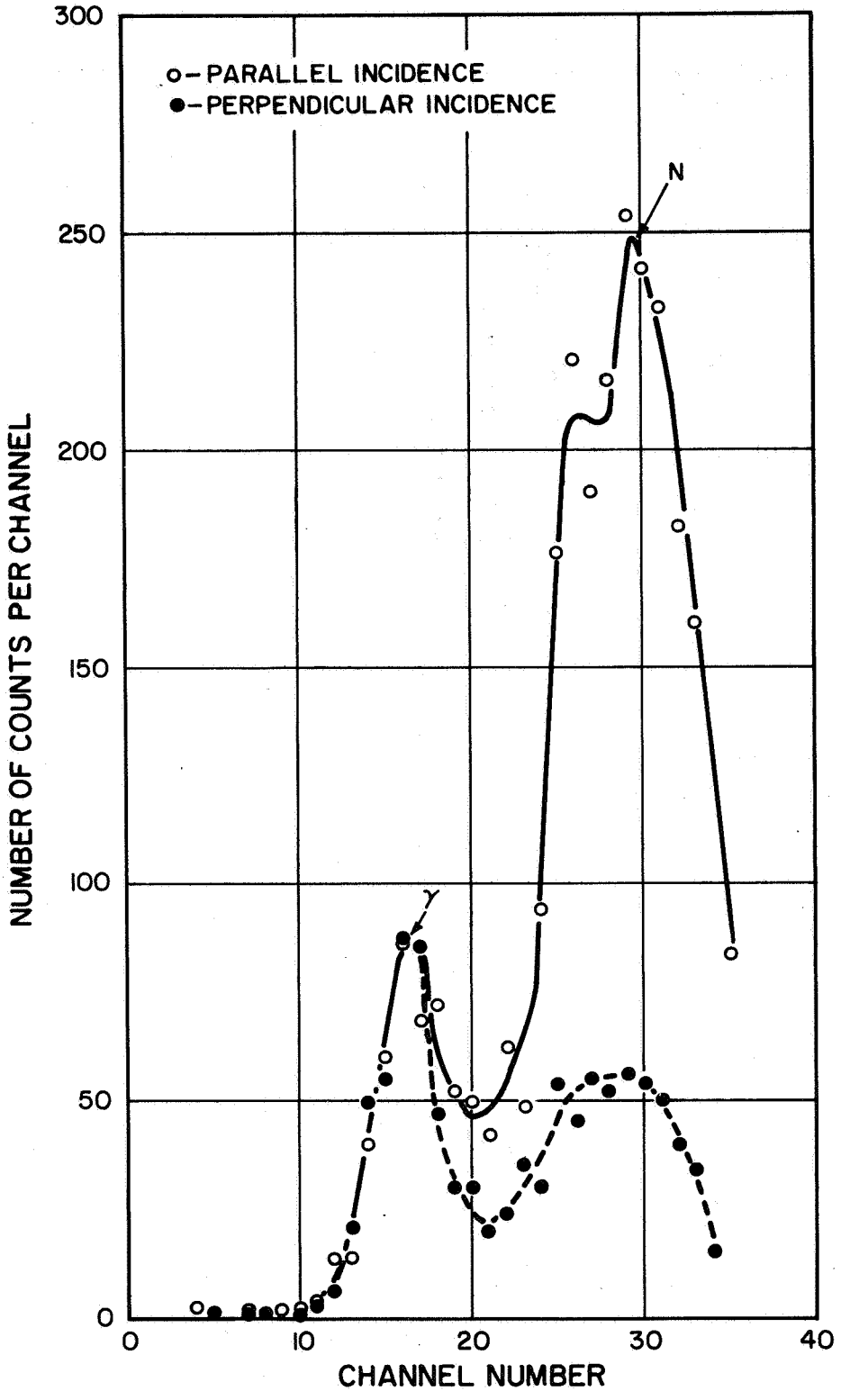

Figure 2-13 Directional Pulse Shape Spectra: Flight Scintillator, Commercial PSD Electronics. The data shown with open circles were taken with the detector axis aligned parallel with the 2.8 MeV neutron source direction; closed circles were perpendicular. The directionality for neutrons, measured by the ratio of the neutron peaks, was 5:1.

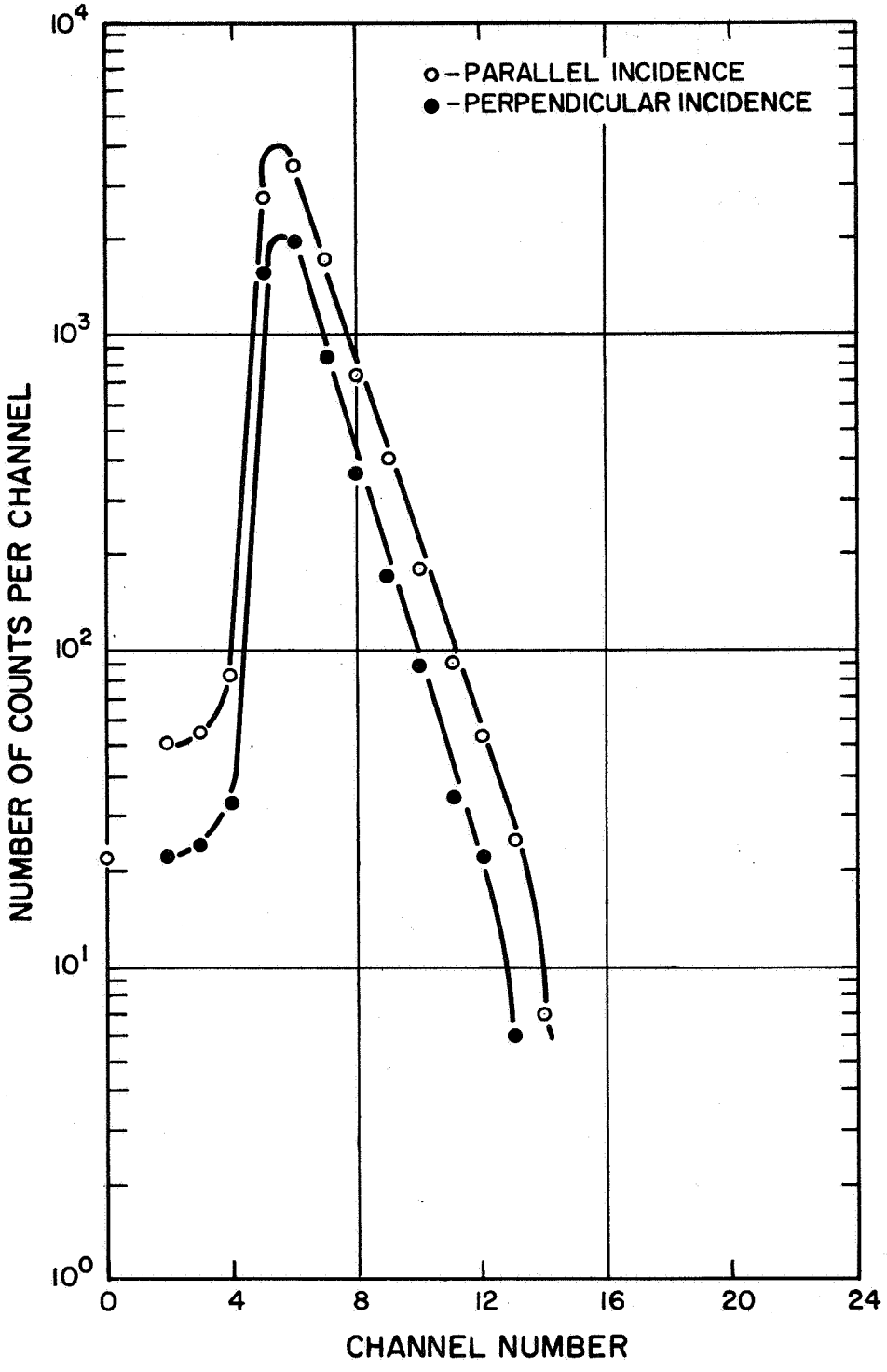

Figure 2-14 Directional Pulse Height Spectra: Flight Scintillator, Commercial PSD Electronics. Source was 2.8 MeV neutrons. Open circles were taken with the detector axis parallel to the neutron source direction; closed circles, perpendicular.

rather than just the largest pulses. This is an indication of the poor pulse height resolution. In analyzing the flight results, the comparison of total neutron counts, as a function of angle, should provide almost as much information about the direction of the incident neutrons as the pulse height spectrum of neutron counts as a function of angle.

The efficiency for neutron detection can be determined from the measurements above, since the strength of the Pu-Be source is known, and since a neutron monitor of known sensitivity was in operation to measure the neutron production from the accelerator. Of course, the efficiency and the quality of the PSD performance both depend on the lowest pulse size which is accepted. Thus, the efficiencies measured with the commercial electronics may be different from the efficiency with the flight electronics.

The efficiency both for D(d, n) He^3 and Pu-Be neutrons was usually between 0.5 and 1 percent. For the monoenergetic neutrons from the accelerator, the efficiency varied by more than a factor of 2 depending on the orientation of the detector axis with respect to the incident neutron direction.

3.0 ELECTRONICS

The flight electronics were designed to obtain particle energy and particle identification information as well as count rates for neutrons, gammas and charged particles. The pulse height and pulse shape information consisted of a variable amplitude fixed width pulse compatible with FM/FM telemetry bandwidth requirements. The count rate information consisted of a staircase waveform obtained from a counter and D/A converter which was self-resetting every sixteen counts. The detector consists of a pair of scintillators in a phoswich configuration coupled to a photomultiplier which is used as a light detector. The scintillator used for neutron and gamma detection is Nuclear Enterprises Type NE 213 which is a liquid organic material. The scintillator light output decay times are shown below.

Decay Constants [8]

	Decay Time		Relative Maximum Amplitudes	
	Electrons	Protons	Electrons	Protons
1st Component	5.2 nsec	5.6 nsec	100	100
2nd Component	107 nsec	138 nsec	2.7	3.5

Particle discrimination is obtained through the use of a pulse width discriminator which uses a zero crossing technique. One of the advantages of this technique is that the zero crossing information is independent of signal amplitude and may be temperature compensated by matching component temperature coefficients. The output signal from the photomultiplier

is integrated directly at the anode with a capacitor. The load resistor in combination with this capacitor determines the discharge time constant (τ_1). The resultant signal is amplified by a linear broad-band video amplifier (Figure 3-1) to obtain a high level signal proportional to the particle energy.

The photomultiplier and preamp were mounted in close physical proximity to minimize such factors as stray capacity, RF pickup, etc. The output signal cable and high voltage input cable were coaxial also to minimize RF pickup.

The processing electronics were located directly below the detector/preamp assembly in an enclosed box. The high voltage power supply was mounted on the back of the electronics box.

The input signal to the electronics box is differentiated (τ_2) and amplified to obtain a bi-polar waveform used to obtain the zero crossing signal. The choice of differentiation time constants of 500 nanoseconds (τ_1) and 200 nanoseconds (τ_2) were used.

A figure of merit approach utilizing the zero crossing time difference between the waveform generated by γ and N particles and the slope of the waveform at the zero crossing location, FM $\cong$ (time difference) $\cdot$ ($\Delta V/\Delta t$), was used to determine τ_1 and τ_2. The theoretical preamp output and zero crossing signals are shown in Figure 3-2.

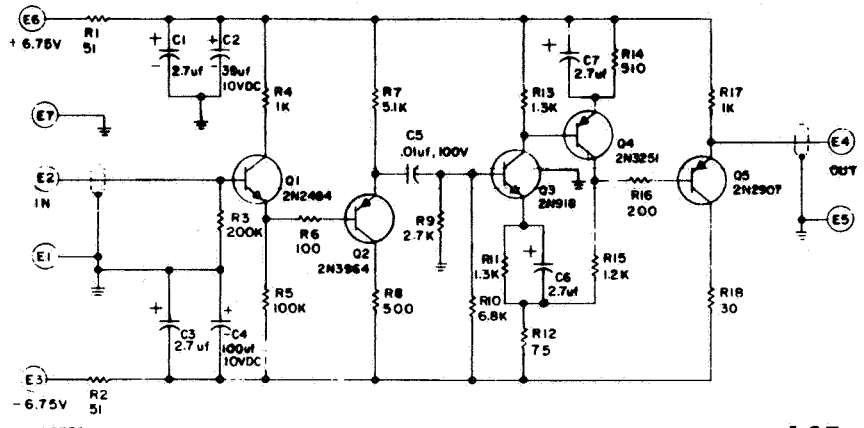

NOTES:
UNLESS OTHERWISE SPECIFIED
1 RESISTORS ARE EXPRESSED IN OHMS, ± 5%, 1/4 W
2 CAPACITOR VALUES ARE ±10%, 15V

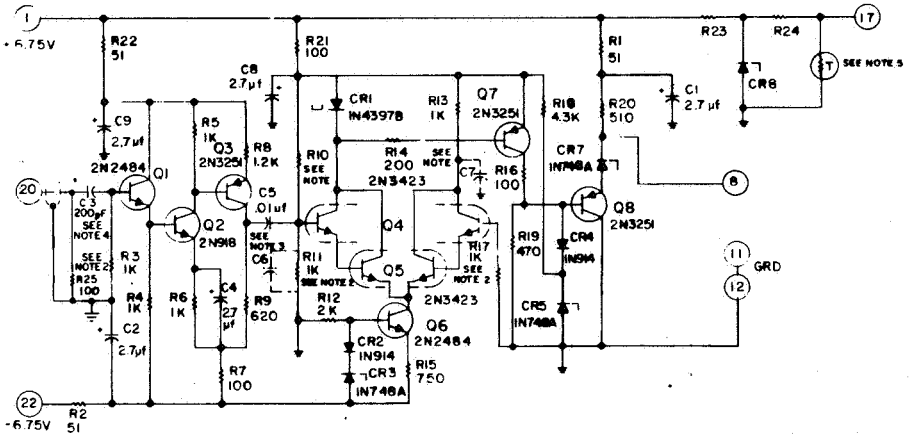

NOTES:
1. UNLESS OTHERWISE SPECIFIED:
RESISTOR VALUES ARE EXPRESSED IN OHMS, 5%, 1/4W
2. R3, R11, R17 ARE FIXED FILM, ± 2%, 1/4W
3. R10, C6, C7 ARE SELECTED AS REQUIRED
4. C3 IS A CORNING TYPE CYFM
5. SELECTED

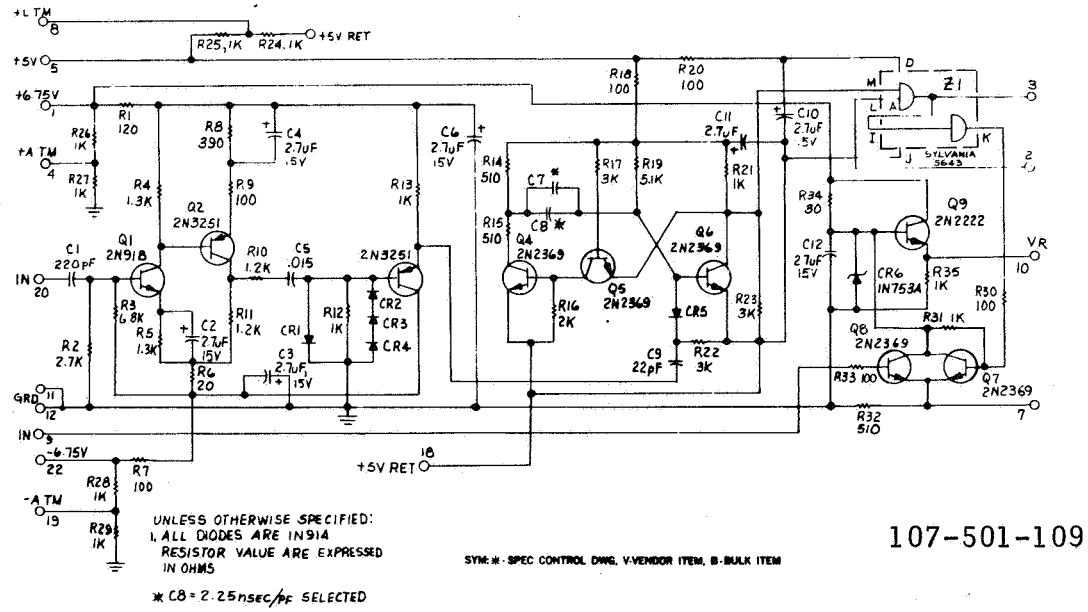

UNLESS OTHERWISE SPECIFIED:
1. ALL DIODES ARE IN914
RESISTOR VALUE ARE EXPRESSED IN OHMS

* C8 = 2.25 nsec/pF SELECTED

SYM: * - SPEC CONTROL DWG, V-VENDOR ITEM, B-BULK ITEM

Figure 3-1 Schematics of Preamp, Shape Detector, Pulse Shaper and Subtractor.

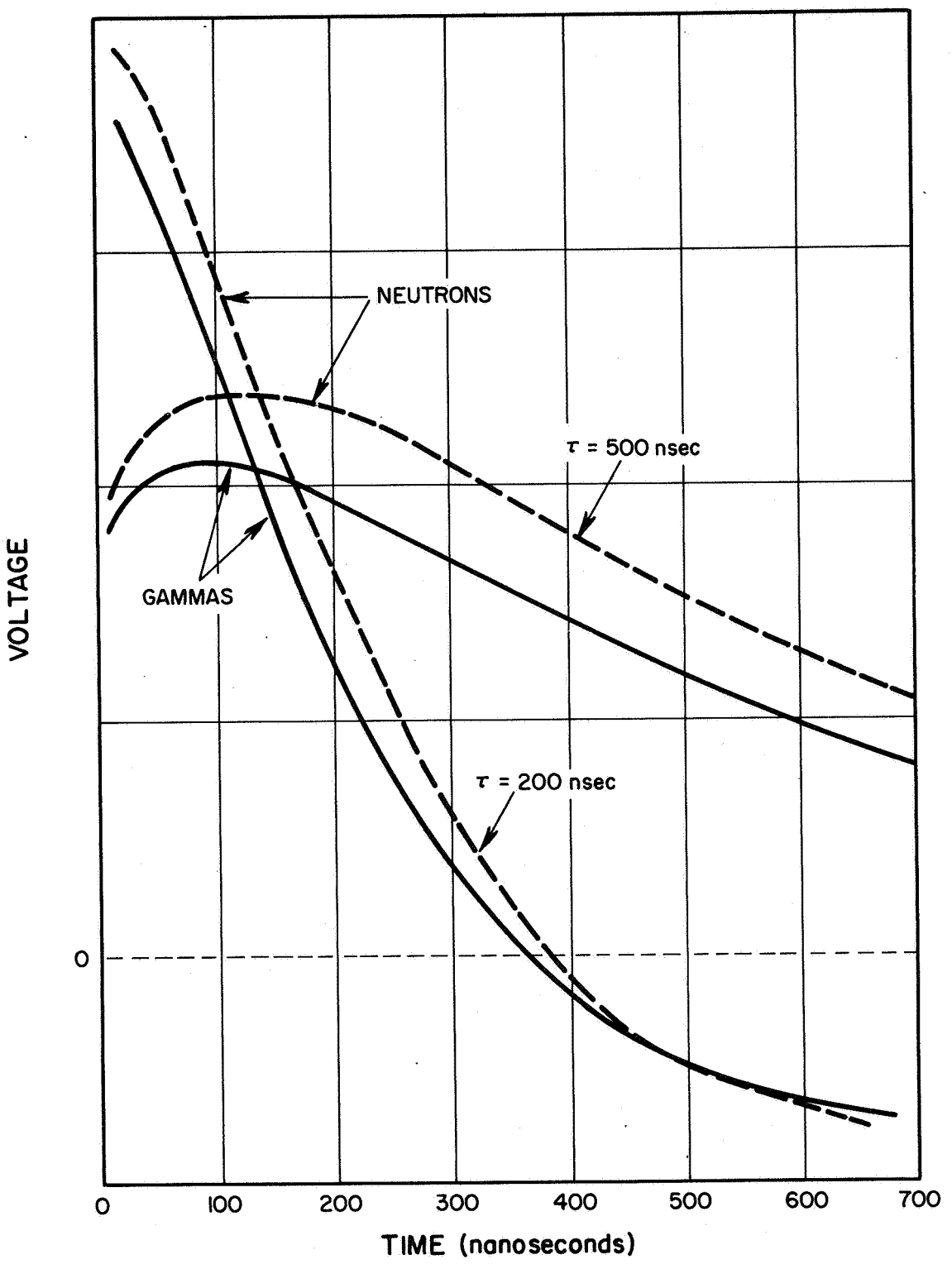

Figure 3-2 Zero-Crossing Waveforms. Showing the integrated waveforms and the differentiated waveforms for neutrons and gammas in NE 213.

Since detection of charged particles excites the slower CsI (Na) detector instead of the NE 213, the zero crossing time for these particles is quite long when compared with NE 213.

Because of the small time differences (30 nanoseconds) between gamma and neutron zero crossings and the relatively long time between the start of the pulse and the zero crossing (400 nanoseconds), a pulse subtraction technique was utilized to increase the percentage difference between the measured zero crossing times.

The pulse subtraction (See Figure 3-1) was accomplished by triggering a temperature compensated one-shot multivibrator from the amplified leading edge of the photomultiplier signal pulse and generating a negative 250 nanosecond pulse which is subtracted from the zero crossing pulse in an analog gate. The resulting pulse widths for the various particles are:

Gammas		100 nsec
Neutrons		140 nsec
Charged Particles	>	500 nsec

A linear time-to-voltage converter using a ramp generator, whose amplitude is proportional to the pulse widths outlined above, is utilized to obtain particle identity. The ramp generator holds its voltage until pulse shape (PS) information transfer to the telemetry circuits is completed (See Figure 3-3).

Simultaneously, with the particle discrimination described above, pulse height information is obtained from the amplified

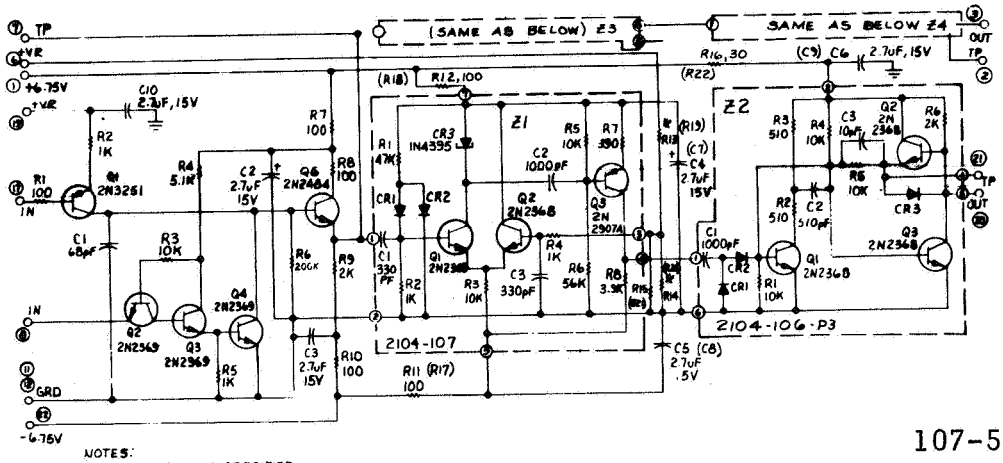

NOTES:
1. UNLESS OTHERWISE SPECIFIED.
ALL DIODES ARE IN914
RESISTOR VALUES ARE EXPRESSED IN OHMS

* R13, R14, R15, R19, R20 & R21 SELECTED FOR THRESHOLD

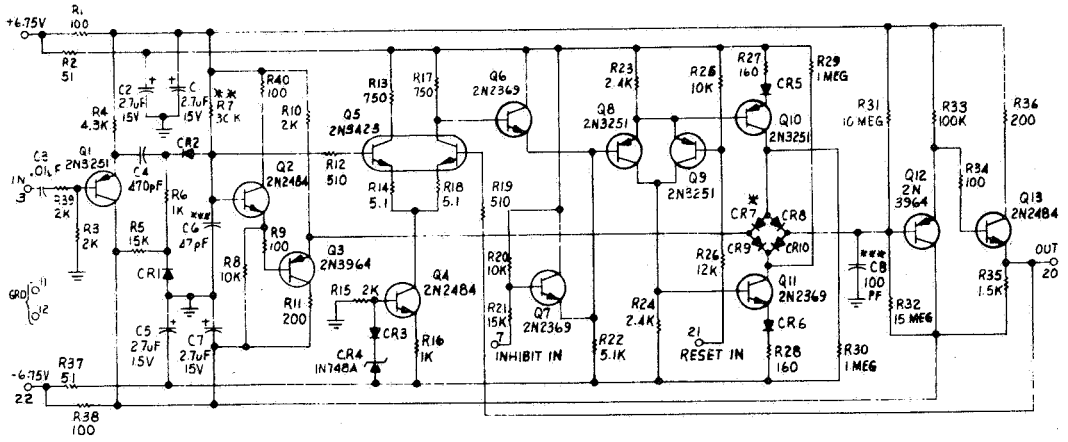

UNLESS OTHERWISE SPECIFIED
ALL DIODES ARE IN914
RESISTOR VALUES ARE EXPRESSED IN OHMS

* CR6 IN914 MATCHED
** CORNING RLO7 1/4W, 2%
*** CORNING CYFM

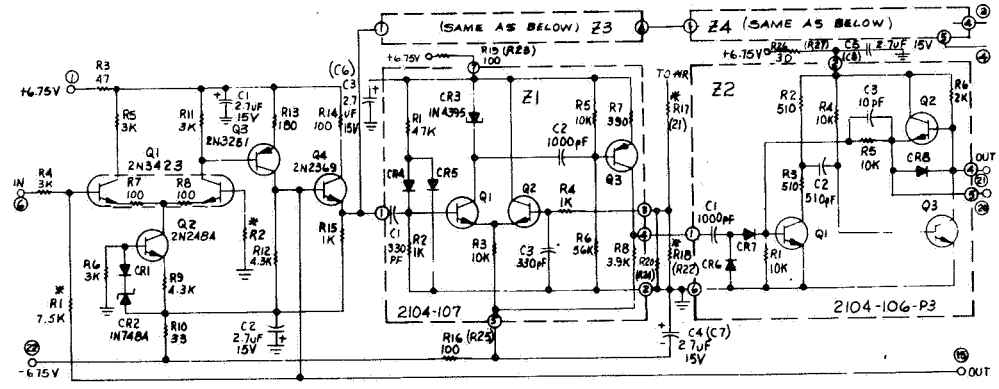

UNLESS OTHERWISE SPECIFIED:
RESISTOR VALUES ARE EXPRESSED IN OHMS
ALL DIODES ARE IN914
ALL TRANSITORS ARE 2N2368

* R1 = (Av)(3K)
* R2 = R1 - 113K
* R17, R18, R20, R21, R22 & R24 SELECTED FOR THRESHOLD

Figure 3-3 Schematics of Pulse Shape and Pulse Height Circuits.

photomultiplier signal. This is accomplished with a fast access (20 - 30 nsec) sample-and-hold circuit shown in Figure 3-4 which stores the pulse height information (PH) until information transferral to the telemetry is completed.

Decoding and pulse coincidence logic (Figure 3-4) are also used to quantize the particle identification information. The resulting particle identification pulses are counted and D/A converted (Figure 3-5) to obtain count rate information for each of the three particle types.

Simultaneously, the sample-and-hold circuits are controlled by these pulses to route the particle energy (signal amplitude or pulse height) and particle identification (pulse shape provided by the ramp generator output voltage) to the proper telemetry channel.

Dynamic ranges of 20:1 for each of the particle types are obtained with the techniques described above. The resultant dynamic ranges for neutrons is typically 1 - 10 MeV and 200 keV - 4 MeV for electrons. The relationship between electron energy and proton energy for the scintillator used has been previously described.

A block diagram of the electronics is shown in Figure 3-6. The time interval for the signal processing to obtain pulse shape, as described above, is approximately 3.0 μsec resulting in a very small dead time loss. The circuits used to interface with telemetry, however, increase the dead-time to $\approx 800\,\mu$sec to maintain consistency with FM/FM telemetry bandwidths.

After acquisition and processing of a single pulse the electronics are completely inhibited for a duration of 800 μsec. This is the width of sample

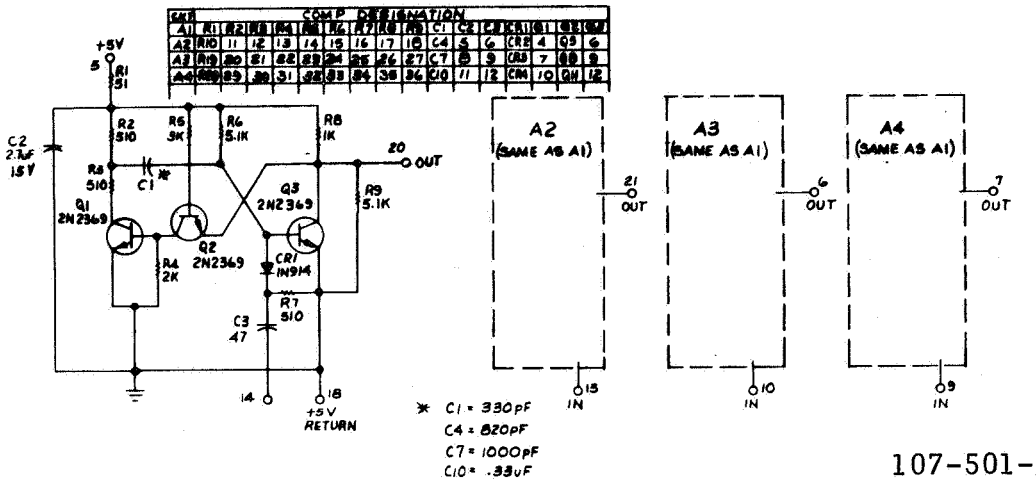

107-501-105

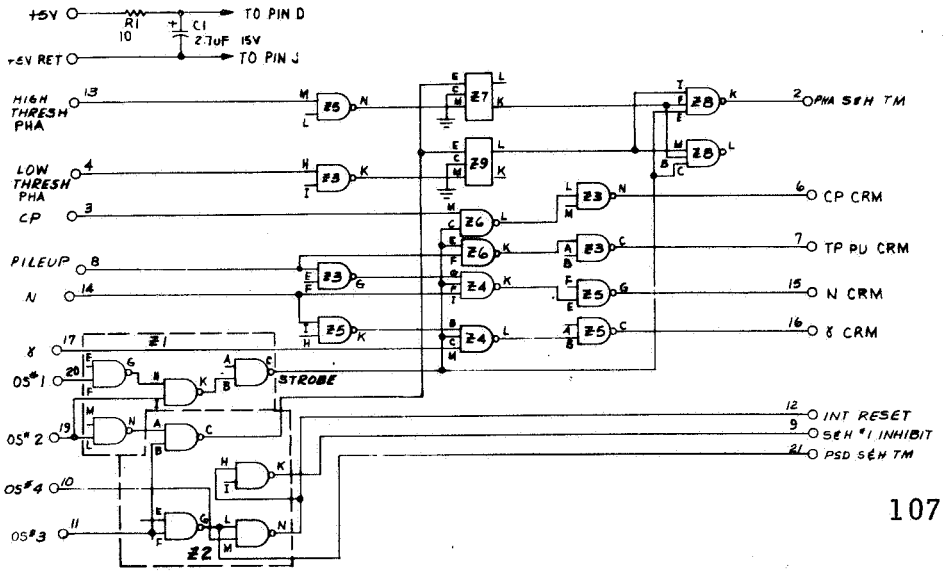

107-501-104

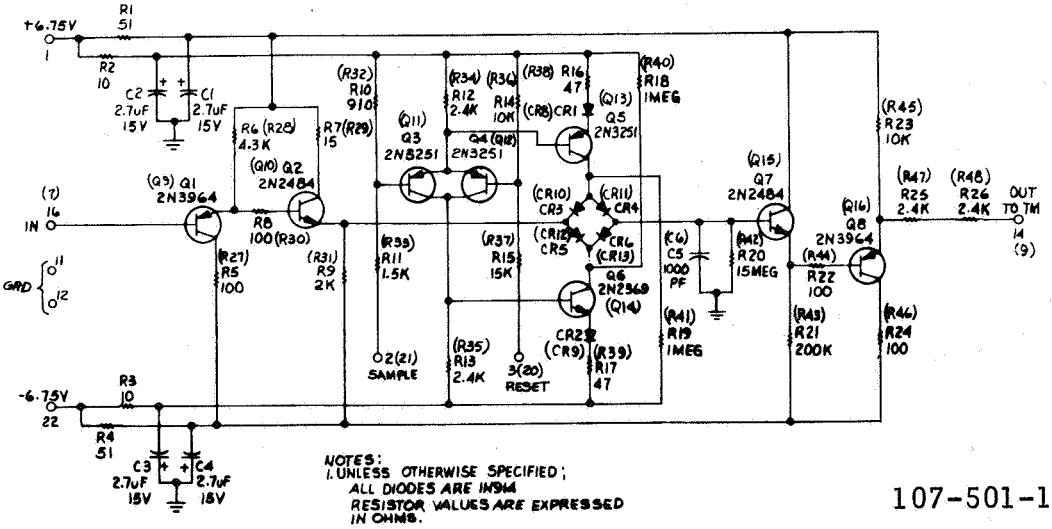

107-501-108

Figure 3-4 Schematics of Logic and Sample-Hold.

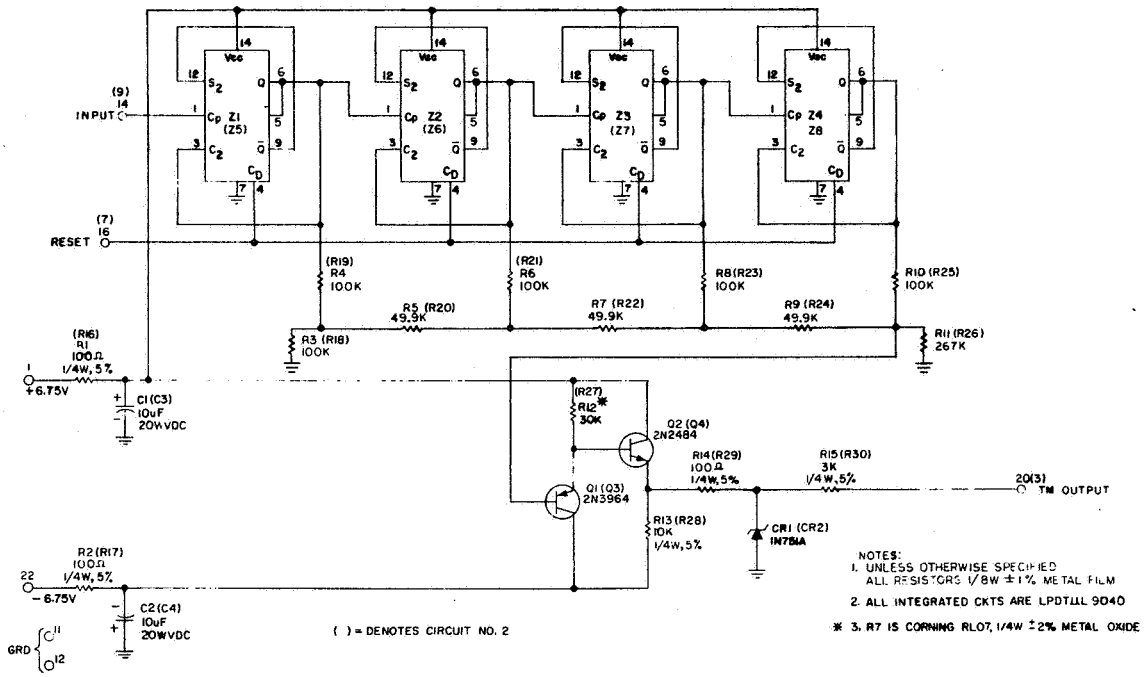

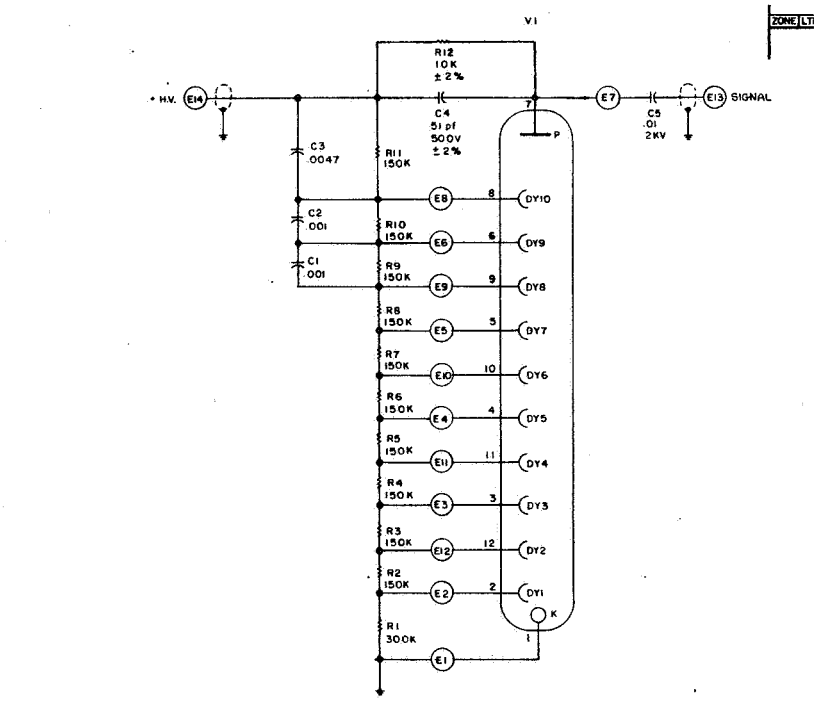

NOTES:
1 UNLESS OTHERWISE SPECIFIED
RESISTOR VALUES ARE EXPRESSED IN OHMS,
CAPACITOR VALUES ARE EXPRESSED IN MICROFARADS.
2 V1=RCA-4461-(SELECTED)

Figure 3-5 Schematics of Counter, D/A Converter and Photomultiplier Biasing.

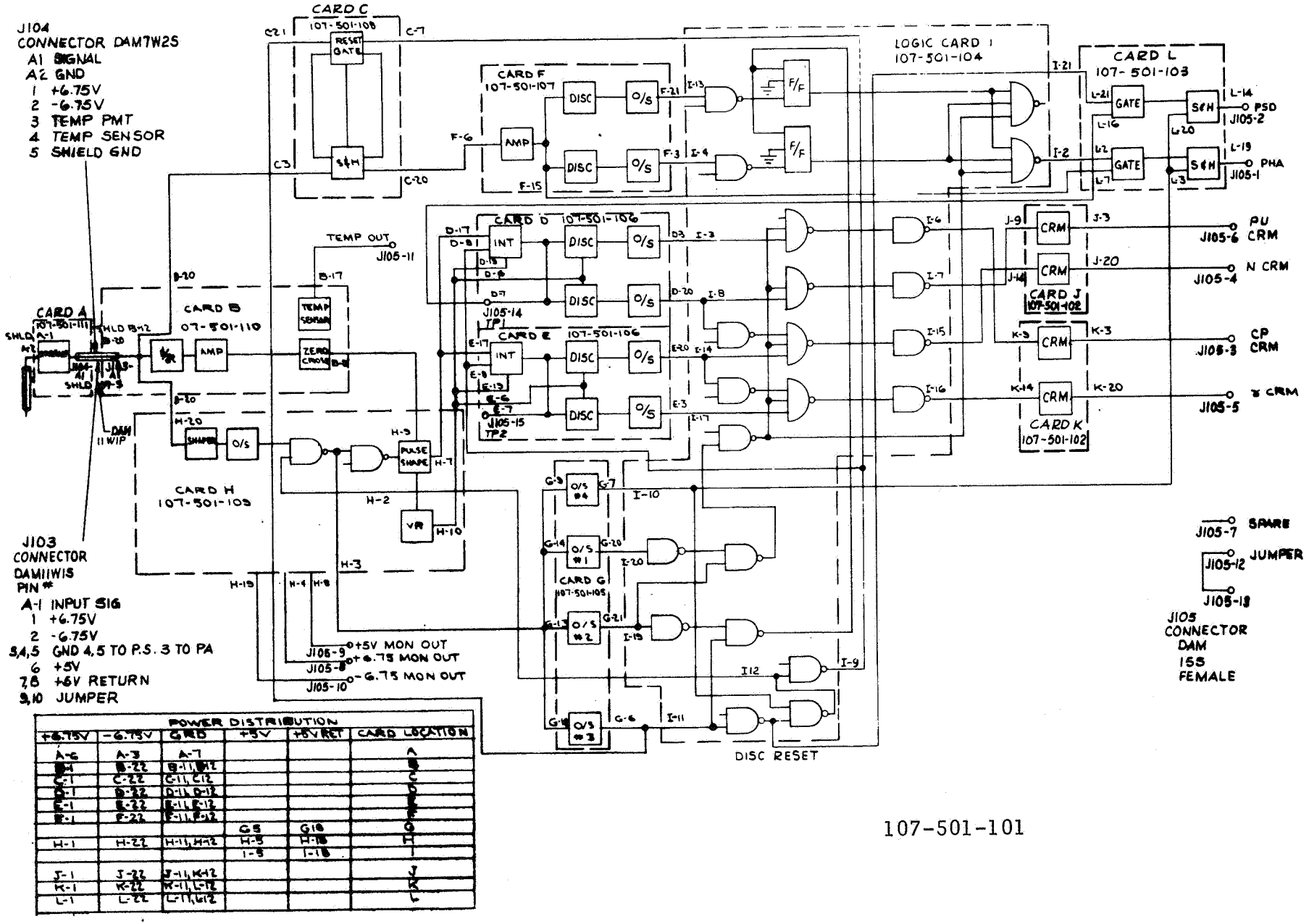

Figure 3-6 System Block Diagram.

and hold telemetry outputs (pulse height and pulse shape). After this time period the inhibits are removed and the next input pulse generates another 800 μsec inhibit period after the 3μsec acquisition period has been completed. The power for the electronics is 3.25 watts and is 5.0 watts for the complete rocket flight instrument package.

Particle Discrimination

The output of the time-to-voltage converter is a pulse for each particle detected. The height of the pulse tells what type of particle was observed. The electronic system's performance was measured by using it to process the light outputs from a bulk NE 213 scintillator which was exposed to gamma ray and neutron sources. The pulse height distribution of the time-to-height converter (called the Pulse Shape Spectrum) was stored in a pulse height analyzer. Figure 3-7 shows the response of the breadboard circuit to Co^{60} gammas and to the output of a neutron generator using the D-D reaction. This output consists mostly of neutrons but with a small number of gammas. The figure shows that gammas give pulses at about channel 58, and neutrons, channel 72. Figure 3-8 shows the response of the flight electronics (with bulk scintillator) to Co^{60} gammas, and to a mixture of gammas and neutrons from a Pu-Be source. The peaks from gammas (channel 28) and neutrons (channel 32) are well separated. This indicates that the electronic system works well with the bulk scintillator.

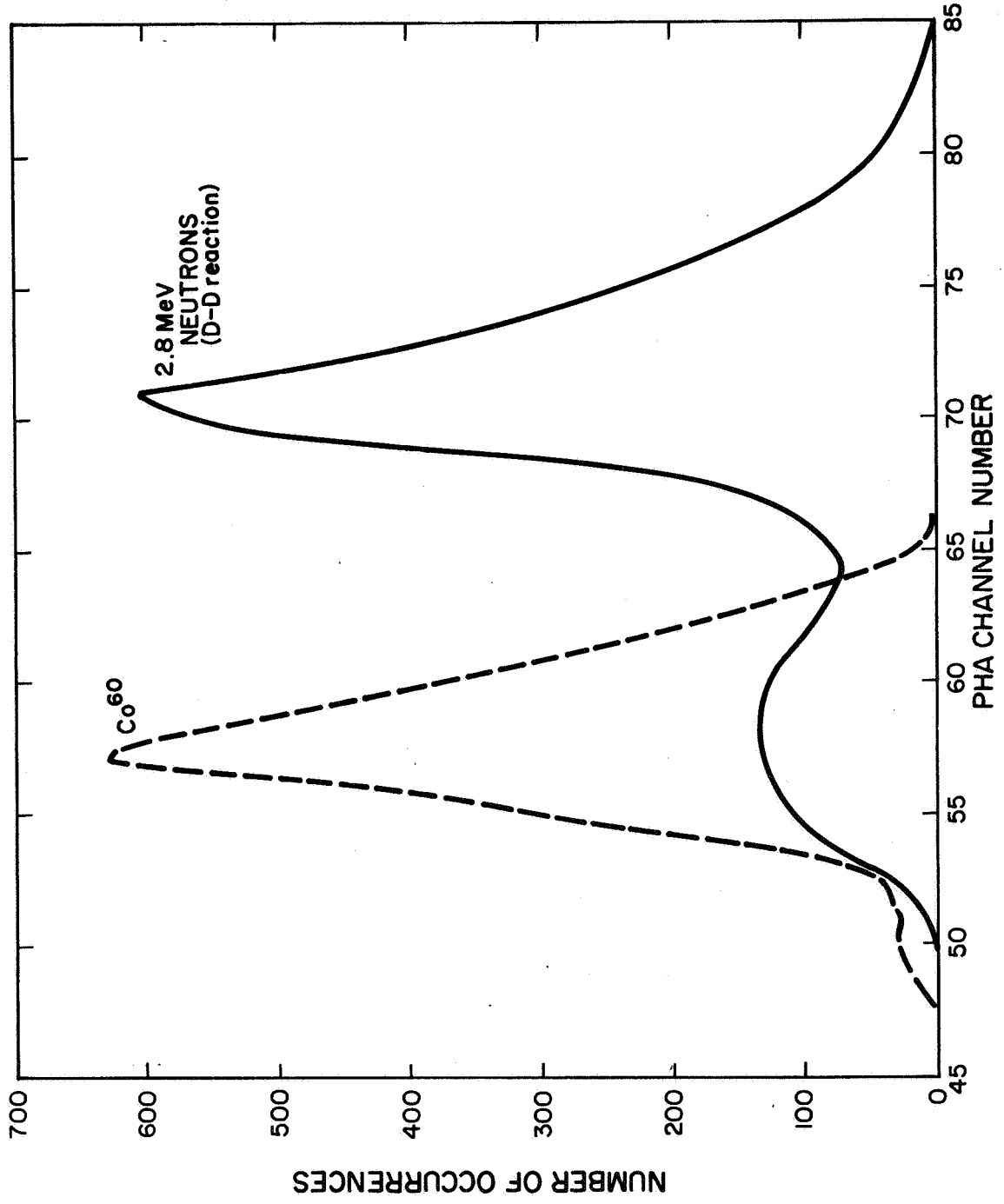

Figure 3-7 Pulse Shape Spectra: Bulk Scintillator, Breadboard Electronics. The dashed curve is from Co^{60} gammas; the solid from D (d, n) reaction.

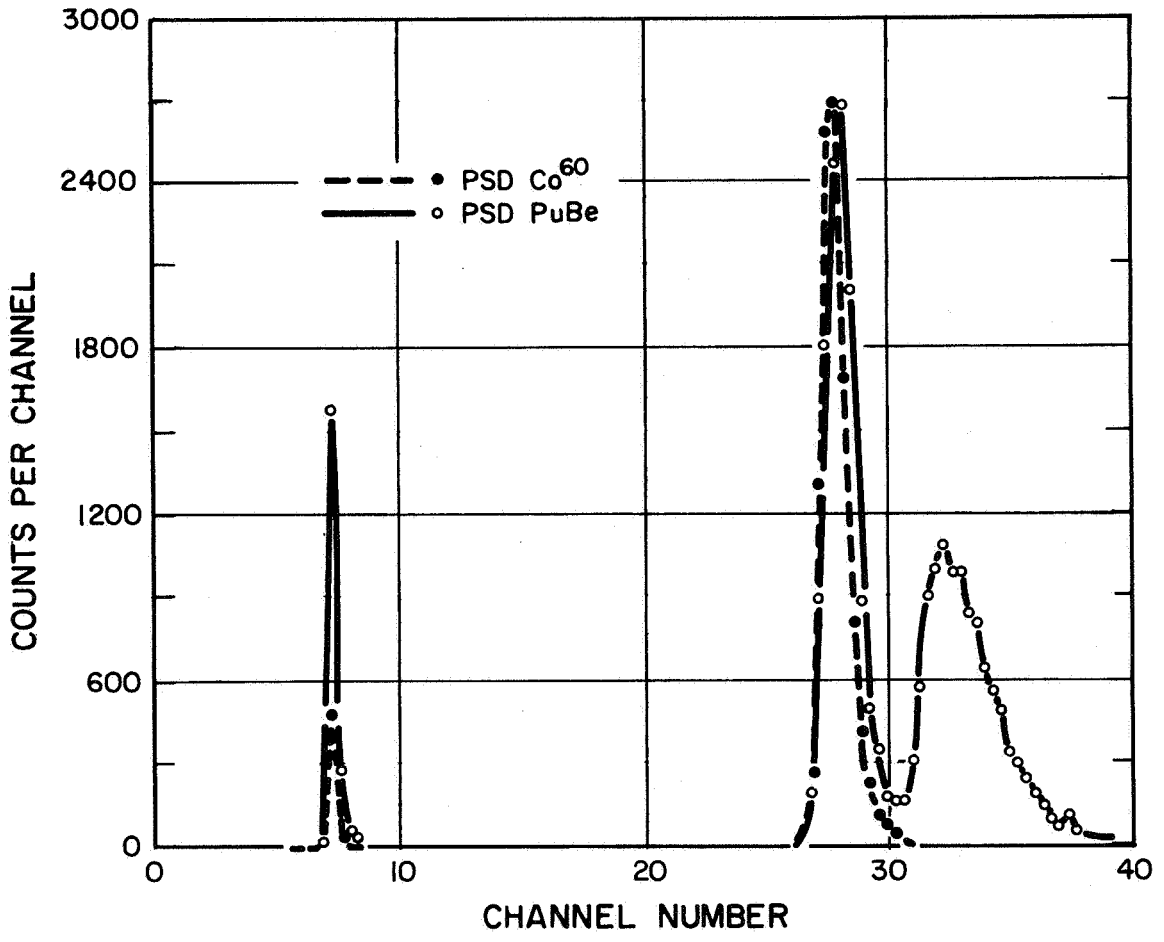

Figure 3-8 Pulse Shape Spectra: Bulk Scintillator, Flight Electronics. The open-circle data were taken with a Pu-Be source, and show a gamma peak and a neutron peak. The closed-circle data were taken with a Co^{60} source, and show only a gamma peak.

1708

4.0 COMPLETION OF THE FLIGHT SYSTEM

4.1 Sun Sensor

To utilize the directional properties of the detector, it is necessary to know the orientation of the glass tubes with respect to the sun at every instant. For this purpose, a holder for a photoconductive cell (Type CL703L, manufactured by Clairex Corporation) was designed, built, and attached to the outside of the photomultiplier housing. Two slits, 0.062 by 0.625 inch, allow sunlight to produce an output pulse from the cell once each revolution as the rocket spins.

The holder and slit system is shown at the bottom of Figure 4-1, while the curve in the insert at the top shows measurements of the cell's output as a function of the angular motion of a light source. The angular resolution (FWHM) is about 9.5 degrees. As the rocket rotates in flight, the detector axis is aligned with the sun at an angle $\alpha = 17.67$ degrees before the sun sensor output signal and will be aligned again, of course, at an angle $\pi - \alpha$ after the signal.

4.2 Nose Cone Ejection System

Proper operation of the sun sensor, and to a lesser extent, of the directional detector itself, requires that the nose cone be ejected when the rocket reaches sufficient altitude. The ejectable nose cone used in this flight was designed, built, and tested by AS&E as a part of the contract. Photographs of two views of the nose cone ejection assembly are shown in Figures 4-2 and 4-3.

Guillotine-type cable cutters operate by the firing of squibs at a preset time after launch. This, in turn, releases three finger clamps so that compressed springs separate the nose cone from the rocket.

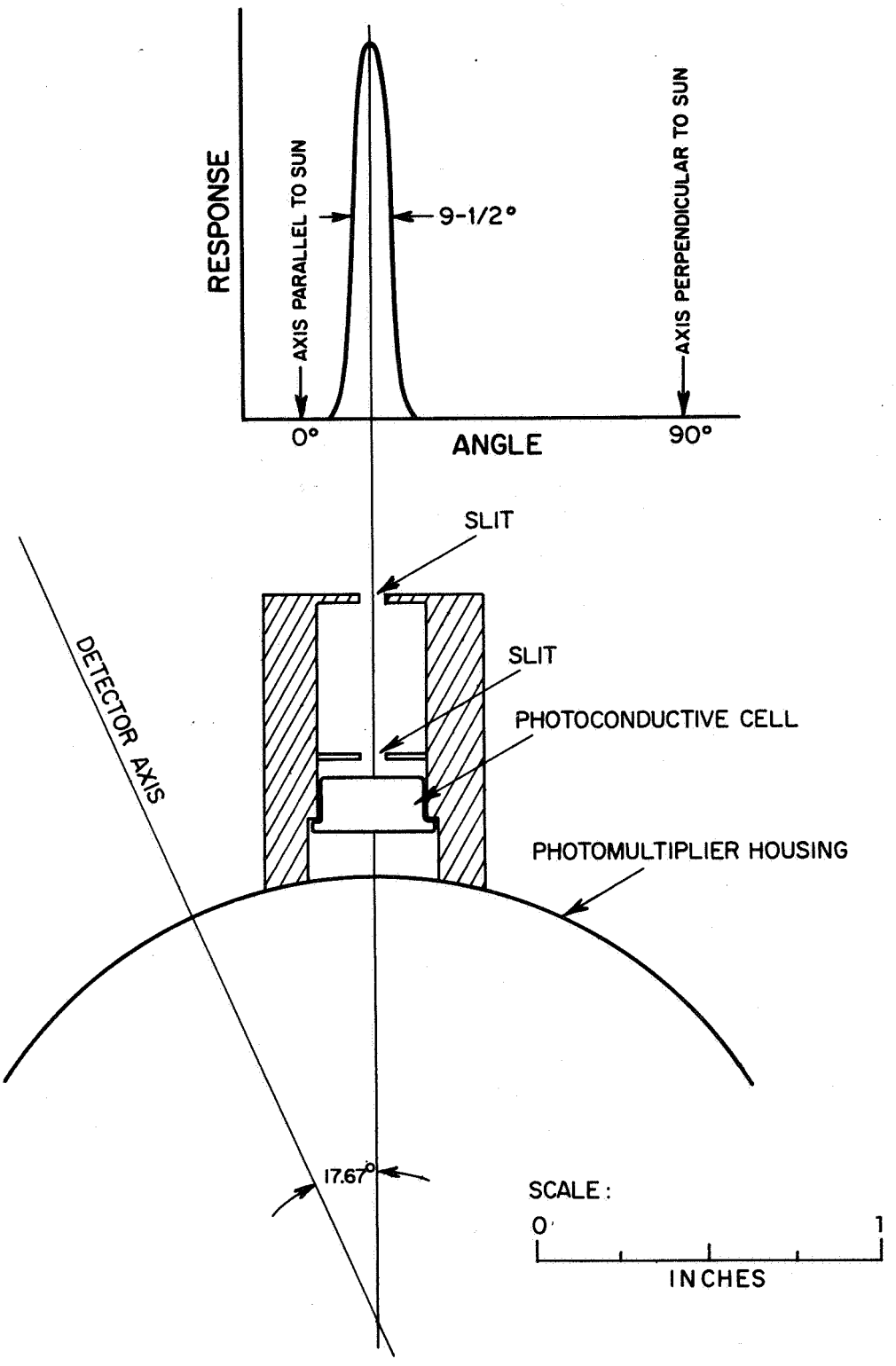

Figure 4-1 Solar Aspect Detector

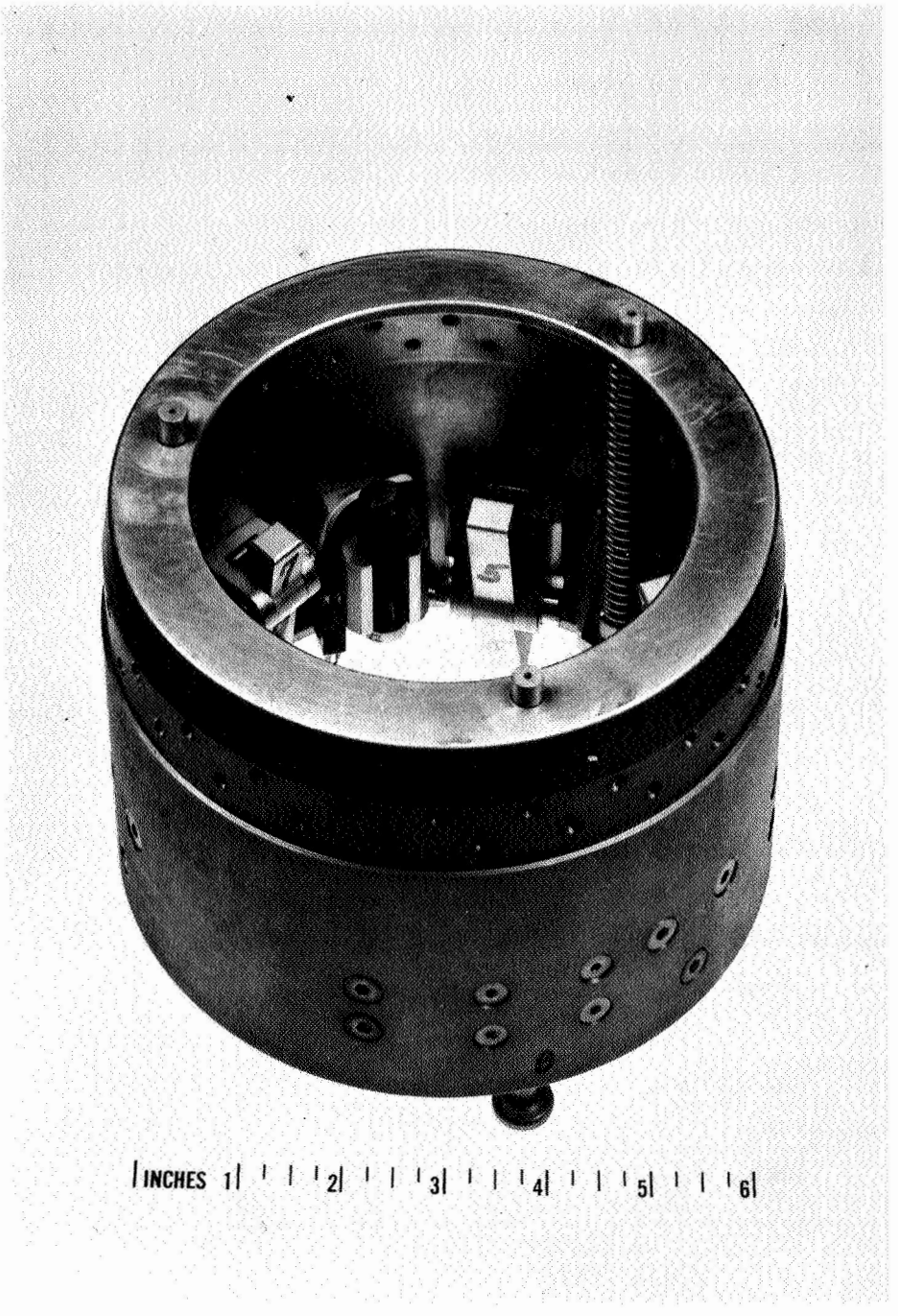

BV-024

Figure 4-2 Nosecone Ejection System, top view.
The rods marked A, B, and C provide the ejection impulse.

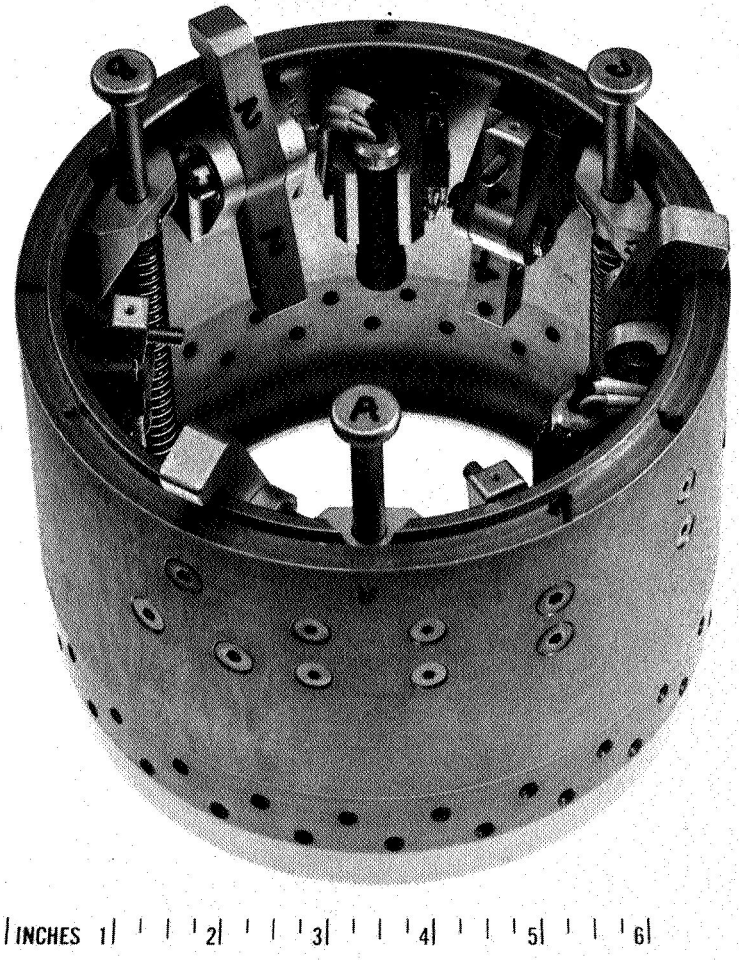

BV-025

Figure 4-3 Nosecone Ejection System, bottom view.

4.3 Power Supplies

Voltage levels of + 5.0, + 6.75, and - 6.75 were required by the electronics. These could be provided either by battery operated internal supplies or a ground support unit attached through the umbilical.

The photomultiplier was powered by a 3 ma, 1500 volt supply manufactured by Mil Associates. The supply was stabilized so that the output remained constant over an input range from 13 to 22 volts. The input was set at 18 volts for the flight.

The umbilical connection, when attached, could be used to recharge the internal batteries and to monitor the internal voltage levels as well as to supply power. During flight, a commutator system continuously sampled these levels and transmitted the information to the ground station by telemetry.

4.4 Telemetry

A standard Nike-Apache telemetry unit was used as provided by Goddard Space Flight Center. Table IV-1 lists the channels for the various signals. Every 36 seconds, transmission was interrupted to allow the generation of a calibration waveform, as each input was stepped from 0.00 to 5.00 volts in integrals of 1.00 volt.

Permanent records of the telemetry signal were produced on magnetic tape and on 12-inch rolls of paper. As discussed in Section 3.0, and as demonstrated in the following sections, simultaneous Pulse Height (PH) and Pulse Shape (PS) information for each event was recorded, allowing two-parameter analysis of the flight data.

TABLE IV-1

Utilization of Telemetering Channels

IRIG Band	Channel	Frequency (kHz)	Filter Frequency (Hz)
18	PS	70.00	1650
17	PH	52.50	790
16	Proton Scaler	40.00	600
15	Neutron Scaler	30.00	450
14	Gamma Scaler	22.00	330
13	Solar Aspect	14.50	220
12	Neutron-Proton Interference	10.50	160
11	Commutator	7.35	110
10	Not Used	5.40	80

4.5 Assembly

The photographs of the completed flight system (Figures 4-4 and 4-5) show the essential parts of the experimental apparatus. The nose cone and outer skin of the rocket do not appear. The directional scintillator is at the top of each picture, just above the housing for the photomultiplier tube. Figure 4-4 provides a view of the sun sensor. Figure 4-5 is taken from the side of the rocket where the high voltage power supply is mounted on the electronics box. Both of these are just below the photomultiplier tube.

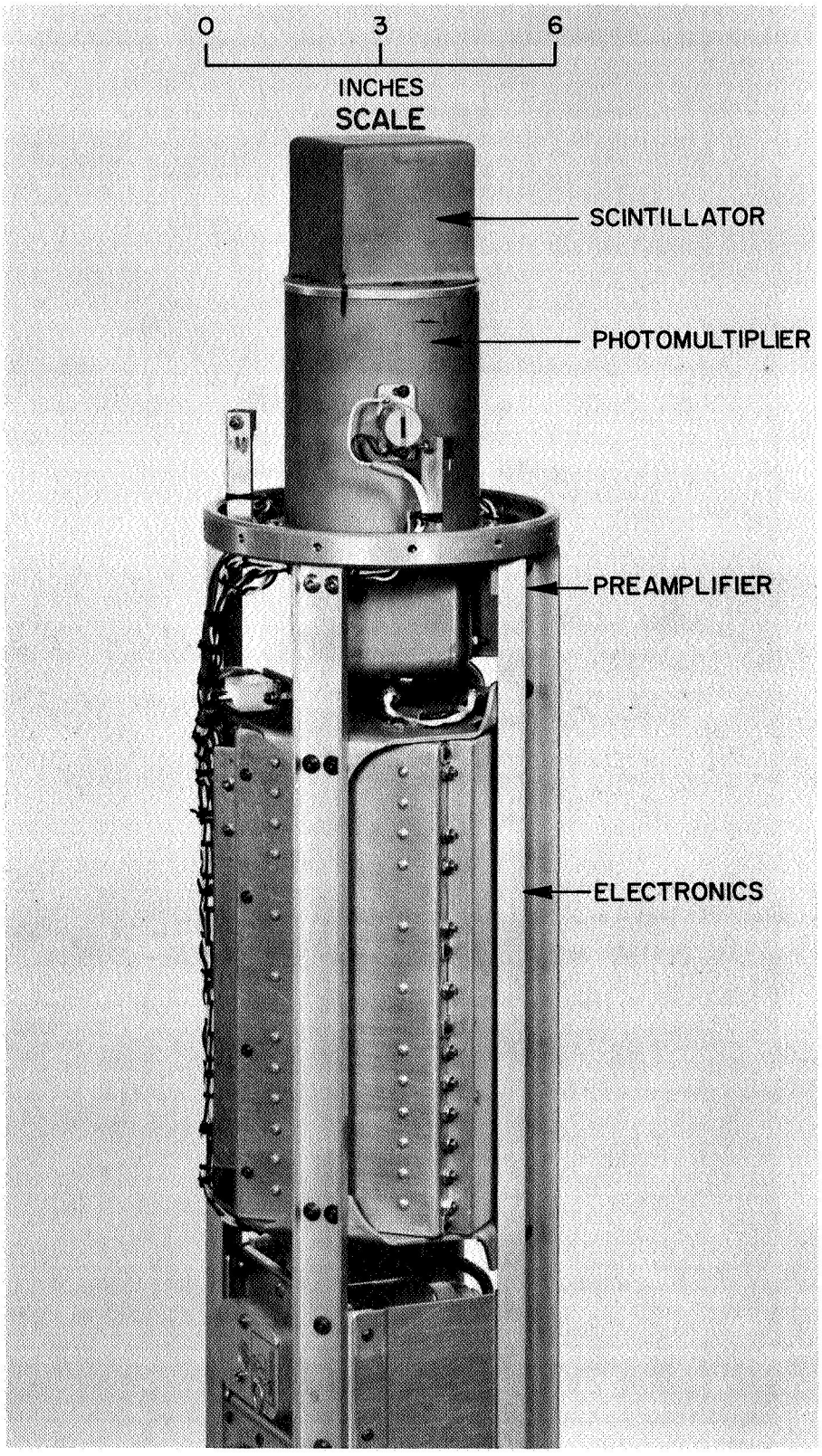

BV-026

Figure 4-4 Payload, Front view. The sun sensor is seen mounted in place on the side of the photomultiplier can.

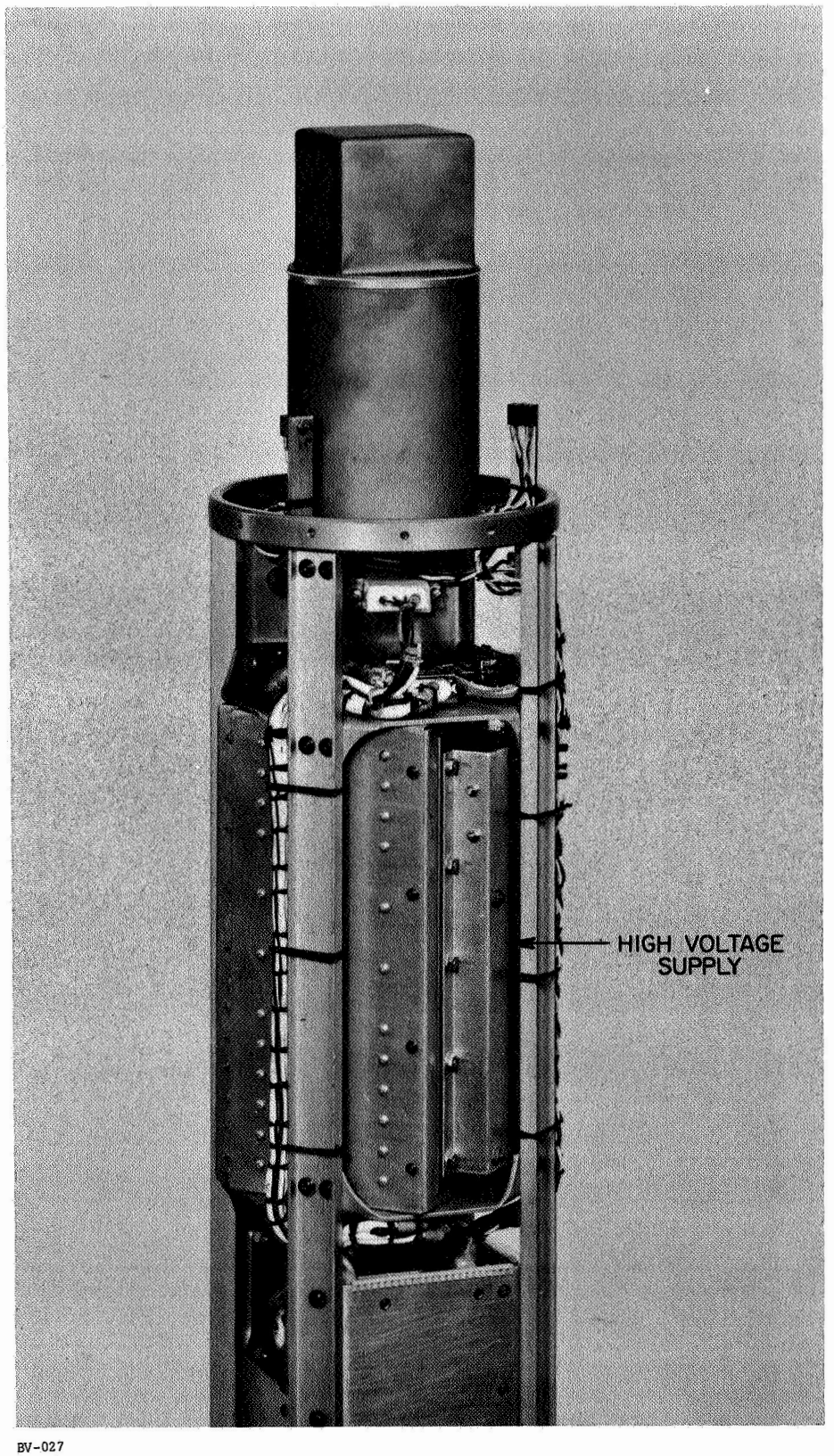

BV-027

Figure 4-5 Payload, Rear View

5.0 TESTS OF DETECTOR WITH PAYLOAD

5.1 Laboratory Tests

The payload, with the exception of the telemetry package, was completely assembled and tested in the laboratory prior to integration tests at Goddard Space Flight Center.

Signals, which are normally input to the telemetry, were instead coupled through emitter followers to a linear pulse shaping circuit, and from there to a pulse height analyzer, oscilloscope, and other circuits. Routing was performed as in earlier tests, by setting the window of a single-channel analyzer to the appropriate position for the PS signal.

Figures 5-1 and 5-2 show the PS and PH spectra, respectively, from Co^{60} and Pu-Be sources as well as for radiation from the neutron generator.

Note that the PSD is not as good as was achieved with commercial electronics, as indicated by the large number of counts in the region of the PS spectrum between the neutron and gamma rays than was observed earlier.

Since the flight electronics works well with the bulk scintillator, the reason for the poor PSD must be attributed, in part, to operating the system with the low pulse heights coming from the flight scintillator. Observation of waveforms in the critical circuit elements just prior to the zero-crossing stage indicated that the principal trouble was probably pick-up from the digital or logic circuits causing a distortion of the analog signal. Subsequent electronics circuits will have to be more carefully designed, incorporating improved isolation and techniques for degrading undesired transient signals.

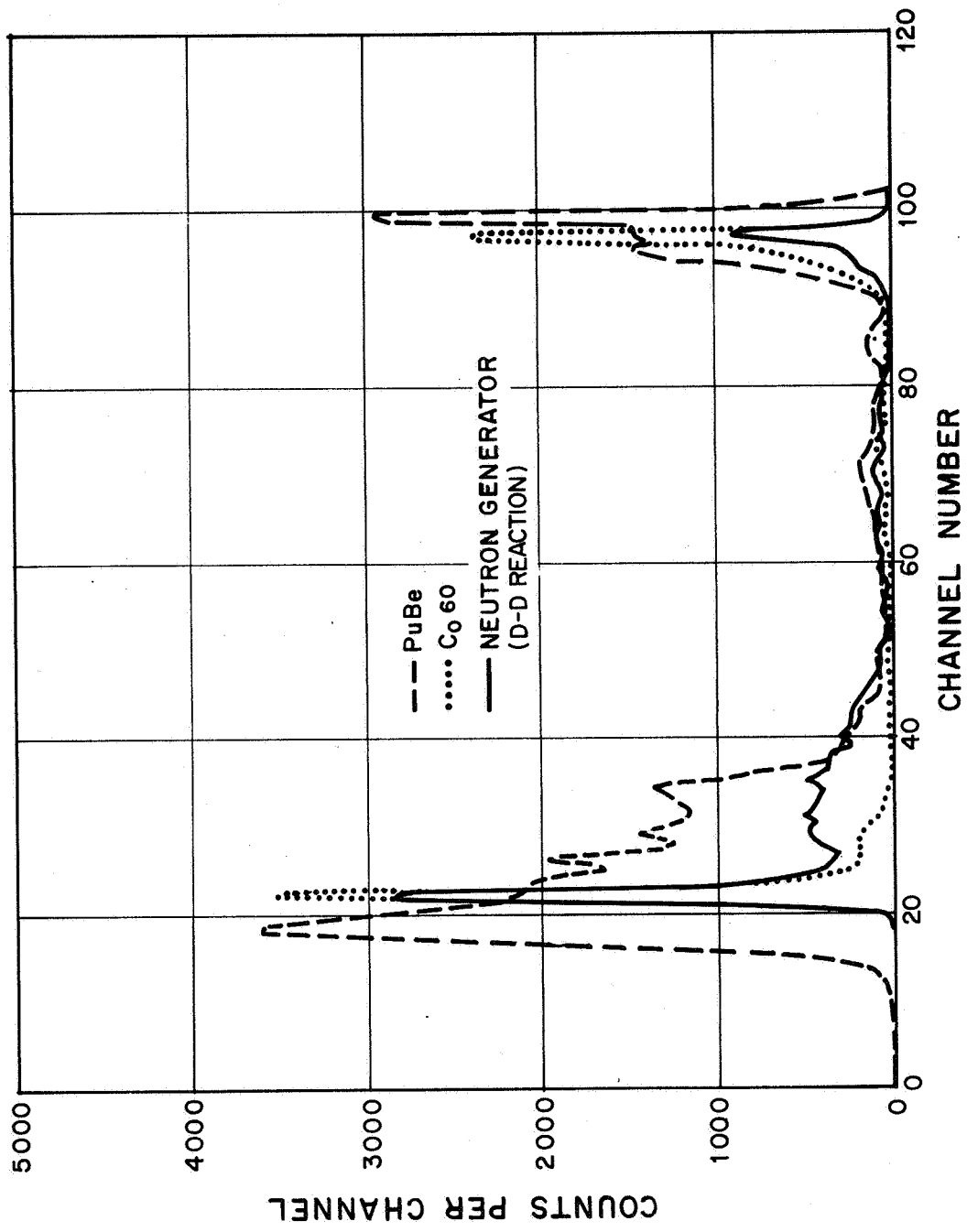

Figure 5-1 Flight Unit Pulse Shape Spectra. Counts between channels 10 and 25 are gammas. From channel 25 to 48 are neutrons. From 48 to 105 are CsI events.

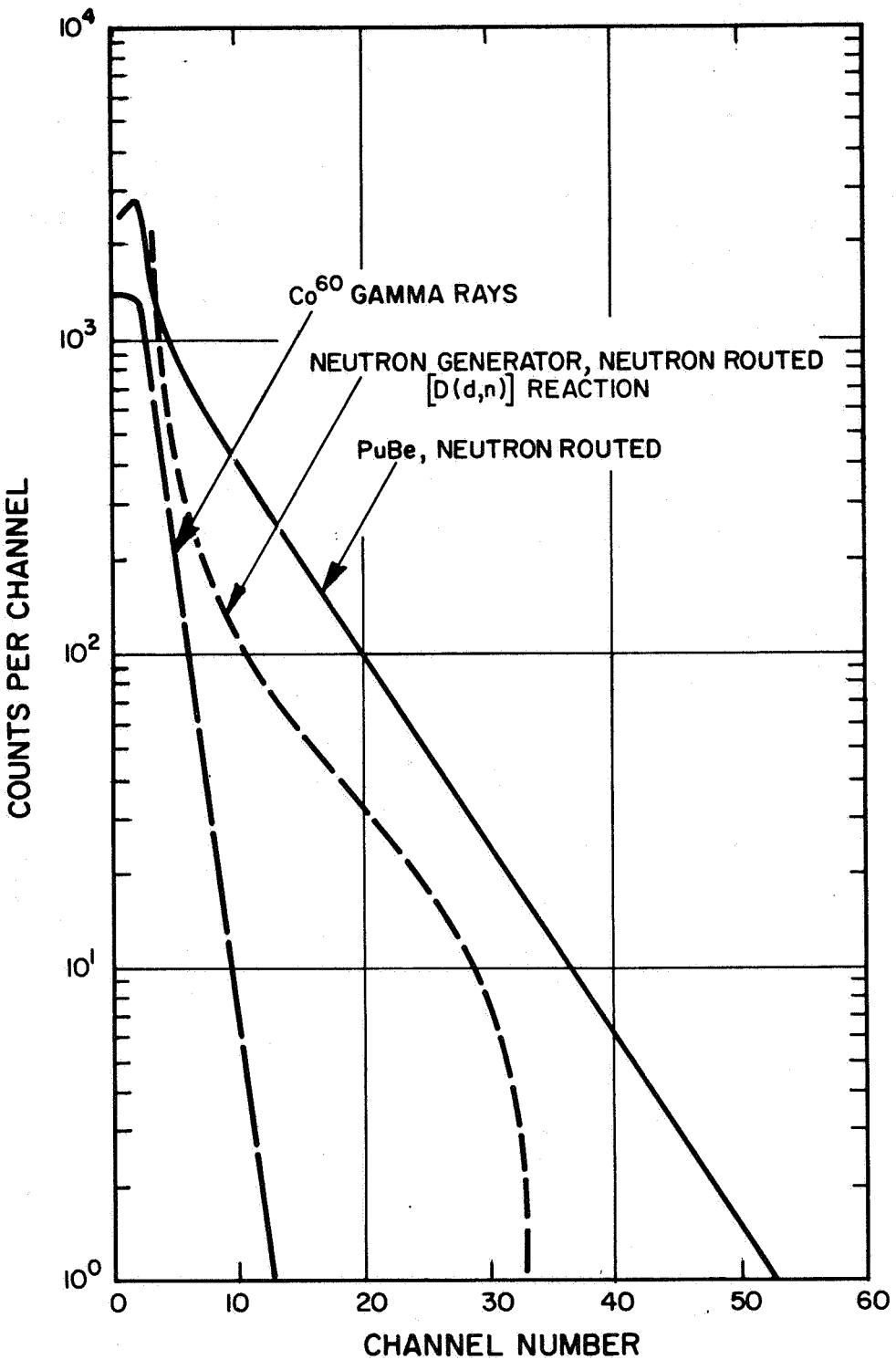

Figure 5-2 Flight Unit Pulse Height Spectra. The spectra from Pu-Be and the D (d,n) reaction are a mixture of gammas and neutrons, so the gamma part was rejected by PSD in these data.

Most of the measurements taken in the laboratory utilized a 512 channel one-parameter pulse height analyzer. Since a two-parameter analysis of PS and PH signals was required, the laboratory tests required multiple runs and did not lend themselves well to simple displays of the data. To aid in visualizing the results, time exposure photographs of an X-Y oscilloscope display were taken with the PH and PS amplitudes determining the coordinates.

The photographs are seen in Figure 5-3. PS and PH signals determine the vertical and horizontal coordinates, respectively. The spots along the top of each photograph represent radiation in the CsI. The response of the NE 213 to gamma rays produces the points one-third of the way up from the bottom. Neutrons, if detected, should appear as a horizontal line slightly above the gamma ray line. Pu-Be, Co^{60}, and generator neutrons were used to produce these photographs. In spite of PSD that is less than ideal, there is a distinct line which can be attributed to neutrons appearing in the Pu-Be and neutron generator exposures, but not in the Co^{60} exposure.

In Figures 5-4 and 5-5 are shown the directional response to Pu-Be and neutron generator radiation. Runs were taken for equal neutron production, with the incident neutrons first parallel and then perpendicular to the axis of the glass tubes. There is a definite directional response of the scintillator, with significantly greater response in the parallel case for generator neutrons. The directionality is much less for the continuous neutron spectrum from Pu-Be.

Vacuum tests were performed on the high voltage supply, detector, and preamplifier. These components were set up in a bell jar which was evacuated to a pressure of 10^{-4} mm while power was supplied. The preamplifier output was not affected by the evacuation.

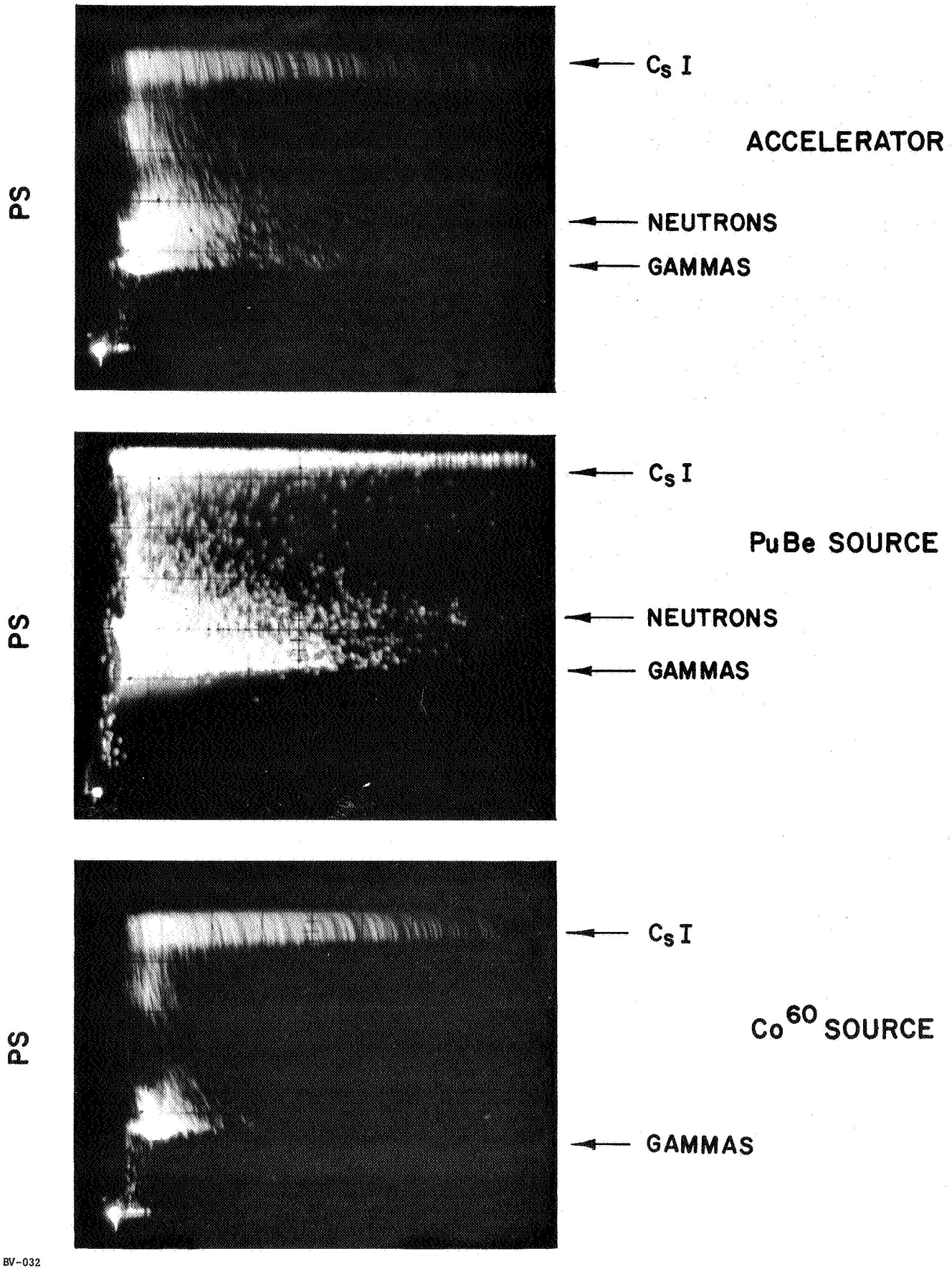

Figure 5-3 Flight Unit Two-Parameter Display.

Each photograph is a time exposure, with every event represented as a dot. The dot's location tells its pulse height and pulse shape. The origin is a bright blotch in the lower left corner of each photograph. PS voltage is the ordinate, increasing upward. PH voltage is the abscissa, increasing rightward.

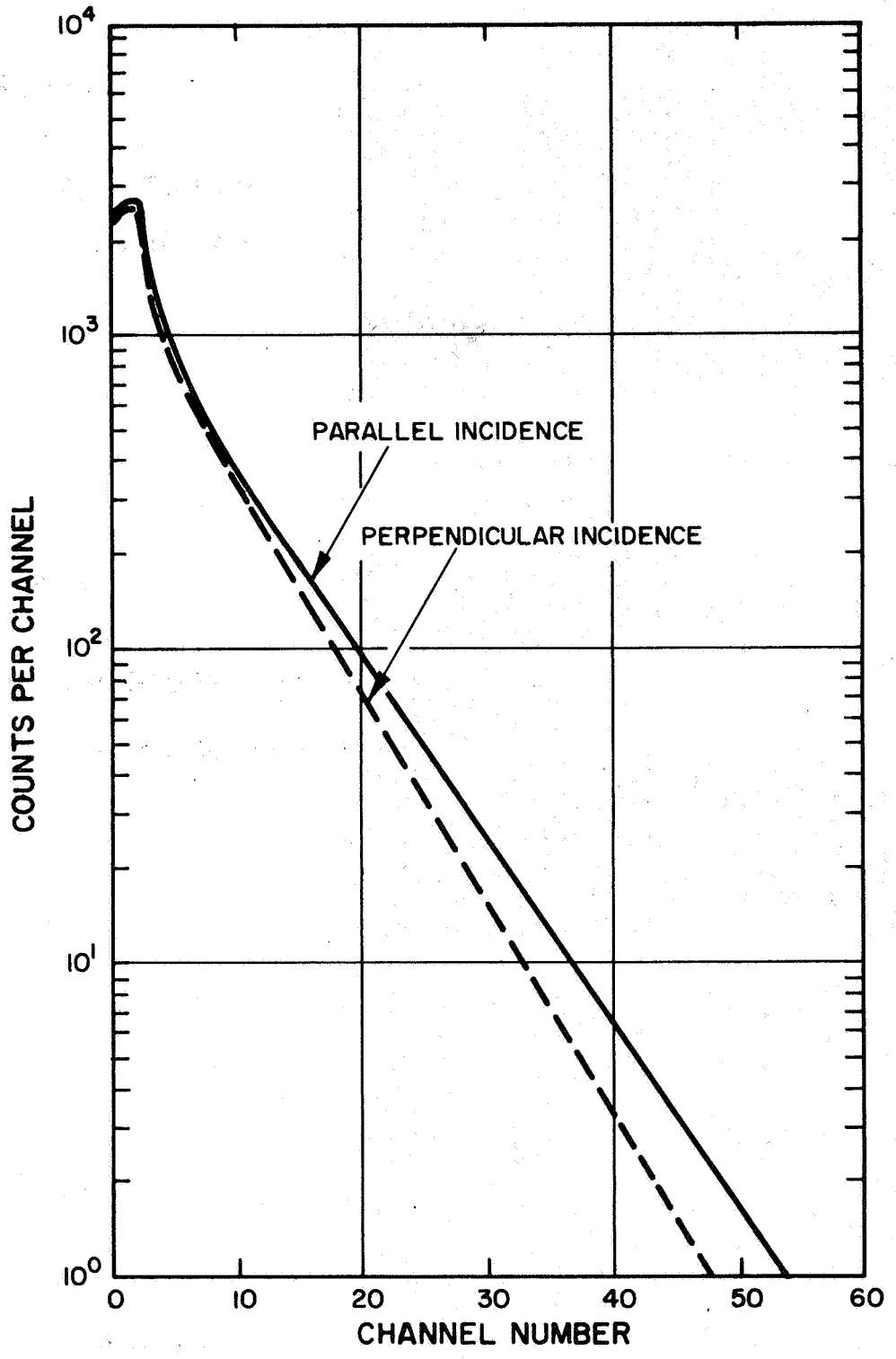

Figure 5-4 Directionality to Pu-Be Neutrons. Taken with the flight detector system. The pulse height spectrum is shown, for all events with PS in the neutron range.

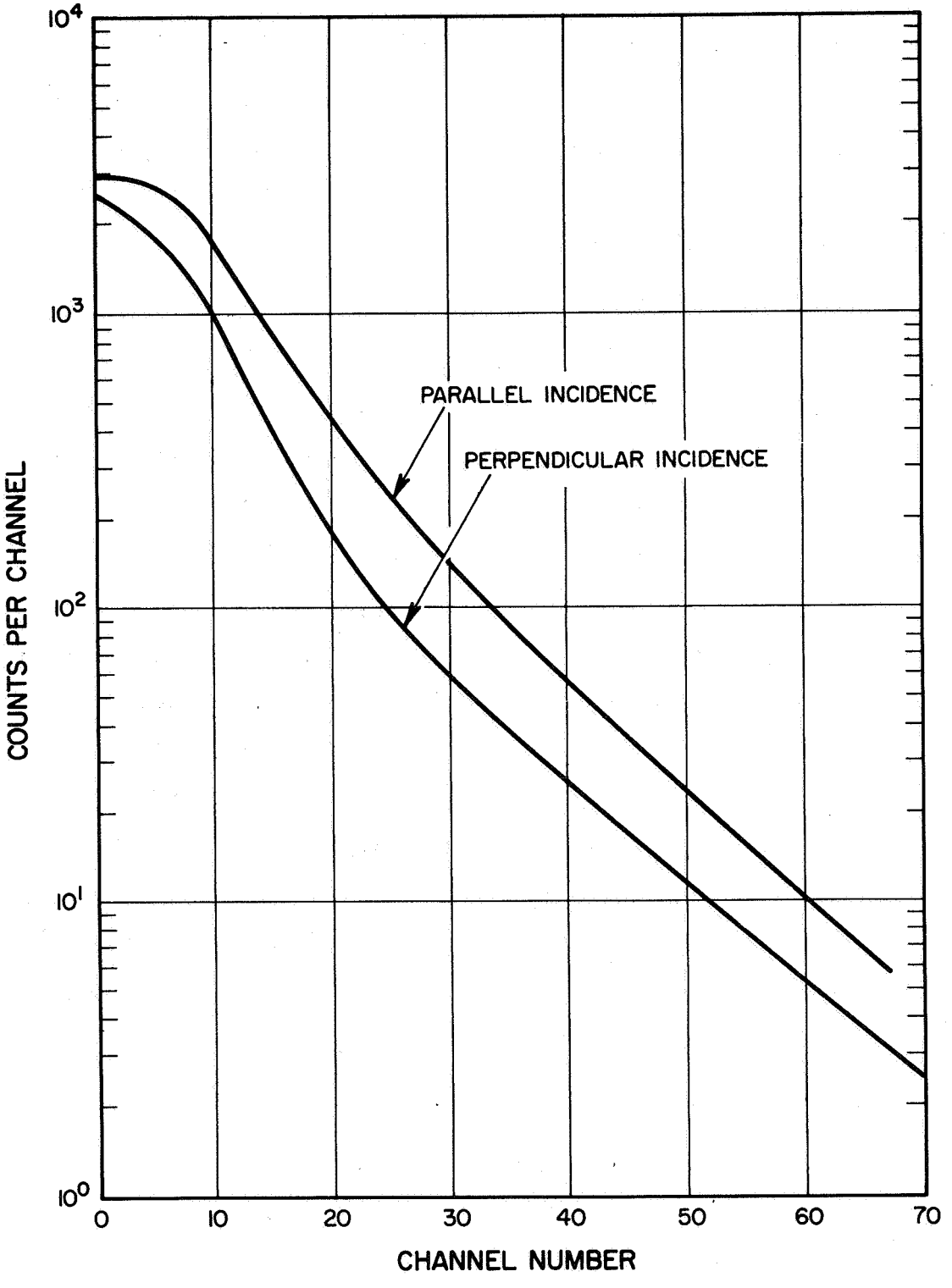

Figure 5-5 Directionality to 2.8 MeV Neutrons.
Taken with the flight system, same settings as in Figure 5-4.

Vibration tests of the entire payload, and also of the high voltage supply separately, were made without incident.

Nose cone ejection was tested several times in the laboratory with no failures. A motion picture of the ejection was examined frame by frame. It was noted that the nose cone was ejected smoothly at a velocity of several ft/sec.

5.2 Integration Tests

On May 22, 1967, integration tests were begun at Goddard Space Flight Center. The payload was disassembled, then carefully re-assembled. Vacuum and shake tests were performed with no problems encountered except for the loosening of a screw. The screw was, of course, retightened.

The electronics were tested with and without the telemetry. By use of telemetry, it was possible to get a quantitative two-parameter analysis of the PH and PS signals. As discussed more fully in the next two sections of this report, an OSCAR data reduction machine was used to measure the heights of the pulse pairs from a paper record. The information was then recorded on data cards.

Such telemetry records were made before and after the shake and vacuum tests, using Pu-Be and Co^{60} radiation. Comparison of the results indicated that the vacuum and shake tests produced no adverse effect on the output.

5.3 Preflight Calibration

One week prior to launch, tests were begun at the launch station at Wallops Island, Va. As in the integration tests, magnetic tape and paper records of the output from Pu-Be and Co^{60} were produced.

Figures 5-6 and 5-7 show the two-parameter output for Pu-Be radiation, for parallel and perpendicular incidence. This was obtained by transmitting a PS (pulse shape) pulse and a PH (pulse height) pulse through the telemetry system for each event occurring in the scintillator. Both pulses arrive and are recorded by the telemetry ground station simultaneously. The telemetry record is then examined, and the pairs of simultaneous PS, PH pulses are measured (in volts). Each event is categorized by two parameters. The two-parameter plot in Figures 5-6 and 5-7 show the number of events observed for each combination of PS and PH voltage. Different dots are plotted to indicate the differing populations of events for various values of PS and PH. The line along PS = 4 volts is events from the CsI shield. The region near PS = 1.7 volts is from gamma rays in the liquid scintillator. Neutrons interacting in the liquid scintillator produce proton recoils with PS = 2.2 volts. Events with PH less than 0.25 volts are subject to electronic malfunction, so were not used in any data analysis. There is very little directionality in the detector's response to the continuous neutron spectrum emitted by the Pu-Be source. This effect was also seen in the earlier payload tests (Figure 5-4). Pulse shape discrimination is at least 90 percent complete for gamma rays in NE 213, and better than 90 percent for events induced in the CsI.

Since the strength and location of the Pu-Be and Co^{60} sources are known, the efficiency of the complete flight system for detection of neutrons and gamma rays from these sources can be determined. Values obtained are 1.30 percent for Pu-Be neutrons, 0.51 percent for Co^{60} gamma rays, and 4.4 percent for the 4.43 MeV gamma rays from the Pu-Be source.

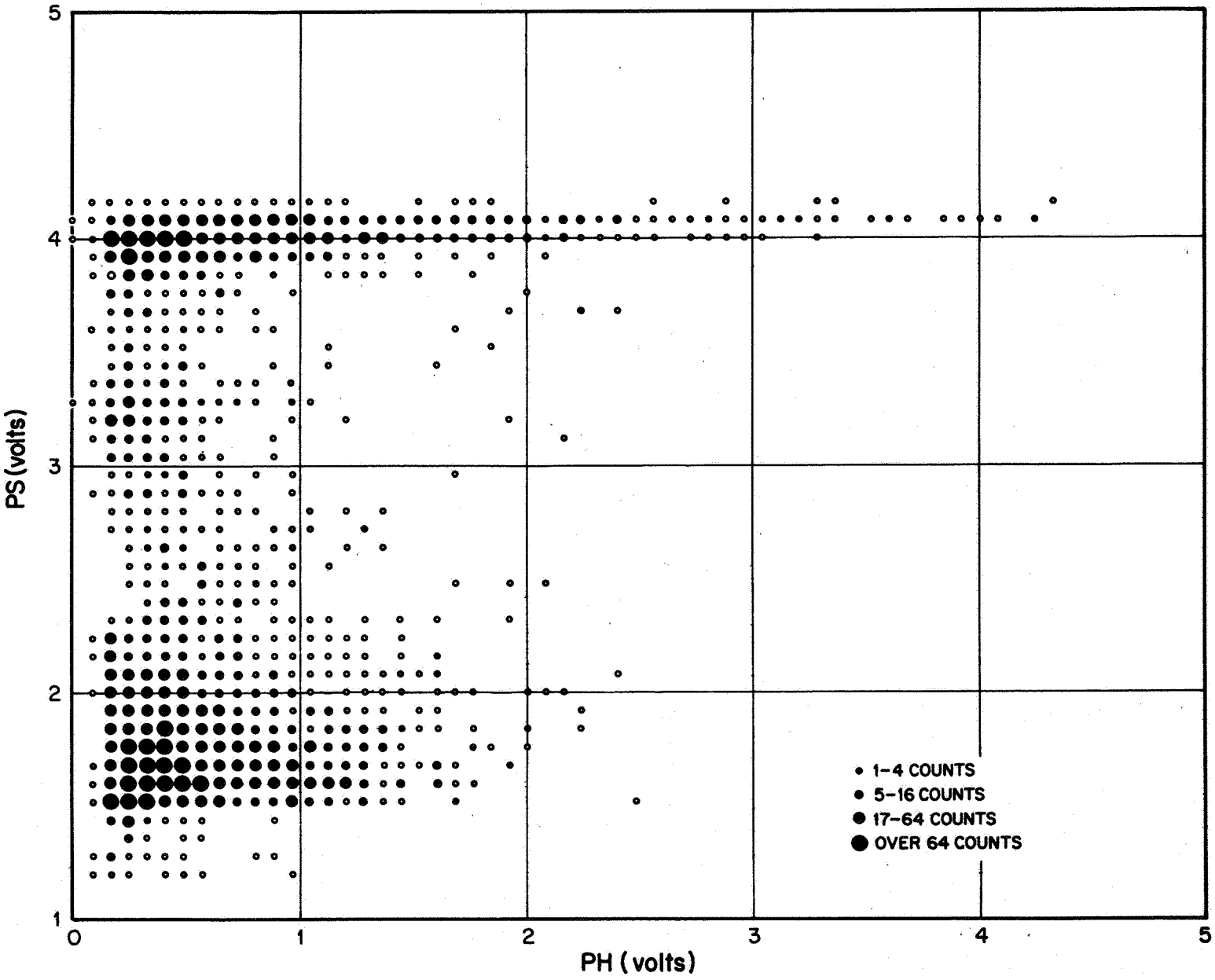

Figure 5-6 Preflight Calibration: Pu-Be Neutrons, parallel incidence. This plot is similar to that of Figure 5-3, with events classified by two parameters, PS and PH.

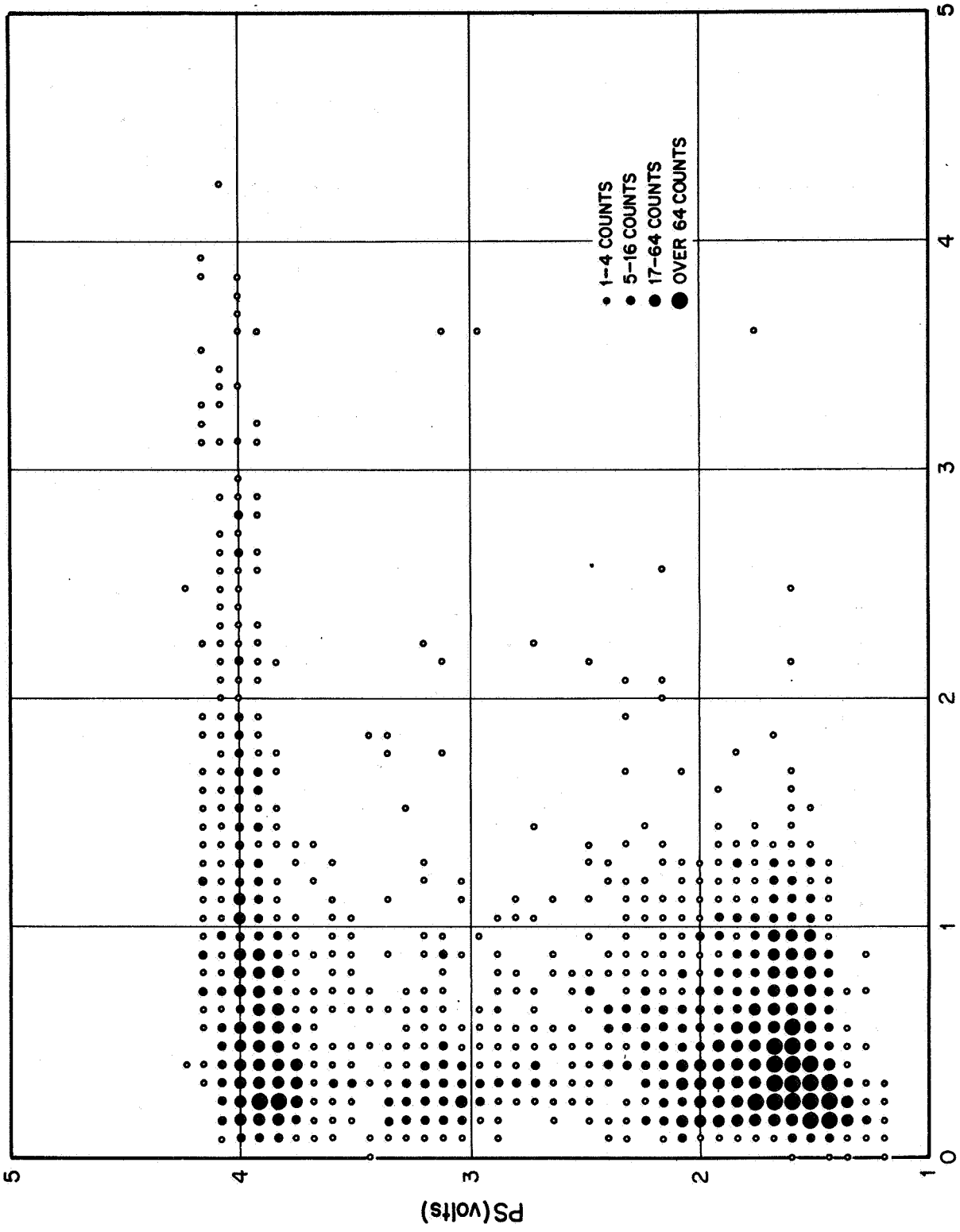

Figure 5-7 Preflight Calibration: Pu-Be Neutrons, perpendicular incidence.

6.0 DESCRIPTION OF THE FLIGHT

6.1 Flight Performance

At 2308:00 GMT on 13 June 1967, the neutron detector payload, pictured in Figure 6-1, was launched from the Wallops Island Range at a Zenith angle of 15.4°. The rocket axis was oriented normal to the earth-sun line. Then as the rocket spun, the detector axis rotated in a plane normal to the spin axis and swept by the sun twice per rotation of the rocket. A graph of the trajectory, obtained from preliminary radar data, appears in Figure 6-2. The maximum altitude and horizontal range were 598,000 feet and 465,000 feet, respectively. The duration of the flight was 435 seconds.

All components of the system worked perfectly during the flight. The nose cone was ejected exactly as planned at T + 54 seconds. Fins on the rocket were set to provide a spin of about six revolutions per second. As will be shown later, the spin was almost exactly seven revolutions per second. A commutator system sampled various voltage levels during the flight, providing continuous information about the stability of voltages and temperature, and the condition of the nose cone. The temperature did not change significantly during any portion of the flight.

During re-entry, a light leak developed in the detector at T + 390. The useful portion of the flight had ended by that time, however, and the detector had not been designed to withstand the stresses associated with re-entry.

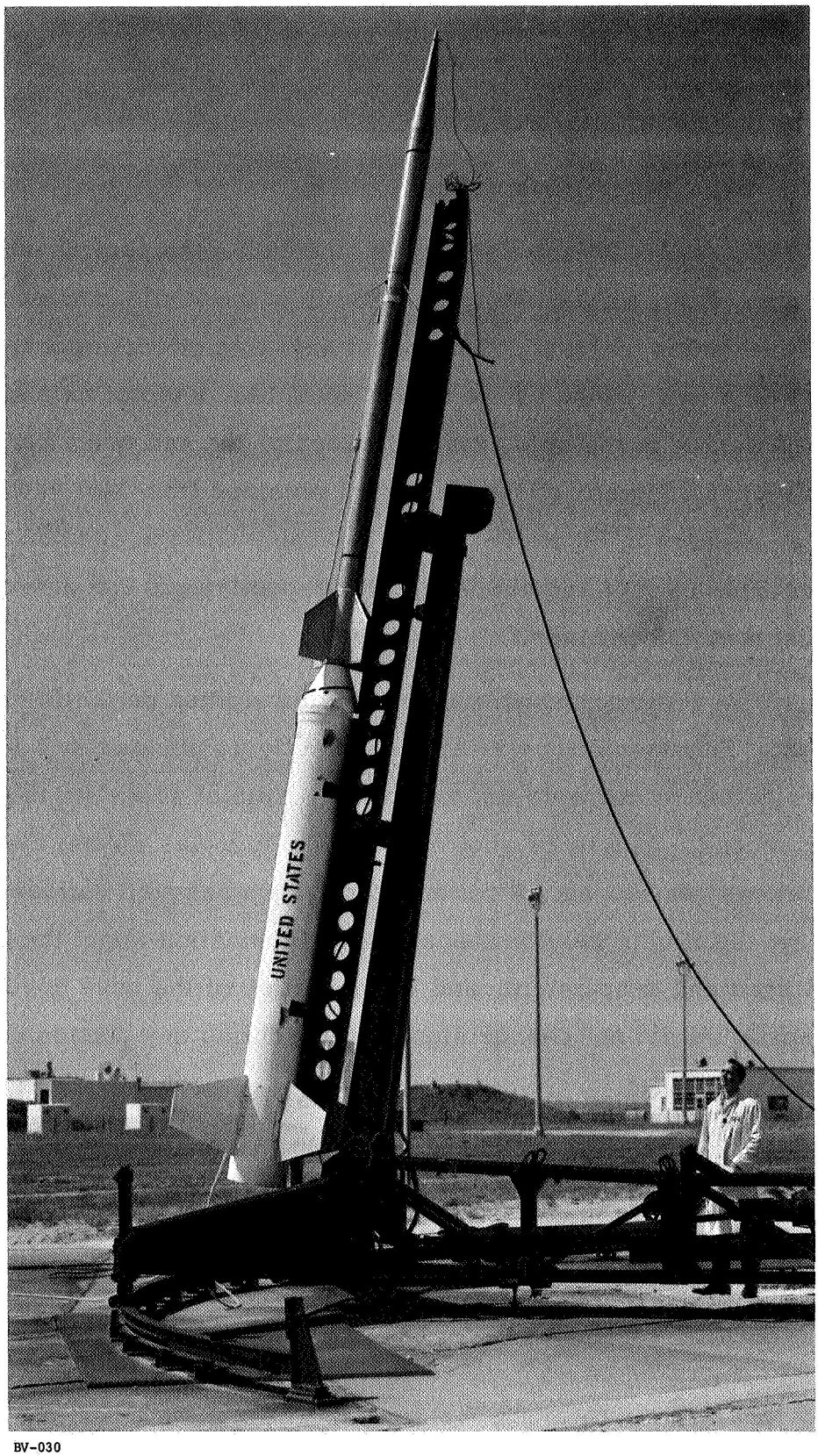

BV-030

Figure 6-1 Nike-Apache, flight 14.297 in launch position.

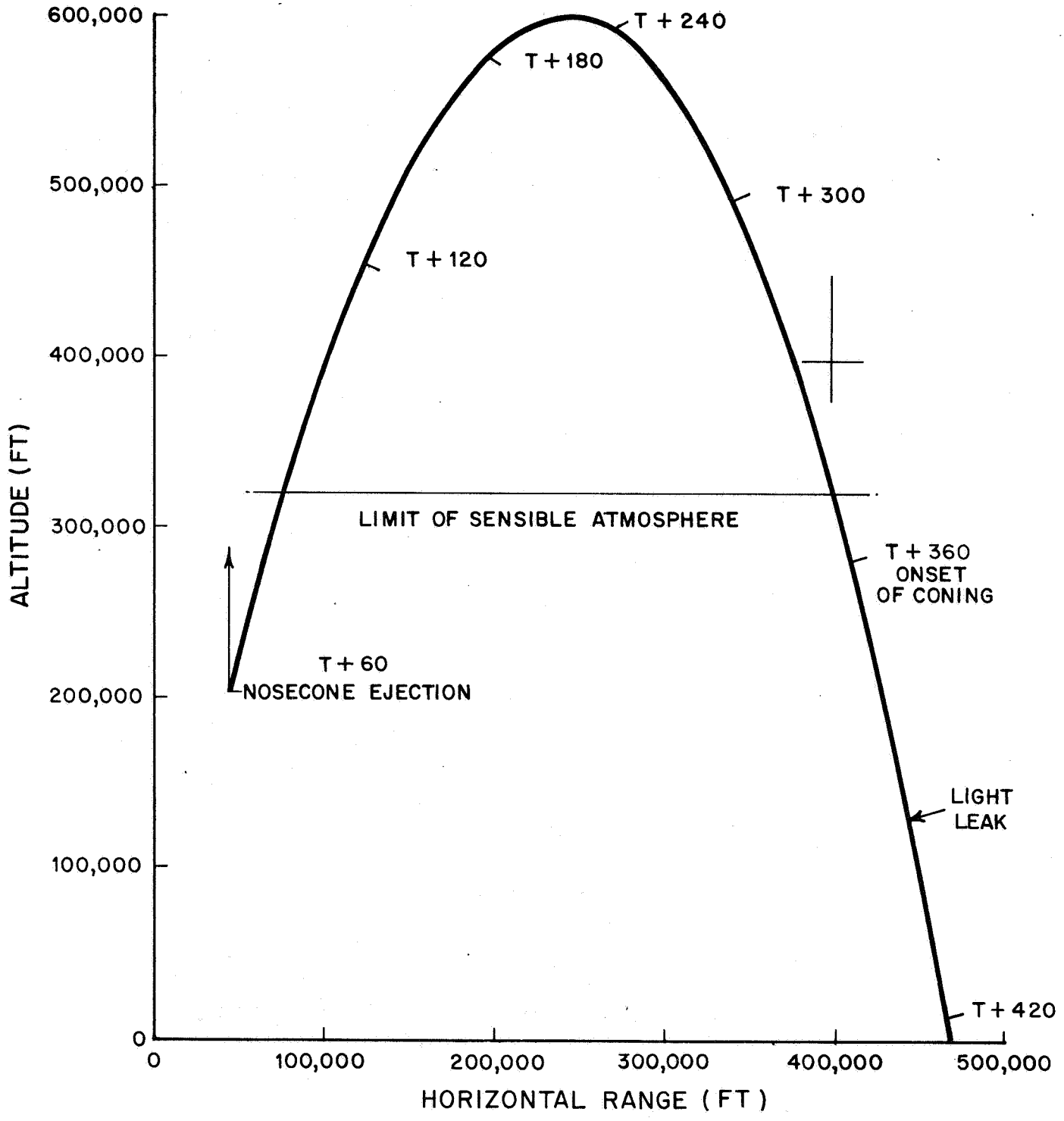

Figure 6-2 Vertical Trajectory Plot. Limit of atmosphere was determined by stability of spin rate.

6.2 Electronic Performance

A short sample of the telemetry output is shown in Figure 6-3. This abscissa is time, whose scale is found by noting that the two peaks in trace 13 are 0.143 sec apart, while the various telemetry channels appear in the same order as in Table IV-1. The height of the PS and PH pulses can be measured to an accuracy of about one percent of the maximum height by an OSCAR data reduction machine. This information is recorded, along with the time of the event, on IBM cards for later correlation studies.

Four scaler outputs were provided. They yield much less information than the two-parameter PS-PH data, by their nature. The scaler data would have been used if the PS or PH channels had not worked properly.

The sun sensor output is seen as a series of light peaks, 143.15 milliseconds apart. The first blip appeared at T + 54.076 seconds, coinciding with nose cone ejection. Secondary light peaks appear on each side of the main peaks. These are caused by internal reflections in the sensor. The time for each main peak was measured with the OSCAR machine, and these data were used to determine the orientation of the detector axis with the sun. This could be done, for each event, to an accuracy of about 2 degrees.

The sun sensor data also allowed determination of the spin of the rocket. This is plotted in Figure 6-4. The frictional effects in the upper atmosphere are apparently responsible for the decrease in angular velocity observed at each end of the graph.

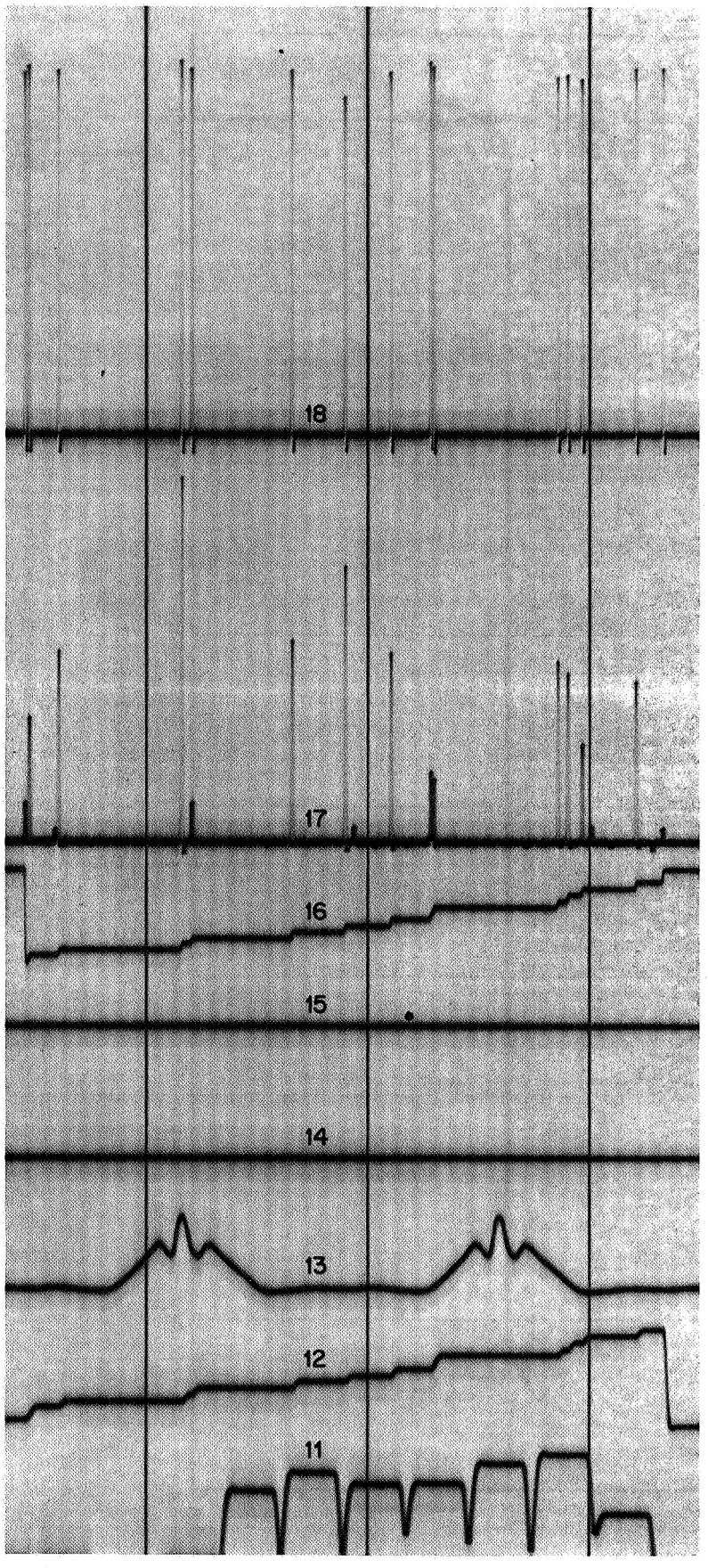

BV-033

Figure 6-3 Telemetry Record Sample. The traces represent, from the top down time code, PS, PH, scaler, scaler, sun sensor, scaler, housekeeping commutator, time code.

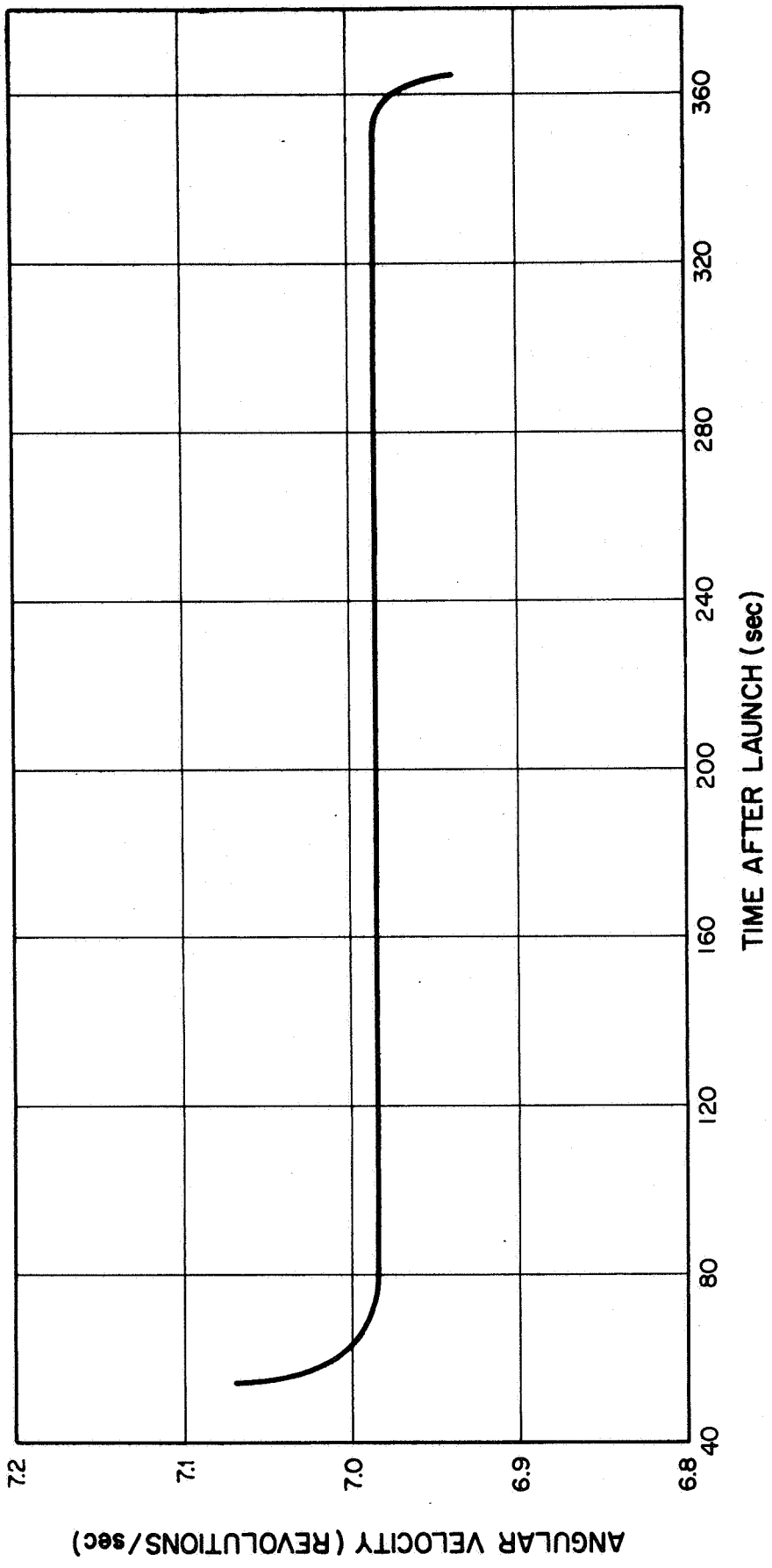

Figure 6-4 Payload Spin Rate. Some drag occurred at the beginning and end of the flight, causing a spin rate decrease.

The lowest channel on the telemetry record is the commutator. Each level was measured by the OSCAR machine at 3-second intervals. A listing of the results was carefully inspected, and no evidence of any major drift of voltage or temperature during the flight was observed. Selected levels are plotted in Figure 6-5 for the period of flight.

A coning of the rocket following re-entry is indicated by a distortion of the sun sensor pulses, beginning at T + 364 seconds, simultaneous with the de-spin noted at the right-hand side of Figure 6-4. The pulses become broader and poorly defined, as though the sun was not directly illuminating the photoconductive cell. This did not affect the usefulness of the data, since the directional properties of the detector could be utilized only above the atmosphere.

In summary, the flight was performed without difficulty and provided a useful engineering test of the directional neutron detector.

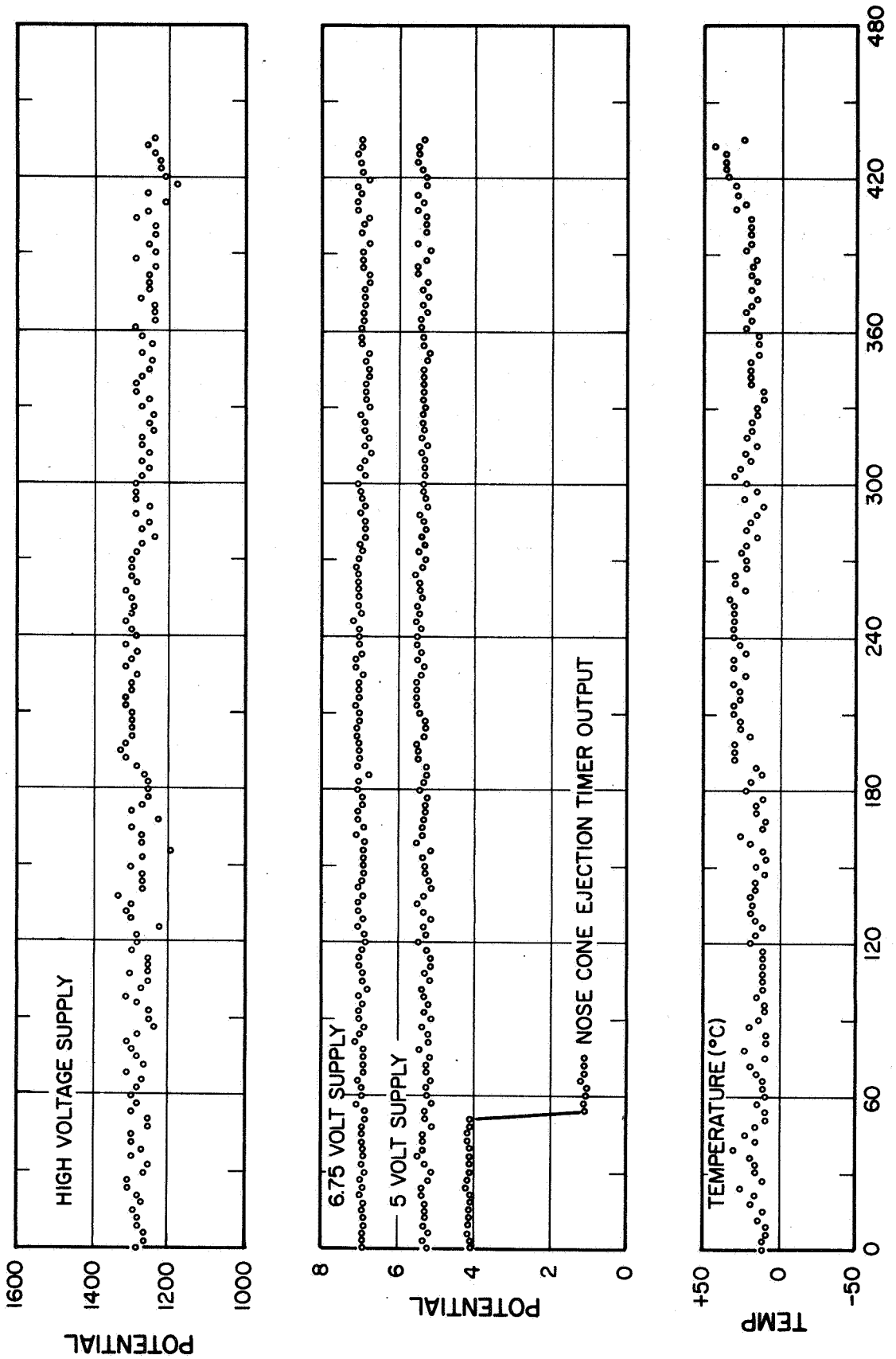

Figure 6-5 Housekeeping Monitors.

7.0 ANALYSIS OF SCIENTIFIC DATA

7.1 Data Reduction

As mentioned previously, data were extracted from the paper records of the flight and placed on IBM cards by use of the OSCAR data reduction machine. The telemetry channels analyzed included PS, PH, sun sensor, and commutator.

Over 18,000 pulse pairs were measured in the PS and PH channels, with the peak heights and time for each event digitized and punched on cards. There were 12 calibration waveforms recorded during the flight which also were measured, providing a means of converting pulse height from arbitrary units of the measuring machine to volts. These calibration waveforms were consistent to within one percent of the full scale deflection.

The sun sensor data were also analyzed by recording on cards the times within each second at which blips occur. A least-squares analysis was then performed, fitting the data to the equation $N_i = T_i/143.15 + b(t)$ to obtain the parameter b for each second of the flight. The parameter b contains the effects of non-constant spin period as well as an initial phase. Here, T_i is the time at which the N_ith blip occurs. With b known, the angular position of the sun sensor relative to the sun at the time T of an event during that second would be $\theta = 2\pi (T/143.15 + b)$. It is then a straight forward matter to determine the angle between the sun and detector axis.

The data were transferred from cards to magnetic tape, with six numbers being recorded for each event, as indicated in Table VII-1.

TABLE VII-1

Form of Reduced Flight Data

Parameter	Form or Units
PH (Pulse Height)	Hundredths of Volts
PS (Pulse Shape)	Hundredths of Volts
Time (Coarse)	Seconds
Time (Fine)	Milliseconds
Angle	Sun-Axis Angle in degrees
Height	Time from Apogee, in seconds, unsigned

7.2 Flight Data from the Scintillator

Once the data were on magnetic tape, they were then sorted out by computer. In Figure 7-1 is a two-parameter display showing PS (vertical) versus PH (horizontal), using data from the entire flight.

7.2.1 Particle Identification

The events for which there is a large PS signal correspond, in most cases, to cosmic ray events. Gamma events in NE 213 should appear at a PS around 1.80 volts, and such a peak is seen. Neutrons are expected over a range from 1.88 to 2.64 Volts, as determined by the preflight calibration.

Many counts are observed in this range, indicating that a large number of events could have been caused by neutrons. In order to verify that neutrons were detected during the flight, we looked at the PS spectrum (i.e., data from Figure 7-1 summed over all values of PH). The spectrum should show a peak at 1.8 volts due to gammas, at 2.2 volts due to neutrons, and a large peak at 4.2 volts due to charged particles. The data as presented in Figure 7-2 show the gamma and charged particle peaks clearly, but the region between is filled in by spillover from the charged particle peak. The only conclusion which Figure 7-2 can lead to is that any neutrons present would be obscured by the charged particle spillover.

At this point the two-parameter data (Figure 7-1) were re-examined. The charged particle spillover appeared to be worse at PH values above one volt. Also, the neutron detection efficiency is better below one volt. (While we cannot make a definite correspondence

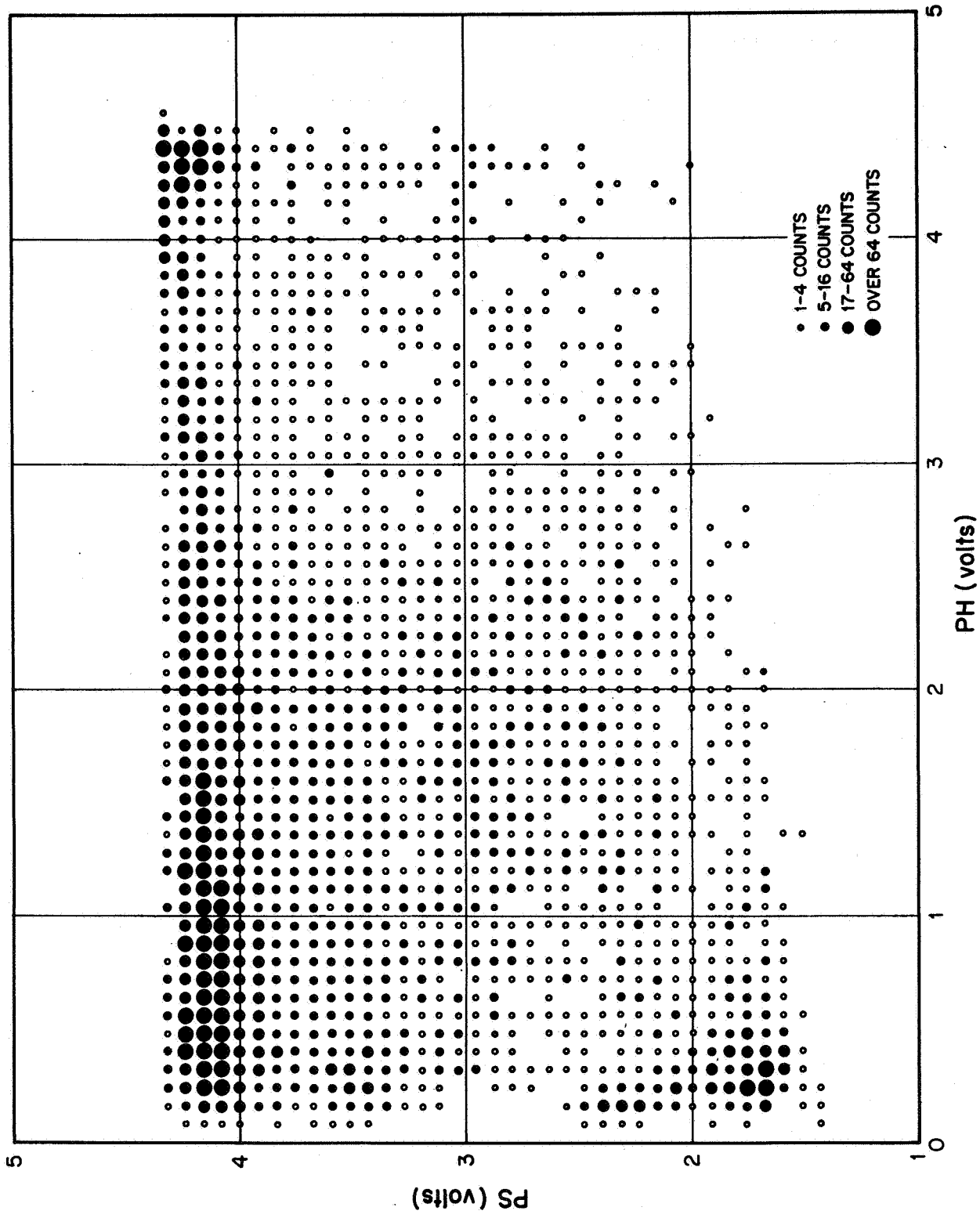

Figure 7-1 Flight Data, Two-Parameter Display.

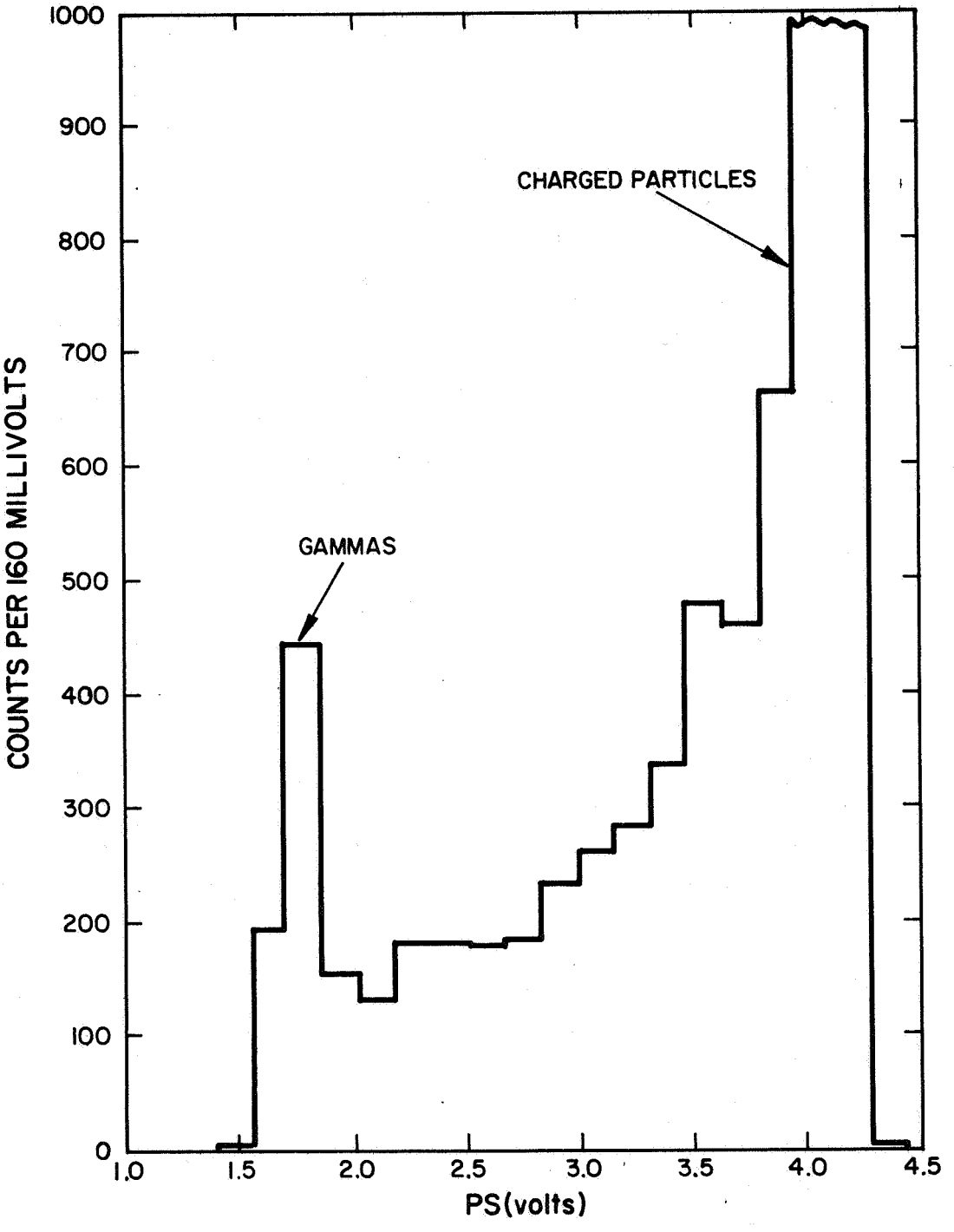

Figure 7-2 Pulse Shape Spectrum, full range of pulse heights. Time after launch: 90 to 350 sec. All angles with Sun.

between pulse height (PH) and neutron energy, it was observed that 2.8 MeV neutrons gave pulses below 1.2 volts.) On the basis of these considerations, a portion of the data having PH between 0.25 and 1.2 volts were re-examined.

Such a selected group of data were summed over PH and plotted as a PS spectrum in Figure 7-3. It was determined from other PH cuts above 1.2 volts that the charged particle spillover does not occur below PS$\leq$ 2.7 volts. The small unresolved peak between 2.0 and 2.5 volts could now be neutrons. Its width and location with respect to the gamma and charged particle peaks are typical of data observed in previous calibrations.

7.2.2 Directional Effects

Using the sun sensor data, we calculated the rocket aspect for all times during the flight. This allowed a presentation of data for various orientations of the detector with respect to the sun. The data were grouped into three intervals, according to θ, the angle between the earth-sun line and detector axis. Results are shown in Figure 7-4. None of the data show any statistically significant dependence on θ.

7.3 Interpretation of Flight Data

The data presented in 7.2 must be interpreted using detector dimensions and efficiencies. This results in three separate flux measurements: charged particle, neutron and gamma. The detector was not expected to be directional for charged particles or gammas, and indeed the results were independent of direction. The neutron data show no correlation with earth-sun line direction either, but there are many more counts than were expected.

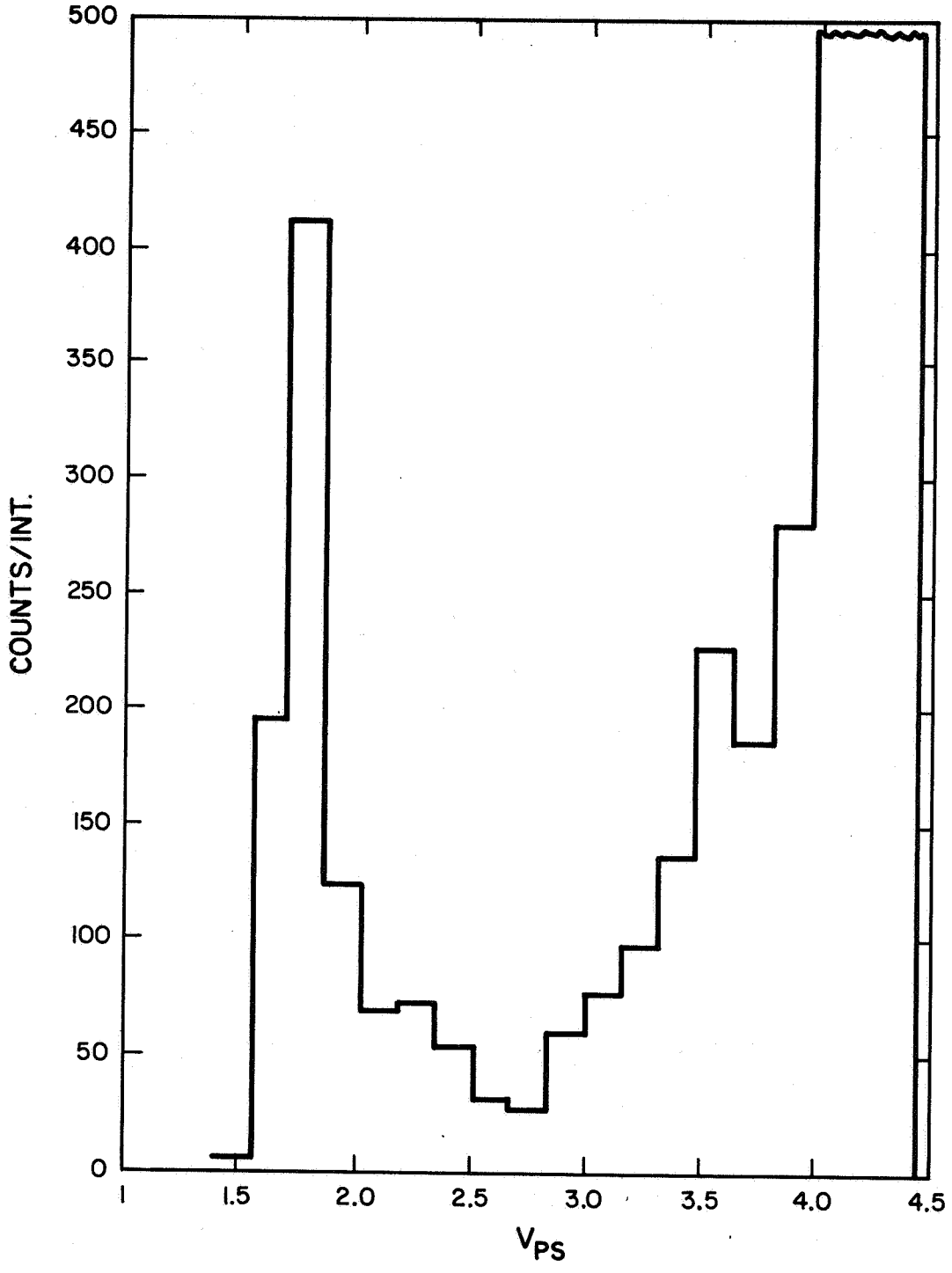

Figure 7-3 Pulse Shape Spectrum, pulse heights up to 1.2 Volts. Time after launch: 90 to 350 sec. All angles.

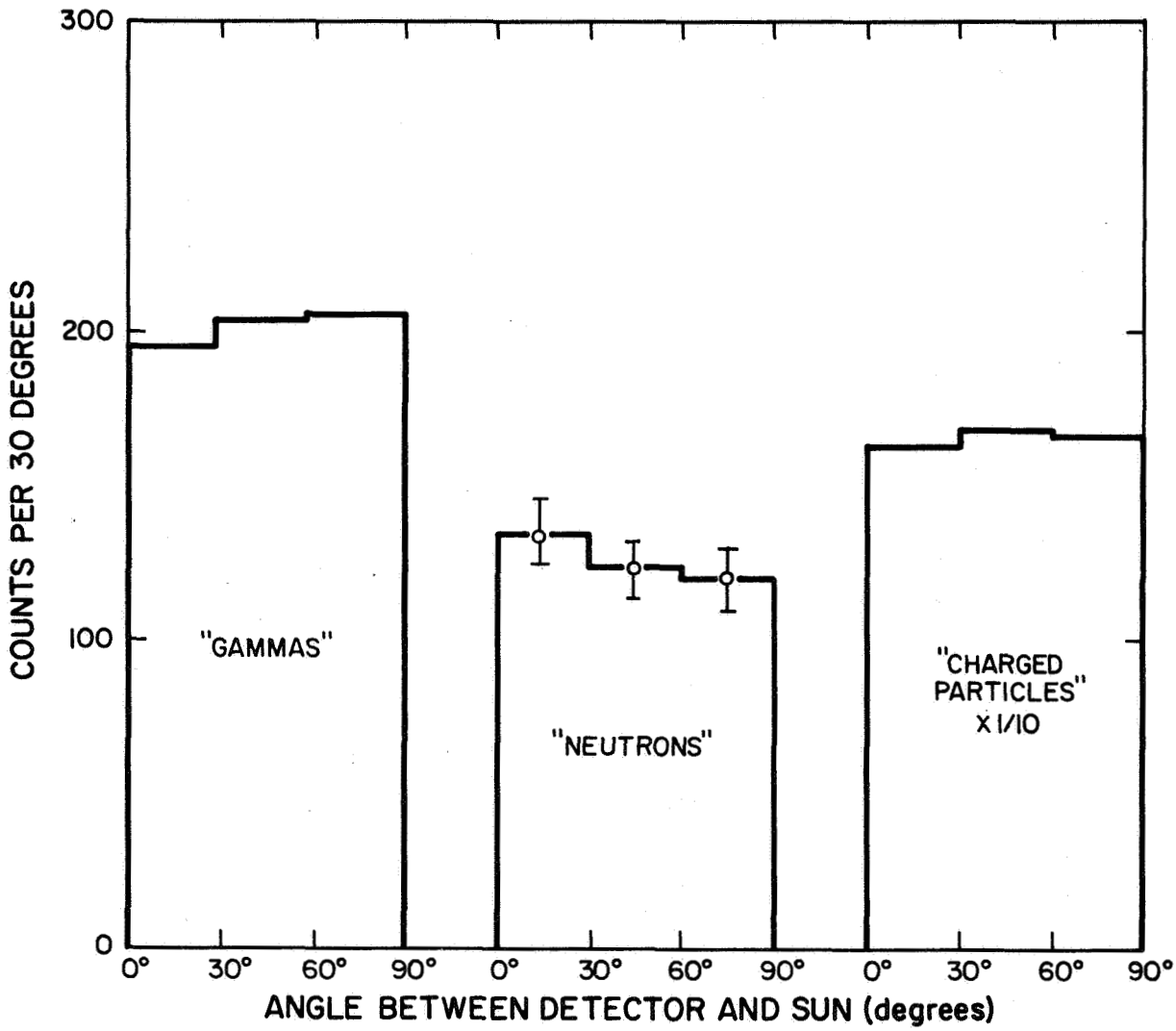

Figure 7-4 Angular Variation of Counts. The three histograms are selections of different ranges of the PS parameter. For gammas, PS ranges up to 1.86 Volts. For neutrons, PS ranges between 1.87 and 2.83 Volts. For charged particles, PS ranges above 2.83 Volts.

7.3.1 Charged Particles

A total of 8362 events were observed in 260 seconds. The effective diagonal area of the CsI(Na) shield was 38 cm^2 ± 10%, giving an omnidirectional flux of 0.76 to 0.96/cm^2 sec (since the efficiency for charged particles is taken to be 100%). The primary proton flux at the top of the atmosphere is[9] 0.12/cm^2 sec ster, giving a 2π flux of 0.76/cm^2 sec. The present data agree with previous measurements of primary proton flux.

7.3.2 Gamma Rays

A total of 615 counts were observed in 260 seconds above the atmosphere. The effective area of the NE 213 cell was 20 cm^2. The detector efficiency was measured before the flight to be 0.5 percent for 1.2 MeV gammas from Co^{60} and 4.4 percent for the 4.43 MeV gammas from the Pu-Be source. Because of the poor resolution resulting from low light output of the cell, it is difficult to calculate the gamma flux. It is believed that the efficiencies measured in the lab represent approximate limits to the efficiency in flight. Thus, the observed counting rate above the atmosphere of 0.11 counts/cm^2 sec suggests a gamma flux between 2.6 and 23.6 photons/cm^2 sec. The lower value is within a factor of two of previous measurements[10].

7.3.3 Neutrons

The number of events occurring where neutrons are expected was 383 for pulse heights between 0.25 and 1.2 volts. The pulse shape discrimination between gammas and neutrons was good enough (10:1 gamma rejection) so that these counts cannot be attributed to gamma spillover. The difficulties with charged particle spillover as shown in Figure 7-2 preclude identifying these counts positively as neutrons.

7.4 Directionality

Since no directional effect was observed, it can be stated that the upper limit on monoenergetic neutron flux at energies from 2-5 MeV from the sun was 5 n/cm^2 sec on June 13, 1967, 2309:30 to 2313:50 GMT.

8.0 CONCLUSIONS

a. The concept of the directional neutron detector has been shown to be valid. Significant directional effects are achievable. Results have been published by Kellogg and Waters[11].

b. The technique of pulse shape discrimination to separate neutron and gamma ray interactions in the scintillator for this particular geometry has been shown to be valid.

c. The charged particle flux in space is known to be much higher than either the neutron or gamma flux. It is desirable to use a separate scintillator for charged particles, otherwise the "break through" that is bound to occur in any electronic separation system will give spurious data in the neutron and gamma ray channel.

d. It is very important to transmit both the pulse height and the pulse shape data on telemetry to allow two dimensional analysis to be performed on the ground. On-board analysis cannot be sophisticated enough without great electronic complexity.

e. The ejectable nose cone and complete payload functioned perfectly during our ground tests and during the flight.

f. The detector operated as predicted. The measured fluxes of protons and gamma rays agree with previous measurements.

g. No significant solar neutron flux was measured. The upper limit was five neutrons per square centimeter-sec.

h. Improvements in the detector are required as follows:

(1) Increase light output from the cell. For example, by reverting to the use of individual glass tubes rather than the monolithic glass block.

(2) Make the charged particle anticoincidence system optically separate by isolating the CsI shield and observing it with a separate photomultiplier.

(3) In the electronics the crosstalk between analog and digital circuitry must be reduced. This problem will be alleviated by increased light output from the detector.

REFERENCES

1. Hess, W. N., Neutrons in Space, Proc. Fifth Inter-American Seminar on Cosmic Rays, LaPaz, Boliva, pp. 17-27, July 1962.

2. Lingenfelter, Flamm, Canfield and Kellman, Geophysical Res. 70, 4087 (1965).

3. Fireman, E. L., Solar Surface Nuclear Reactions, Proc. of Cosmic Ray Conference, Jaipur, India

4. Haynes, R. C., J. Geophys. Res. 69, 841 (1964)

5. Bame and Asbridge, J. Geophys. Res. 71, 4605 (1966)

6. Daniel, Joseph, Lavakare, and Sunnderajan, Nature, 213, 21 (1967)

7. Rothberg, Anderson, Bleser, Lederman, Meyer, Rosen and Wang, Phys. Rev. 132, 2664 (1963)

8. Peuckert, K., Nuclear Instr. and Methods, 17, 257 (1962)

9. Gangnes, Jenkins and Van Allen, Phys. Rev. 75, 57 (1949)

10. Peterson, L., private communication

11. Kellogg and Waters, IEEE Trans. Nucl. Science NS-14